

**TRANSITION METAL-CONTAINING CARBON MOLECULAR
SIEVE MEMBRANES FOR ADVANCED OLEFIN/PARAFFIN
SEPARATIONS**

A Dissertation
Presented to
The Academic Faculty

by

Yu-Han Chu

In Partial Fulfillment
of the Requirements for the Degree
Doctor of Philosophy in the
School of Chemical & Biomolecular Engineering

Georgia Institute of Technology
August 2017

COPYRIGHT © 2017 BY YU-HAN CHU

**TRANSITION METAL-CONTAINING CARBON MOLECULAR
SIEVE MEMBRANES FOR ADVANCED OLEFIN/PARAFFIN
SEPARATIONS**

Approved by:

Dr. William J. Koros, Advisor
School of Chemical & Biomolecular
Engineering
Georgia Institute of Technology

Dr. David G. Bucknall
School of Material Science and
Engineering
Georgia Institute of Technology

Dr. Pradeep K. Agrawal
School of Chemical & Biomolecular
Engineering
Georgia Institute of Technology

Mr. Mark K. Brayden
Hydrocarbon R&D
The Dow Chemical Company

Dr. Christopher W. Jones
School of Chemical & Biomolecular
Engineering
Georgia Institute of Technology

Dr. Liren Xu
Hydrocarbon R&D
The Dow Chemical Company

Date Approved: July 17, 2017

This work is dedicated to my beloved mother and brother.

ACKNOWLEDGEMENTS

During the journey of pursuing Ph.D., I have met several intelligent and warm-hearted individuals. This dissertation would not have been possible without the supports and encouragements provided from each of them.

First and foremost, I would like to extend my sincere gratitude to my advisor, Dr. William J. Koros. I would not have completed my Ph.D. study without his guidance and inspiration. His enthusiasm, intelligence, and positive attitude will always continue to inspire me to be a better person.

Funding support from The Dow Chemical Company is greatly acknowledged. I have been fortunate to collaborate with Mr. Mark Brayden, Mr. Marcos Martinez, and Dr. Liren Xu on this exciting research project. Their insightful inputs and continuous supports are highly appreciated. I also would like to express my sincere appreciation to Dr. David Yancey for his assistance on XANES characterization.

I would like to thank my thesis committee members, Dr. Pradeep K. Agrawal, Dr. Christopher W. Jones, and Dr. David G. Bucknall for their technical suggestions on this dissertation.

I am lucky to be the last graduate student in the Koros group. I am thankful for all the supports and guidance from each previous and current group member. It has been a pleasure to work with Dr. Wulin Qiu, Dr. Justin Vaughn, and John Hessler on the Dow projects, and I would like to appreciate the feedbacks they provided during the meetings. I am also grateful to Dr. Dai Ying, Dr. Shouliang Yi, Dr. Kuang Zhang, and Dr. Chen Zhang

for sharing their extensive research experiences. I would like to greatly appreciate Dr. Manjeshwar Kamath and Dr. Vinod Babu for their efforts on lab safety. I have been enjoying sharing the office with Dr. Shweta Karwa or Dr. Oishi Sanyal, and I owe thanks to them for all the cheers. Dr. Gongping Liu, Dr. Shilu Fu, and Dr. Graham Wenz are good friends for enjoyable conversations on either technical discussions or fun things, and I would like to appreciate the great time they gave me. Besides the group members, I would like to specially acknowledge Mrs. Michelle Martin and Mr. Rod Sefton for their responsible administrative assistances.

Last but not the last, I would like to thank my mother, my brother, and all other lovely family members. Their encouragements, love, and supports have helped me go through the ups and downs in this journey.

TABLE OF CONTENTS

ACKNOWLEDGEMENTS	iv
LIST OF TABLES	x
LIST OF FIGURES	xii
SUMMARY	xvi
CHAPTER 1. INTRODUCTION	1
1.1 Production of Olefins	1
1.2 Membrane Technology for Gas Separations	5
1.3 Olefin-Selective CMS Membranes	6
1.4 Research Objectives	8
1.5 Dissertation Organization	11
1.6 References	13
CHAPTER 2. BACKGROUND AND THEORY	16
2.1 Overview	16
2.2 Structure of Carbon Molecular Sieve Membranes	16
2.3 Formation of Carbon Molecular Sieve Membranes	18
2.3.1 Polymer Precursor	18
2.3.2 Pre-Treatment of Polymer Precursor	20
2.3.3 Pyrolysis Temperature Protocol	21
2.3.4 Pyrolysis Atmosphere	23
2.3.5 Post-Treatment of CMS Membranes	24
2.4 Gas Transport in Membranes	25
2.4.1 Permeation	25
2.4.2 Sorption	28
2.4.3 Diffusion	29
2.4.4 Temperature Dependence of Gas Transport	31
2.4.5 Energetic and Entropic Factors in Diffusion Selectivity	33

2.5	References	36
CHAPTER 3. MATERIALS AND EXPERIMENTAL METHODS		
3.1	Overview	40
3.2	Materials	40
3.2.1	Gases	40
3.2.2	Polymers	40
3.2.3	Metal Salts	42
3.3	Membrane Formation	43
3.3.1	Polymer Dense Film Membrane Formation	43
3.3.2	Carbon Molecular Sieve Dense Film Membrane Formation	45
3.4	Characterization Techniques	49
3.4.1	Dense Film Permeation Measurements	49
3.4.2	Pressure Decay Sorption	53
3.4.3	X-Ray Absorption Near Edge Structure	54
3.5	References	55
CHAPTER 4. EVALUATION OF VIABILITY OF IRON IN CARBON MOLECULAR SIEVE MEMBRANES FOR INCREASING OLEFIN/PARAFFIN SORPTION SELECTIVITY		
4.1	Overview	56
4.2	Olefin/Paraffin Separation with CMS Membranes	56
4.3	Selective Olefin/Paraffin Adsorption with Metal-Organic Frameworks	58
4.4	Strategy for Improving Olefin/Paraffin Separation with Fe in CMS Membranes	59
4.5	Sorption Performance of Fe-Containing CMS Membranes	60
4.5.1	Effects of Pyrolysis Protocols	61
4.5.2	Olefin-Selective CMS Membranes with Fe	67
4.5.3	Effects of DABA Group in Polymer Precursor	68
4.6	XANES Spectra of Fe-Containing CMS Membranes	69
4.7	Summary and Conclusions	72

4.8	References	73
CHAPTER 5. INVESTIGATION OF EFFECTS OF IRON LOADINGS & STUDIES ON ALTERNATIVE METAL SPECIES FOR OLEFIN-SELECTIVE CARBON MOLECULAR SIEVE MEMBRANES		
5.1	Overview	75
5.2	Effects of Fe Loadings in CMS Membranes	75
5.3	Stability of Fe-Containing CMS Membranes	79
5.4	Effects of Metal Species for Metal-Containing CMS Membranes	80
5.5	Summary and Conclusions	84
5.6	References	85
CHAPTER 6. ANALYSIS OF EFFECTS OF IRON ON PERFORMANCE OF IRON-CONTAINING CARBON MOLECULAR SIEVE MEMBRANES		
6.1	Overview	86
6.2	Transport Properties of Polymer Precursors	86
6.2.1	Permeation Performance	87
6.2.2	Sorption Performance	89
6.2.3	Diffusion Performance	91
6.3	Transport Properties of CMS Membranes	91
6.3.1	Sorption and Diffusion Factors in Separation Efficiency	92
6.3.2	Mixed Gas Permeation Performance	96
6.4	Summary and Conclusions	101
6.5	References	102
CHAPTER 7. CHARACTERIZATION OF EFFECTS OF TESTING TEMPERATURE ON OLEFIN/PARAFFIN SEPARATION PERFORMANCE OF IRON-CONTAINING CARBON MOLECULAR SIEVE MEMBRANES		
7.1	Overview	103
7.2	Temperature Dependence of Permeation Performance	104

7.3	Temperature Dependence of Sorption Performance	109
7.4	Temperature Dependence of Diffusion Performance	114
7.5	Energetic and Entropic Factors in Diffusion Selectivity	118
7.6	Summary and Conclusions	121
7.7	References	123
CHAPTER 8. CONCLUSIONS & RECOMMENDATIONS		124
8.1	Overview	124
8.2	Conclusions	124
8.2.1	Evaluation of Viability of Selected Metal in CMS Membranes for Increasing Olefin/Paraffin Sorption Selectivity	124
8.2.2	Investigation of Effects of Iron Loadings & Studies on Alternative Metal Species for Olefin-Selective CMS Membranes	126
8.2.3	Analysis of Effects of Iron on Performance of Iron-Containing CMS Membranes	127
8.2.4	Characterization of Effects of Testing Temperature on Olefin/Paraffin Separation Performance of Iron-Containing CMS Membranes	128
8.3	Recommendations	129
8.3.1	Exploration of Higher Metal Loadings in CMS Membranes with Alternative Processing Procedures and Precursor Materials	129
8.3.2	Investigation of Physical Aging in Fe-Containing CMS Membranes	130
8.3.3	Translation of Fe-Containing CMS Dense Films to Hollow Fiber Membranes	131
8.4	References	132
APPENDIX A. GAS COMPRESSIBILITY FACTORS		133

LIST OF TABLES

Table 3.1.	Chemical structures and names of polymers-----	41
Table 3.2.	Chemical structures of metal salts-----	43
Table 3.3.	Casting solution formulation for metal-containing polymer dense film ---	44
Table 3.4.	Programmed pyrolysis heating protocols ($T_{\text{pyro}}=550\text{ }^{\circ}\text{C}$ or $675\text{ }^{\circ}\text{C}$) -----	48
Table 4.1.	XANES linear combination fitting results -----	71
Table 5.1.	Compositions of feed and permeate streams for CMS membranes derived from 6FDA-DAM:DABA (3:2) precursor with various Fe loadings -----	77
Table 6.1.	Permeation performance of C_2H_4 and C_2H_6 (50 psia) at $35\text{ }^{\circ}\text{C}$ for Fe-free and Fe-containing 6FDA-DAM:DABA (3:2) polymer precursors -----	87
Table 6.2.	Sorption performance of C_2H_4 and C_2H_6 (50 psia) at $35\text{ }^{\circ}\text{C}$ for Fe-free and Fe-containing 6FDA-DAM:DABA (3:2) polymer precursors -----	90
Table 6.3.	Diffusion performance of C_2H_4 and C_2H_6 (50 psia) at $35\text{ }^{\circ}\text{C}$ for Fe-free and Fe-containing 6FDA-DAM:DABA (3:2) polymer precursors -----	91
Table 7.1.	Permeation performance of C_2H_4 and C_2H_6 (50 psia) at $35\text{--}50\text{ }^{\circ}\text{C}$ for Fe-free and Fe-containing 6FDA-DAM:DABA (3:2) polymeric and CMS membranes-----	107
Table 7.2.	Permeation activation energy (E_p) and permeation pre-exponential factor (P_o) of C_2H_4 and C_2H_6 (50 psia) between $35\text{--}50\text{ }^{\circ}\text{C}$ for Fe-free and Fe-containing 6FDA-DAM:DABA (3:2) polymeric and CMS membranes --	107
Table 7.3.	Sorption performance of C_2H_4 and C_2H_6 (50 psia) at $35\text{--}50\text{ }^{\circ}\text{C}$ for Fe-free and Fe-containing 6FDA-DAM:DABA (3:2) polymeric and CMS membranes-----	112
Table 7.4.	Apparent heat of sorption (H_S) and sorption pre-exponential factor (S_o) of C_2H_4 and C_2H_6 (50 psia) between $35\text{--}50\text{ }^{\circ}\text{C}$ for Fe-free and Fe-containing 6FDA-DAM:DABA (3:2) polymeric and CMS membranes-----	112
Table 7.5.	Diffusion performance of C_2H_4 and C_2H_6 (50 psia) at $35\text{--}50\text{ }^{\circ}\text{C}$ for Fe-free and Fe-containing 6FDA-DAM:DABA (3:2) polymeric and CMS membranes-----	116

Table 7.6. Diffusion activation energy (E_D) and diffusion pre-exponential factor (D_o) of C_2H_4 and C_2H_6 (50 psia) at 35–50 °C for Fe-free and Fe-containing 6FDA-DAM:DABA (3:2) polymeric and CMS membranes ----- 116

Table A.1. Compressibility factor equations of gases, with pressure (p) in psia----- 134

LIST OF FIGURES

Figure 1.1. Historical and projected global production capacities for ethylene and propylene after 2010 -----	2
Figure 1.2. Schematic of a simplified steam cracking route for producing olefins ----	3
Figure 1.3. Schematic of flow paths of ethylene and propylene in a simplified olefin plant-----	4
Figure 1.4. (a) C ₂ H ₄ /C ₂ H ₆ and (b) C ₃ H ₆ /C ₃ H ₈ experimental upper bound plot for polymer dense membranes -----	6
Figure 1.5. Schematic of hybrid membrane-distillation systems for olefin recovery--	8
Figure 2.1. Schematic of turbostratic structure of CMS membranes with disordered sp ² hybridized carbon sheets -----	17
Figure 2.2. (a) idealized ‘slit-like’ pore structure of CMS membranes and (b) idealized bimodal pore size distribution in CMS membranes-----	18
Figure 2.3. Representative pyrolysis temperature protocol with three phases: ramp, soak, and cooling -----	21
Figure 2.4. Schematic of gas transport through a membrane by solution-diffusion model -----	26
Figure 2.5. Schematic depiction of a diffusion step in polymer membranes-----	30
Figure 2.6. Schematic depiction of a diffusion step in CMS membranes -----	31
Figure 3.1. Reaction scheme for 6FDA-DAM:DABA (3:2) synthesis -----	42
Figure 3.2. Schematic of solution-casting method for polymer dense film -----	45
Figure 3.3. Schematic of pyrolysis furnace setup for fabricating CMS materials-----	46
Figure 3.4. Custom made quartz plate for dense film pyrolysis -----	47
Figure 3.5. Temperature profiles of programmed pyrolysis protocols-----	48
Figure 3.6. Schematic of masking a dense film into a permeation cell -----	50
Figure 3.7. Schematic of a constant-volume permeation system -----	51

Figure 3.8. Schematic of a pressure decay sorption system -----	54
Figure 4.1. C ₂ H ₄ /C ₂ H ₆ selectivities based on permeability, sorption, and diffusion for CMS membranes derived from Matrimid [®] and 6FDA:BPDA-DAM (reproduced from reported data)-----	57
Figure 4.2. Ionic cross-linking of DABA-containing polyimide with Fe(II) acetylacetonate -----	60
Figure 4.3. Sorption isotherms of single-component ethylene and ethane at 35 °C for Fe-containing 6FDA-DAM:DABA (3:2) derived CMS membranes from (a) Slow 675 °C and (b) Slow 550 °C pyrolysis protocols -----	62
Figure 4.4. Effects of final pyrolysis temperature (T _{pyro}) on idealized pore structures of CMS membranes -----	63
Figure 4.5. Sorption isotherms of single-component ethylene and ethane at 35 °C for Fe-containing 6FDA-DAM:DABA (3:2) derived CMS membranes from (a) Fast 675 °C and (b) Fast 550 °C pyrolysis protocols-----	65
Figure 4.6. Sorption isotherms of single-component ethylene and ethane at 35 °C for Fe-free 6FDA-DAM:DABA (3:2) derived CMS membranes from Fast 550 °C pyrolysis protocol -----	66
Figure 4.7. Conceptual interaction between ethylene and active Fe complex in idealized pore structures of CMS membranes-----	67
Figure 4.8. Sorption isotherms of single-component propylene and propane at 35 °C for (a) Fe-containing and (b) Fe-free 6FDA-DAM:DABA (3:2) derived CMS membranes from Fast 550 °C pyrolysis protocol -----	68
Figure 4.9. Sorption isotherms of single-component ethylene and ethane at 35 °C for Fe-containing 6FDA-DAM derived CMS membranes from Fast 550 °C pyrolysis protocol-----	69
Figure 4.10. XANES spectra of Fe-containing CMS membranes derived from various pyrolysis protocols -----	71
Figure 5.1. Effects of Fe loading on (a) gas permeability and (b) selectivity at 35 °C for 6FDA-DAM:DABA (3:2) derived CMS membranes from Fast 550 °C pyrolysis protocol (50 psia quaternary mixture feed) -----	77
Figure 5.2. (a) Gas permeability and (b) selectivity at 35 °C over ~60 testing days for Fe-containing 6FDA-DAM:DABA (3:2) derived CMS membranes from Fast 550 °C pyrolysis protocol-----	80

Figure 5.3. Effects of metal species on (a) gas permeability and (b) selectivity at 35 °C for 6FDA-DAM:DABA (3:2) derived CMS membranes from Fast 550 °C pyrolysis protocol (50 psia quaternary mixture feed) -----	83
Figure 5.4. Sorption isotherms of single-component ethylene and ethane at 35 °C for Fe(III)-containing 6FDA-DAM:DABA (3:2) derived CMS membranes with Fast 550 °C pyrolysis protocol -----	84
Figure 6.1. Relationship between pure C ₂ H ₄ permeability and C ₂ H ₄ /C ₂ H ₆ permselectivity at 35 °C for various polymer precursors (results of non-DABA polyimides are reproduced from reported data)-----	88
Figure 6.2. Sorption isotherms of single-component ethylene and ethane at 35 °C for (a) Fe-free and (b) Fe-containing 6FDA-DAM:DABA (3:2) polymer precursors -----	90
Figure 6.3. C ₂ H ₄ /C ₂ H ₆ selectivity in (a) permeation (b) sorption and (c) diffusion at 35 °C for polymer precursors and CMS membranes derived from Fast 550 °C pyrolysis protocol (50 psia single-component gas)-----	94
Figure 6.4. Idealized ultramicropore size distribution in (a) Fe-free CMS membranes and (b) Fe-containing CMS membranes -----	95
Figure 6.5. Schematic of Fe complex in ultramicropores and micropores of idealized pore structure of Fe-containing CMS membranes based on observed sorption and permeation results -----	96
Figure 6.6. C ₂ H ₄ /C ₂ H ₆ mixed-gas permeation results at 35 °C for Fe-free 6FDA-DAM:DABA (3:2) derived CMS membranes from various pyrolysis protocols (50 psia quaternary mixture feed) -----	98
Figure 6.7. Effects of final pyrolysis temperature (T _{pyro}) on idealized pore structures of CMS membranes -----	99
Figure 6.8. C ₂ H ₄ /C ₂ H ₆ mixed-gas permeation results at 35 °C for Fe-free and Fe-containing 6FDA-DAM:DABA (3:2) derived CMS membranes with various pyrolysis protocols (results of PIM-polyimide CMS made at 800 °C are reproduced from reported data) -----	100
Figure 7.1. Temperature dependence of permeability for C ₂ H ₄ and C ₂ H ₆ (50 psia) for Fe-free and Fe-containing 6FDA-DAM:DABA (3:2) polymeric and CMS membranes (Equations are shown with $\ln(P) = \left(\frac{-E_P}{R}\right) \cdot \frac{1}{T} + \ln(P_o)$) -----	108

- Figure 7.2.** Temperature dependence of sorption coefficient for C₂H₄ and C₂H₆ (50 psia) for Fe-free and Fe-containing 6FDA-DAM:DABA (3:2) polymeric and CMS membranes (Equations are shown with $\ln(S) = \left(\frac{-H_S}{R}\right) \cdot \frac{1}{T} + \ln(S_o)$)----- 113
- Figure 7.3.** Temperature dependence of diffusion coefficient for C₂H₄ and C₂H₆ (50 psia) for Fe-free and Fe-containing 6FDA-DAM:DABA (3:2) polymeric and CMS membranes (Equations are shown with $\ln(D) = \left(\frac{-E_D}{R}\right) \cdot \frac{1}{T} + \ln(D_o)$)----- 117
- Figure 7.4.** Permeation, sorption, and diffusion selectivities of C₂H₄/C₂H₆ (50 psia) between 35–50 °C for Fe-free and Fe-containing 6FDA-DAM:DABA (3:2) polymeric and CMS membranes----- 118
- Figure 7.5.** Diffusion, energetic, and entropic selectivities of C₂H₄/C₂H₆ (50 psia) between 35–50 °C for Fe-free and Fe-containing 6FDA-DAM:DABA (3:2) polymeric and CMS membranes----- 120
- Figure 7.6.** Idealized bimodal pore size distribution in Fe-containing CMS materials (shaded area represents cross-over region of “large” ultramicropores and “small” micropores as possible range for Fe complex to present)----- 121

SUMMARY

In this work, carbon molecular sieve (CMS) dense film membranes derived from 6FDA-DAM:DABA (3:2) polyimide precursor were studied for separation of mixed olefins (C_2H_4 and C_3H_6) from paraffins (C_2H_6 and C_3H_8). Olefin-selective CMS membranes with high performance can be made by pyrolysis of metal-containing polymeric precursors. Pyrolyzed at $550^\circ C$ with a fast ramp rate, CMS membranes with integrated Fe^{2+} (2.2 wt% in the precursor) showed 19% higher C_2H_4/C_2H_6 and 11% higher C_3H_6/C_3H_8 sorption selectivity than that of the neat CMS membrane. Additional investigations with a quaternary mixture feed (C2 and C3 hydrocarbons) show that C_2H_4 permeability above 10 Barrers with C_2H_4/C_2H_6 permselectivity near 11 were achieved for the 3.2 wt% Fe loading case. Although Fe incorporation did not appear to promote C_3H_6/C_2H_6 permselectivity, Fe is useful to achieve impressive C2 pair olefin/paraffin separation. Deconvolution of the C_2H_4/C_2H_6 permselectivity for the more extensively studied 2.2 wt% loading case was also revealing. While both sorption and diffusion selectivity increased due to the Fe incorporation, a larger influence is seen on the diffusion selectivity versus the sorption selectivity. This added diffusion selectivity was dominated by a contribution from an entropic factor with Fe, which is the feature for CMS materials to surpass conventional polymer membranes.

CHAPTER 1. INTRODUCTION

1.1 Production of Olefins

Light olefins, such as ethylene (C_2H_4) and propylene (C_3H_6), are key building blocks for a wide range of petrochemicals and valuable polymers. Ethylene and its derivatives are used to produce various polymers, such as polyethylene (PE), polyethylene terephthalate (PET), and polyvinyl chloride (PVC)¹. On the other hand, propylene is the raw material for chemical derivatives such as polypropylene (PP), acrylonitrile (ACN), propylene oxide (PO), cumene, and acrylic acid². The global production capacity for ethylene and propylene in 2015 is 171 million metric tons per year (MTPA) and 111 MTPA, respectively. Based on the high demands for olefins, their global production capacities are considered to grow 34.7% (ethylene) and 18.7% (propylene) between 2015 and 2020³⁻⁵, as shown in **Figure 1.1**.

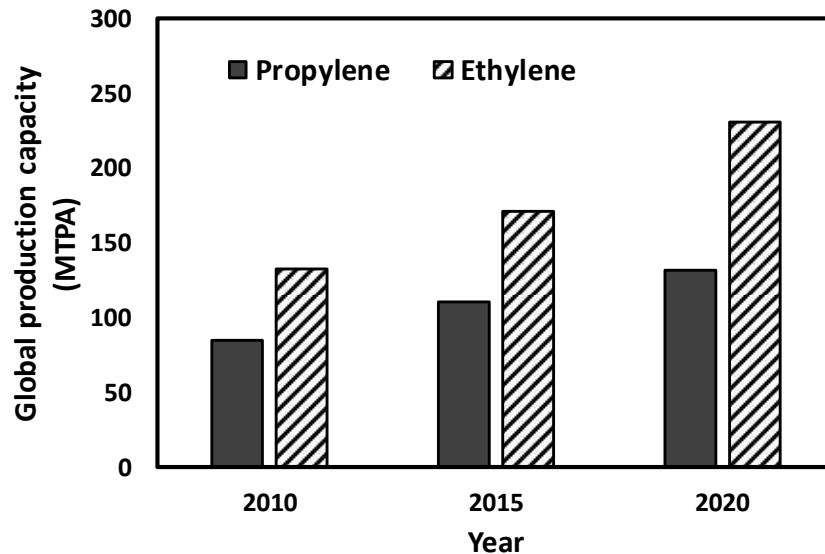


Figure 1.1. Historical and projected global production capacities for ethylene and propylene after 2010³⁻⁷

Currently, the majority of olefins are produced by steam cracking of hydrocarbon feedstocks derived from either naphtha or natural gas liquids. A simplified steam cracking route for producing ethylene and propylene is shown in **Figure 1.2**. A mixture of the feedstocks is heated at high temperature inside a furnace, and this cracking process break down the long chain hydrocarbons into smaller molecules, including methane, hydrogen, ethylene, propylene, butadiene, butylenes, benzene, toluene, and other co-products. To meet the specifications for various products, a series of separation processes is essential for recovering the desired products from by-products. Among the separation units, olefin/paraffin separation is normally the final step in the production of olefins.

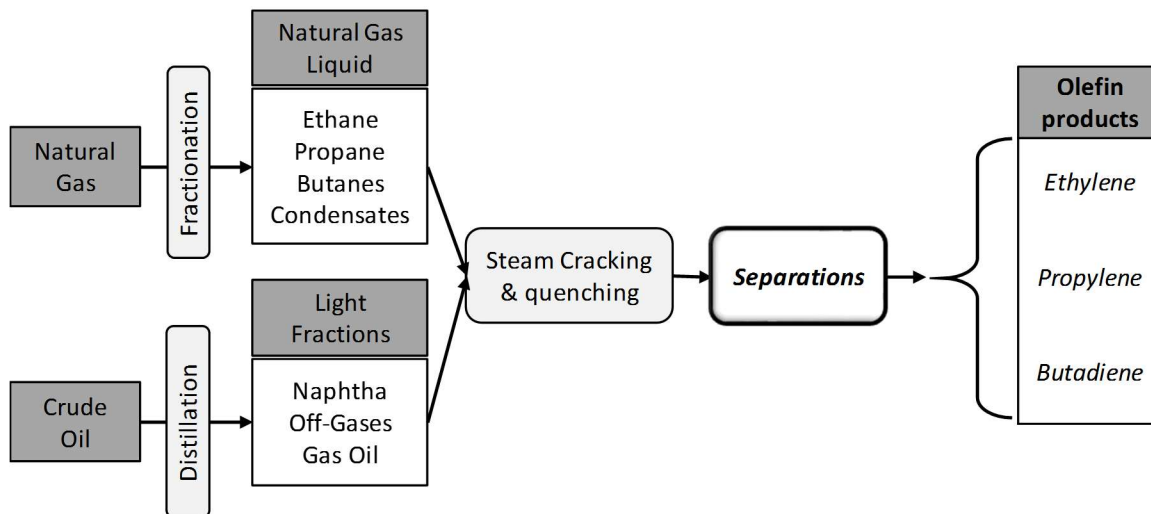


Figure 1.2. Schematic of a simplified steam cracking route for producing olefins

The separation of olefin from paraffin is typically carried out by distillation, and the flow scheme of a simplified olefin plant is shown in **Figure 1.3**. As highlighted in the figure, a deethanizer separate C2 hydrocarbons (ethylene and ethane) from C3 hydrocarbons (propylene and propane). At the top product stream of the deethanizer, there is a C2-splitter for separating ethylene from ethane, while at the bottom product stream, a C3-splitter is used to separate propylene from propane. Because of the similar boiling points of the olefin and its corresponding paraffin pairs, a large scale of distillation column with 120 to 180 trays and high reflux ratios are required to meet industrial scale production levels. In addition, since the critical temperature of ethylene is about 10 °C (~92 °C for propylene), moderately low temperatures and high pressures are typically used for optimum operating conditions, which can cost more for capital design. Hence, the distillation technology for olefin/paraffin separation has high capital cost and high energy

consumption. It is, therefore, appealing to develop an alternative technology to replace or modify such conventional method of olefin/paraffin separation.

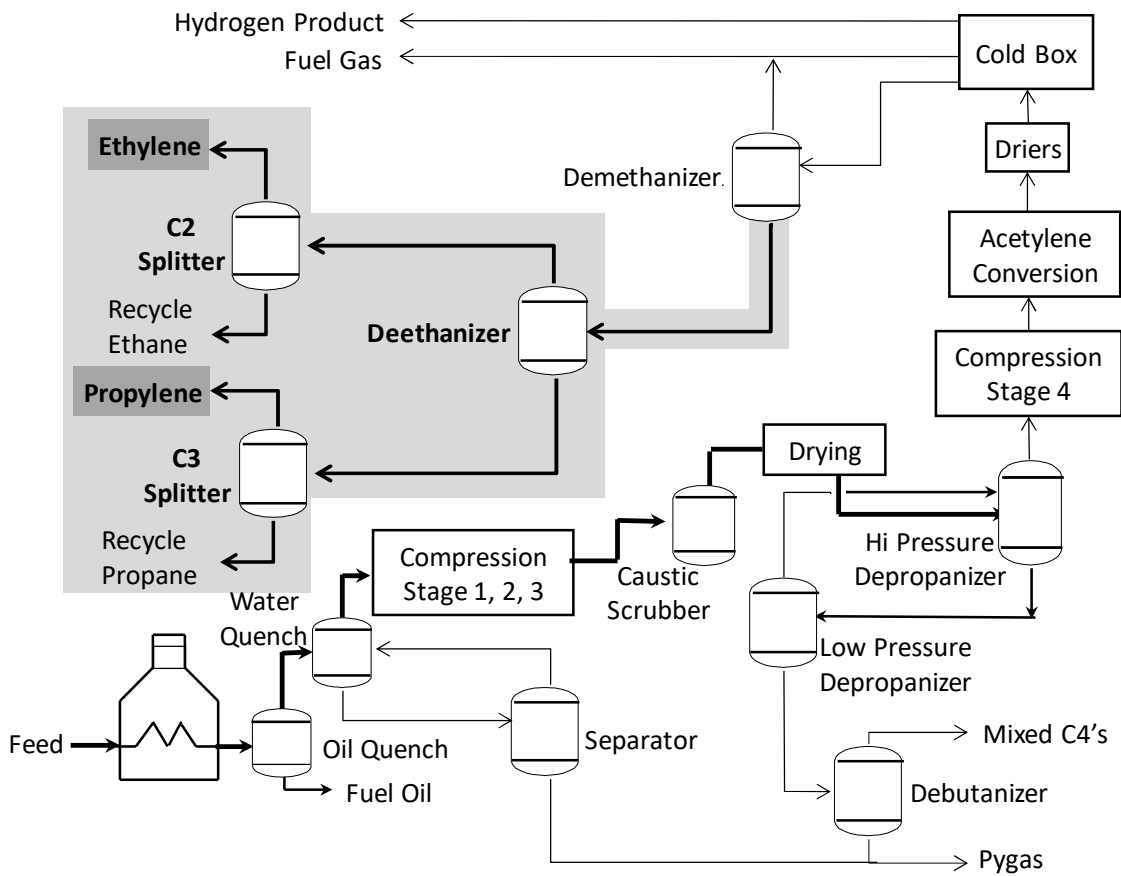


Figure 1.3. Schematic of flow paths of ethylene and propylene in a simplified olefin plant⁸

1.2 Membrane Technology for Gas Separations

Membrane separation is an emerging technology, and it has been suggested that membrane technology may provide attractive alternative to traditional thermally driven methods for gas separation because of lower capital and operating costs⁹. Currently, insufficient selectivity, a narrow range of useful operation conditions, and high manufacturing costs limit the application of membranes for distillation replacement¹⁰. Nevertheless, several studies have shown that a combination of membranes and conventional distillation units can provide better separation performance with attractive energy and economic savings^{11,12}.

Conventional polymeric membranes have been well studied for gas separations. Polymer membranes have good mechanical and chemical properties, and the membranes are currently implemented in industry for gas separation applications, except for olefin/paraffin separation¹³. In 1991, Robeson¹⁴ reported that the performances of solution-processable polymers are limited by a trade-off relationship (commonly referred to as the polymer upper bound) between productivity (permeability) and separation efficiency (selectivity) for common gas pairs. Recently, Rungta *et al.*¹⁵, and Burns and Koros¹⁶ reviewed published extensions to include upper bounds for C₂H₄/C₂H₆ and C₃H₆/C₃H₈ separation respectively (see **Figure 1.4 (a)** and **(b)**). The plots show that polymeric membranes are limited with respect to olefin/paraffin separation performance, and it is desirable to surpass these upper bounds.

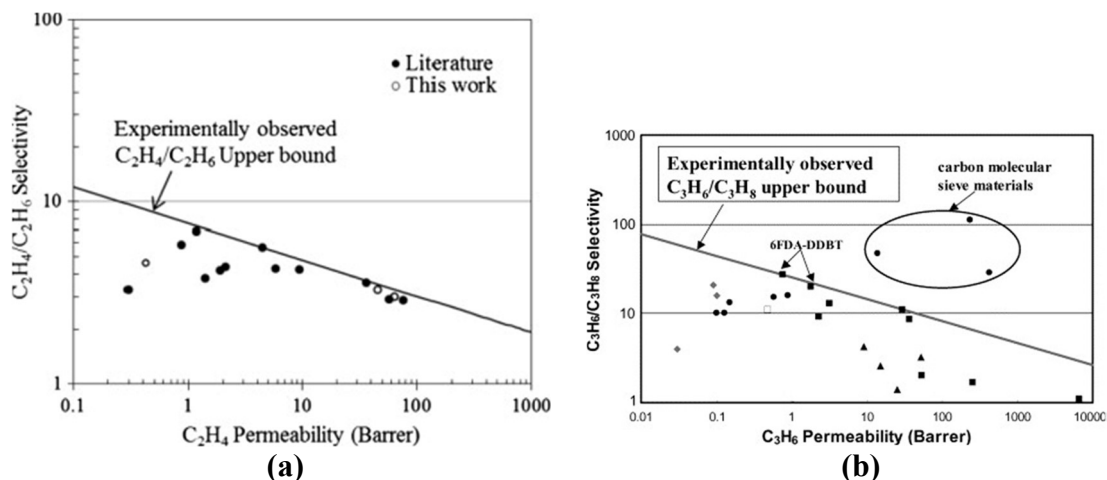


Figure 1.4. (a) C_2H_4/C_2H_6 and (b) C_3H_6/C_3H_8 experimental upper bound plot for polymer dense membranes^{15,16}

A new class of materials for gas separations, carbon molecular sieve (CMS) membranes, has been shown to achieve performances well above the upper bound relationship for many gas pair separations, such as O_2/N_2 , CO_2/CH_4 , C_2H_4/C_2H_6 , and C_3H_6/C_3H_8 ¹⁷⁻²². The rigid size-selective ultramicropores in CMS membranes allow them to surpass conventional polymer membranes. Although CMS membranes are still in their infancy, they are believed to be promising candidates for gas separations.

1.3 Olefin-Selective CMS Membranes

Standard binary olefin/paraffin membrane separations (C_2H_4/C_2H_6 and C_3H_6/C_3H_8) have been investigated by several researchers, and hybrid membrane-distillation systems were proposed for energy and economic savings. A possible implementation of C2 and C3 separation membrane units in process is shown in **Figure 1.5 (a)**²³. For each distillation column, a parallel membrane unit is installed for debottlenecking. Xu *et al.*²³ have demonstrated that the ‘slit-like’ structures of CMS membranes enable separation of bulk

olefins (C_2H_4 and C_3H_6) from paraffins (C_2H_6 and C_3H_8). A proof of concept study further demonstrated that a hybrid system with this olefin-selective membrane can not only debottleneck a C2 splitter but also potentially eliminate the need for a costly C3 splitter, as illustrated in **Figure 1.5 (b)**²³. In this work, this approach was further pursued and novel CMS membranes containing metal ions for such separation of bulk olefins from paraffins were studied.

As will be discussed, achieving this goal requires balancing more factors than is needed for a standard binary olefin/paraffin separation (C_2H_4/C_2H_6 or C_3H_6/C_3H_8) based solely on size. Specifically, the large olefin (C_3H_6) is only slightly more compact in molecular sieving size than the small paraffin (C_2H_6), which makes an olefin-selective membrane challenging. Nevertheless, by including metal ions into CMS membranes, the C_3H_6 has the potential for sorption selectivity enhancement to further promote its permselectivity relative to C_2H_6 . The advanced metal-containing CMS membranes made in this work have significantly improved bulk olefin/paraffin separation performance, which will be reported later.

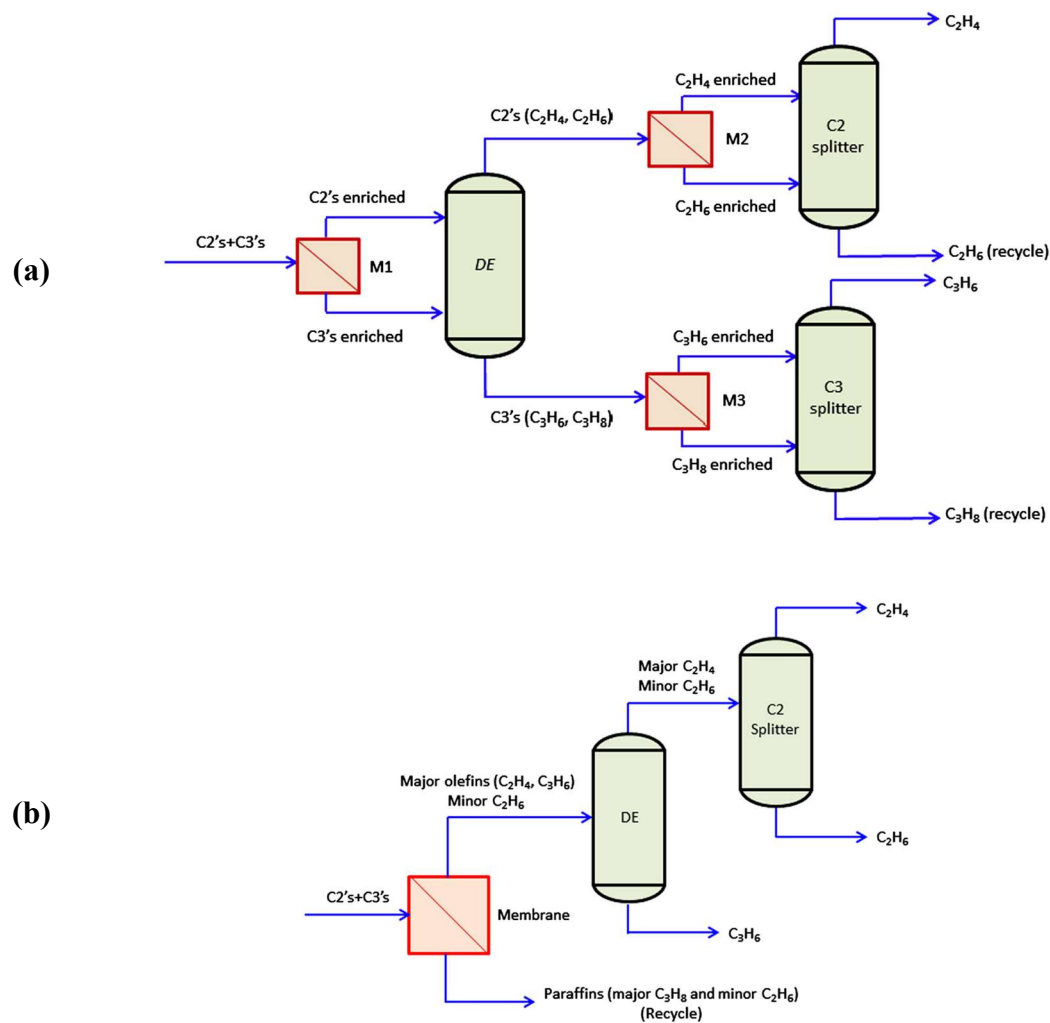


Figure 1.5. Schematic of hybrid membrane-distillation systems for olefin purification²³

1.4 Research Objectives

The principal goal of this work is to understand the factors controlling performance of carbon molecular sieve (CMS) dense membranes for the separation of mixed olefins (C_2H_4 and C_3H_6) from paraffins (C_2H_6 and C_3H_8). In collaboration with The Dow Chemical Company, we envision that the application of olefin-selective membranes can achieve

significant energy savings and even reduced process footprint. The specific objectives are illustrated below.

Objective 1: Evaluation of viability of selected metal in CMS membranes for increasing olefin/paraffin sorption selectivity (Chapter 4)

For either glassy polymer or carbon membranes, separation of olefin from the corresponding paraffin is dominated by diffusion selectivity, while sorption selectivity has little influence^{24,25}. Since this work focuses on developing olefin-selective CMS membranes for the separation of mixed olefins (C₂H₄ and C₃H₆) from paraffins (C₂H₆ and C₃H₈), improving olefin/paraffin sorption selectivity was felt to be a good strategy to separate the large olefin (C₃H₆) from the small paraffin (C₂H₆) more efficiently. A key difference between olefins and paraffins is the fact that olefins have carbon-carbon double bonds. Bloch *et al.*²⁶ indicated that coordinatively unsaturated Fe²⁺ cation sites in metal-organic frameworks (MOFs) can selectively interact with unsaturated bonds in olefin molecules and increase C₂ and C₃ olefin/paraffin pairs adsorption selectivity. Also, several researchers have successfully made metal-containing CMS membranes to improve the separation performances²⁷⁻³¹, but none of them have studied the effects of Fe²⁺ on olefin/paraffin separation.

If correctly tailored, CMS membranes with metal incorporation may be able to separate mixed olefins from paraffins more efficiently. This work proposed that integrating selected metal ions into polymer precursors can enable CMS membranes to significantly raise sorption selectivity for olefin/paraffin, and ultimately permselectivity. The first objective in this work is to evaluate the effects of metal ions on the sorption of olefins by

pressure decay sorption measurements. Starting materials and pyrolysis conditions for forming the metal-containing CMS membranes were investigated to explore the impacts on the separation properties.

Objective 2: Investigation of effects of iron loadings & studies on alternative metal species for olefin-selective CMS membranes (Chapter 5)

This work focuses on developing an advanced olefin-selective CMS membrane with high C_2H_4/C_2H_6 , C_3H_6/C_3H_8 , and most importantly, C_3H_6/C_2H_6 permselectivities. Preliminarily, 2.2 wt% of Fe(II) in a form of $Fe(acac)_2$ was studied for the metal incorporation into CMS membranes, and the improved C2 and C3 pairs sorption selectivities have been observed when a suitable pyrolysis protocol was applied. The added favorable properties with Fe can be further pursued by altering the loading of Fe as well as by substituting alternative metal species into membranes. The second objective is to investigate the effects of Fe loadings as well as metal species on the separation performance for olefin-selective CMS membranes. While permeation performance is more critical than sorption for the gas separation applications, this work explored permeation measurements with a mixture consisting C2 and C3 hydrocarbons to determine gas transport properties in the membranes.

Objective 3: Analysis of effects of iron on performance of iron-containing CMS membranes (Chapter 6)

As an improvement in C_2H_4/C_2H_6 separation has been observed with the Fe incorporation into the Fe-containing CMS membranes, it is important to better understand the effects of Fe on the fundamental gas transport properties. This objective is to decouple

the effects of Fe on C₂H₄/C₂H₆ separation performance into a sorption contribution and a diffusion contribution. Permeation, sorption, and diffusion properties of the single-component C₂H₄ & C₂H₆ for the Fe-containing CMS membranes will be reported. Besides, the trade-off in terms of separation efficiency and productivity of various CMS films (Fe-containing and Fe-free CMS materials derived from different pyrolysis protocols) will be analyzed. To confirm the competitive performance of the Fe-containing CMS membranes studied in this work, the performance of the membranes will be compared with other membrane materials reported previously.

Objective 4: Characterization of effects of testing temperature on olefin/paraffin separation performance of iron-containing CMS membranes (Chapter 7)

Gas transport properties, including permeation, sorption, and diffusion performance, are temperature-dependent. As the Fe-containing CMS membranes developed in this work have shown impressive olefin/paraffin separation performance, studying the temperature dependence of the membranes performance will be pursued in this objective to better understand the properties of this type of CMS membranes. By analyzing the temperature dependence results, the feature of added diffusion selectivity based on an entropic factor for the CMS membranes will be proven in this objective as well.

1.5 Dissertation Organization

Including this introductory chapter, this dissertation contains 8 chapters. Chapter 2 outlines the background knowledge and fundamental theories relevant to this work. Chapter 3 describes the materials, experimental procedures, and characterization

techniques used in this work. Chapter 4–7 are the main chapters, presenting the research results corresponding to the four objectives listed above. Finally, Chapter 8 summarizes the key findings and contributions for each objective in this work, and recommendations for the future studies are outlined in the chapter as well. Appendices are provided at the end of this dissertation as supplemental information.

1.6 References

1. Ethylene Uses and Market Data. *ICIS* (2007). Available at: <https://www.icis.com/resources/news/2007/11/05/9075777/ethylene-uses-and-market-data>.
2. Propylene Uses and Market Data. *ICIS* (2007). Available at: <https://www.icis.com/resources/news/2007/11/06/9076455/propylene-uses-and-market-data>.
3. *Q3 Global Ethylene Capacity and Capital Expenditure Outlook - Asia and North America impel Ethylene Industry Expansion*. (GlobalData).
4. *Q4 Global Propylene Capacity and Capital Expenditure Outlook - Asia and North America to Propel Propylene Industry Expansion*. (GlobalData).
5. *Q4 Global Ethylene Capacity and Capital Expenditure Outlook - The US and China to Spearhead Ethylene Industry Expansion*. (GlobalData).
6. Global demand and Production of Ethylene and Propylene in 2005-2010 is expected to recover. Available at: http://216.169.121.148/upload/literature/Global_demand_of_ethylene.asp.
7. True, W. R. Global ethylene capacity continues advance in 2011. *Oil Gas J.* **110**, 78–93 (2012).
8. Brayden, M. K. &Barbay, G. A. The Dow Chemical Company's Membrane Test Unit. in *2011 North American Membrane Society Annual Meeting* (2011).
9. Koros, W. J. Evolving beyond the thermal age of separation processes: membranes can lead the way. *AIChE J.* **50**, 2326–2334 (2004).
10. Angelini, P. *et al.* Materials for Separation Technologies: Energy and Emission Reduction Opportunities. *DOE, EERE Off. Washington, DC* 103 (2005).
11. Benali, M. &Aydin, B. Ethane/ethylene and propane/propylene separation in hybrid membrane distillation systems: Optimization and economic analysis. *Sep. Purif. Technol.* **73**, 377–390 (2010).
12. Pedram, S., Kaghazchi, T. &Ravanchi, M. T. Performance and Energy Consumption of Membrane-Distillation Hybrid Systems for Olefin-Paraffin Separation. *Chem. Eng. Technol.* **37**, 587–596 (2014).
13. Alqaheem, Y., Alomair, A., Vinoba, M. &Pérez, A. Polymeric Gas-Separation Membranes for Petroleum Refining. *Int. J. Polym. Sci.* **2017**, (2017).
14. Robeson, L. M. Correlation of separation factor versus permeability for polymeric

- membranes. *J. Memb. Sci.* **62**, 165–185 (1991).
15. Rungta, M., Xu, L. & Koros, W. J. Carbon molecular sieve dense film membranes derived from Matrimid® for ethylene/ethane separation. *Carbon N. Y.* **50**, 1488–1502 (2012).
 16. Burns, R. L. & Koros, W. J. Defining the challenges for C₃H₆/C₃H₈ separation using polymeric membranes. *J. Memb. Sci.* **211**, 299–309 (2003).
 17. Hayashi, J. *et al.* Separation of ethane/ethylene and propane/propylene systems with a carbonized BPDA–pp ‘ODA polyimide membrane. *Ind. Eng. Chem. Res.* **35**, 4176–4181 (1996).
 18. Okamoto, K. *et al.* Olefin/paraffin separation through carbonized membranes derived from an asymmetric polyimide hollow fiber membrane. *Ind. Eng. Chem. Res.* **38**, 4424–4432 (1999).
 19. Kiyono, M., Williams, P. J. & Koros, W. J. Effect of pyrolysis atmosphere on separation performance of carbon molecular sieve membranes. *J. Memb. Sci.* **359**, 2–10 (2010).
 20. Rungta, M., Zhang, C., Koros, W. J. & Xu, L. Membrane-based ethylene/ethane separation: The upper bound and beyond. *AIChE J.* **59**, 3475–3489 (2013).
 21. Steel, K. M. & Koros, W. J. An investigation of the effects of pyrolysis parameters on gas separation properties of carbon materials. *Carbon N. Y.* **43**, 1843–1856 (2005).
 22. Jones, C. W. & Koros, W. J. Carbon molecular sieve gas separation membranes-I. Preparation and characterization based on polyimide precursors. *Carbon N. Y.* **32**, 1419–1425 (1994).
 23. Xu, L. *et al.* Olefins-selective asymmetric carbon molecular sieve hollow fiber membranes for hybrid membrane-distillation processes for olefin/paraffin separations. *J. Memb. Sci.* **423**, 314–323 (2012).
 24. Rungta, M. Carbon molecular sieve dense film membranes for ethylene/ethane separations. (Georgia Institute of Technology, 2012).
 25. Tanaka, K., Taguchi, A., Hao, J., Kita, H. & Okamoto, K. Permeation and separation properties of polyimide membranes to olefins and paraffins. *J. Memb. Sci.* **121**, 197–207 (1996).
 26. Bloch, E. D. *et al.* Hydrocarbon separations in a metal-organic framework with open iron (II) coordination sites. *Science (80-.)*. **335**, 1606–1610 (2012).
 27. Yoshimune, M., Fujiwara, I., Suda, H. & Haraya, K. Gas transport properties of carbon molecular sieve membranes derived from metal containing sulfonated poly

- (phenylene oxide). *Desalination* **193**, 66–72 (2006).
28. Yoda, S. *et al.* Preparation of a platinum and palladium/polyimide nanocomposite film as a precursor of metal-doped carbon molecular sieve membrane via supercritical impregnation. *Chem. Mater.* **16**, 2363–2368 (2004).
 29. Barsema, J. N., van derVegt, N. F. A., Koops, G. H. &Wessling, M. Ag-Functionalized Carbon Molecular-Sieve Membranes Based on Polyelectrolyte/Polyimide Blend Precursors. *Adv. Funct. Mater.* **15**, 69–75 (2005).
 30. Kim, Y. K., Park, H. B. &Lee, Y. M. Carbon molecular sieve membranes derived from metal-substituted sulfonated polyimide and their gas separation properties. *J. Memb. Sci.* **226**, 145–158 (2003).
 31. Barsema, J. N., Balster, J., Jordan, V., Van derVegt, N. F. A. &Wessling, M. Functionalized carbon molecular sieve membranes containing Ag-nanoclusters. *J. Memb. Sci.* **219**, 47–57 (2003).

CHAPTER 2. BACKGROUND AND THEORY

2.1 Overview

This chapter outlines the background knowledge and fundamental theories relevant to this work. Section 2.2 introduces the structure of carbon molecular sieve (CMS) material and its attractive pore distribution for gas separation applications. Section 2.3 reviews important fabrication factors controlling the performance of optimized CMS membranes. Section 2.4 describes the transport theories of gas penetrating through both polymer and CMS membranes, and major advantages of CMS membranes over polymer membranes are also discussed in this section.

2.2 Structure of Carbon Molecular Sieve Membranes

CMS membranes can be formed by thermal decomposition of polymer precursors through heating in an inert or vacuum environment. The residual material is primarily carbon after removal of volatile decomposition compounds during pyrolysis. Most CMS membranes used for gas separation have a disordered sp^2 hybridized carbon sheet morphology, which is amorphous and more or less isotropic; referred to as a so-called turbostratic structure as illustrated in **Figure 2.1**^{1,2}.

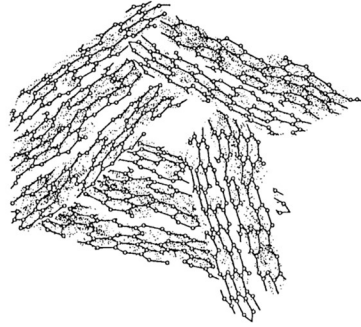


Figure 2.1. Schematic of turbostratic structure of CMS membranes with disordered sp^2 hybridized carbon sheets^{1,2}

The resulting CMS membranes consist of ultramicropores ($<7 \text{ \AA}$) within the carbon sheets while micropores ($7\sim 20 \text{ \AA}$) can be formed from packing imperfections between the carbon sheets. Unlike crystalline molecular sieve materials (e.g., zeolites), the pore distribution of CMS materials is not sharply defined. Still, the pore structure of a CMS membrane can be idealized with a ‘slit-like’ structure, as shown in **Figure 2.2 (a)**. The micropores are connected by the ultramicropores, forming a selective passageway for gas to be transported. An idealized pore size distribution in a CMS membrane is envisioned as being bimodal, as illustrated in **Figure 2.2 (b)**³. For gas separation applications, the ultramicropores offer selective molecular sieving, while micropores allow for sorption sites and high diffusion coefficients. The combination of ultramicropores and micropores make CMS membranes an attractive material for gas separations.

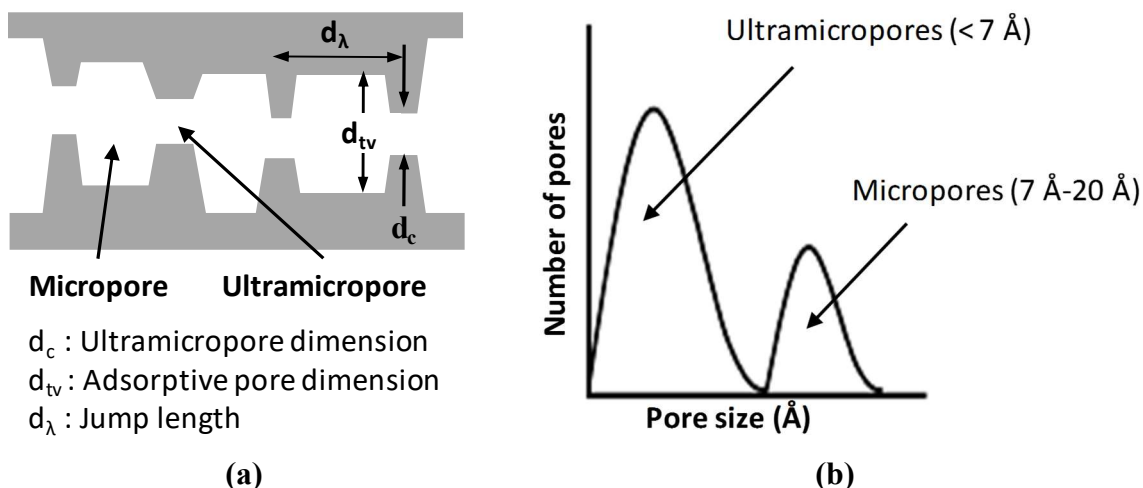


Figure 2.2. (a) idealized ‘slit-like’ pore structure of CMS membranes and (b) idealized bimodal pore size distribution in CMS membranes³

2.3 Formation of Carbon Molecular Sieve Membranes

As mentioned before, CMS membranes are formed by thermal decomposition of polymer precursors, and the separation performance is strongly dependent on the pore size distribution. Some factors have been identified critical as in carbon membrane fabrication, such as (a) polymer precursor, (b) pre-treatment of polymer precursor, (c) pyrolysis temperature protocol, (d) pyrolysis atmosphere, and (e) post-treatment of CMS membranes. The effects of each factor are discussed below.

2.3.1 Polymer Precursor

The choice of polymer precursor is influential in the properties of the resulting CMS membrane. This precursor variable can even span different polymer families. A variety of thermosetting polymers have been studied as precursors for CMS membranes, such as polyacrylonitrile (PAN)⁴, phenolic resin⁵, poly(furfuryl alcohol) (PFA)^{6,7},

poly(vinylidene)-based polymers⁸, cellulose derivatives⁹, and polyimides¹⁰⁻¹⁶. Among those precursors, polyimides have drawn much attention due to their ease of processability, attractive CMS transport, and good mechanical properties^{17,18}.

The intrinsic properties of polymer precursors that have significant effects on the resulting CMS membranes include fractional free volume (FFV), chemical structure, glass transition temperature (T_g), and decomposition temperature (T_d). The relationship between above properties of polyimides and the performance of the resulting CMS membranes have attracted research interest.

The relationship between chemical structure of polyimides and gas permeation properties of their CMS membranes has been studied by many researchers. Park *et al.*¹¹ suggested that the increase of FFV in the polyimides by methyl substituents led to more permeable CMS membranes. Kiyono¹⁹ indicated that 6FDA-based polyimide with bulky CF_3 group had higher FFV and that the evolution of this CF_3 group during pyrolysis provided higher microporosity in the resulting CMS membranes.

The difference between T_g and T_d of a polymer precursor have impacts on the morphology of resulting asymmetric membrane during pyrolysis. Xu *et al.*^{20,21} showed that 6FDA-based polyimide with a small temperature interval between T_g and T_d could retain the porous supporting layer in hollow fiber during pyrolysis, resulting in higher permeance.

As discussed later, 6FDA-based polyimides are suitable precursors for CMS membranes, and for the purpose of this work, 6FDA-DAM:DABA (3:2) was chosen as the starting material derived to CMS membranes for improved olefin/paraffin separations.

2.3.2 Pre-Treatment of Polymer Precursor

Pre-treatments have been used to ensure the stability of porous polymer precursors and the preservation of their structure during pyrolysis. Sometimes, multiple pre-treatment methods are used to achieve desired properties of the resulting CMS membranes.

Oxidation pre-treatment of polymer precursors has been commonly used to prevent asymmetric membranes from collapsing and to stabilize the structure during pyrolysis. Kusuki *et al.*²² indicated that pre-oxidizing asymmetric polyimide hollow fiber membranes under air at 400 °C could maintain the asymmetric structure and result in CMS membranes with high separation performance. Besides oxidation, chemical treatments are also used to provide an enhanced porosity of the resulting CMS membranes. Bhuwania *et al.*²³ recently developed a novel method to restrict the morphology collapse in asymmetric CMS hollow fiber membranes by a sol-gel cross-linking reaction between organic-alkoxy silane and moisture on polyimides. This treatment contributed to a 5–6 fold reduction in apparent membrane separation layer thickness compared to the CMS membranes derived from untreated precursors, leading to the retention of the asymmetric morphology for the resulting CMS membranes.

In the current study, pre-treatment methods of the *dense* film polymer precursors were not explored since porosity collapse is not a problem. The goal of this work is to investigate other approaches, such as fabrication of polymer precursors and pyrolysis process, to enhance the separation performance of the resulting CMS membranes.

2.3.3 Pyrolysis Temperature Protocol

Polymer precursors can turn into carbon materials when heated under a controlled temperature protocol during pyrolysis. A typical pyrolysis temperature protocol is represented by **Figure 2.3** showing three phases: ramp, soak and cooling. A pyrolysis protocol consists of several parameters: pyrolysis temperature (the highest temperature during pyrolysis process), ramp rate (the heating rate reaching the highest temperature), and thermal soak time (the time held at highest temperature). Each of the parameters can have impacts on the performance of the resulting CMS membranes, and their effects are discussed in below subsections.

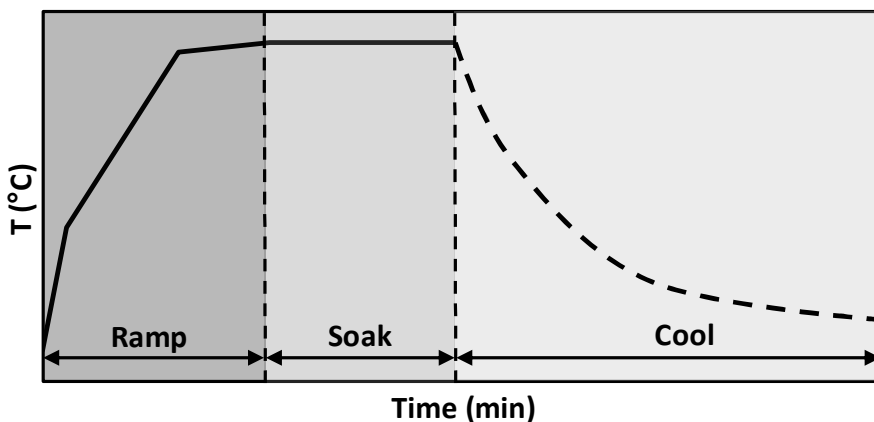


Figure 2.3. Representative pyrolysis temperature protocol with three phases: ramp, soak, and cooling

2.3.3.1 Pyrolysis Temperature

Final pyrolysis temperature has a remarkable influence on the properties of the resulting CMS membranes, and it usually lies between decomposition temperature and graphitization temperature of the polymer precursor²⁴, typically in the range of ~500–1000 °C in the current literature. Generally, higher pyrolysis temperature allows for tighter pore structures in the resulting CMS membranes, leading to higher selectivity but less permeation. This trend has been confirmed by several studies on various polyimides for gas separation applications of O₂/N₂, CO₂/CH₄, CO₂/N₂, C₂H₄/C₂H₆, and C₃H₆/C₃H₈^{15,25–28}.

Steel and Koros¹⁵ studied the effects of pyrolysis temperature on gas separation by pyrolyzing two different polyimides (Matrimid[®] and 6FDA:BPDA-DAM (1:1)) at a final temperature in a range of 500 °C and 800 °C. For small gas pairs (O₂/N₂ and CO₂/CH₄), the results showed that as pyrolysis temperature increased from 550 °C to 800 °C, the permeability of the fast gas decreased while the permselectivity increased, and this trend was found with CMS membranes derived from both polymer precursors. For larger penetrants, such as C₃H₆ and C₃H₈, CMS membranes derived from Matrimid[®] with 500 °C pyrolysis temperature had optimum performance in both permeabilities of fast gas and permselectivity, while the optimum performance of CMS membranes derived from 6FDA:BPDA-DAM (1:1) was found to be at 550 °C pyrolysis temperature.

Overall, the pyrolysis temperature has significant impacts on the performance of the resulting CMS membranes. The optimum pyrolysis temperature depends on the selection of polymer precursors and the aspects of applications.

2.3.3.2 Ramp Rate

Ramp rate, the heating rate reaching the highest temperature, used for pyrolysis can also tune the performance of CMS membranes. Suda and Haraya²⁹ investigated the ramp rates between 1.33–13.3 °C/min for CMS membranes derived at 1000 °C from Kapton[®] polyimide. The results showed that the increasing ramp rate tended to increase permeability and reduce selectivity. It is believed that at a slower ramp rate, the combination of a slower evolution rate of volatile compounds and a longer overall pyrolysis time can allow for pore sintering. This then results in smaller pore size of CMS membranes and lower permeability.

2.3.3.3 Thermal Soak Time

After reaching the pyrolysis temperature, the carbon materials can be soaked at the final temperature to finely tune the microstructure in CMS membranes for desired transport properties. Some studies have shown that increasing soak time gives rise to higher selectivity with lower permeability, and it is because that increasing soak time leads to microstructural rearrangements and pore sintering^{15,30}.

2.3.4 *Pyrolysis Atmosphere*

Pyrolysis environment in which the pyrolysis is conducted can also have significant effects on the resulting CMS membranes structure and performance. Pyrolysis is usually performed with inert gas purge or under vacuum to prevent undesired burn off and chemical damage of the precursors. Previous studies have shown that vacuum atmosphere yielded more selectivity but less permeable CMS membranes than that with inert gas purge^{27,31}.

Geiszler and Koros³¹ studied the type of inert purge gas for pyrolysis of 6FDA:BPDA-DAM (1:1) at 550 °C for O₂/N₂ and H₂/N₂ separations. They found that little difference was seen among the CMS membranes pyrolyzed in the three purge gases: argon, helium, and carbon dioxide. On the other hand, Kiyono *et al.*^{19,32,33} have found that ppm level of oxygen in argon as purge gas could finely tune the CMS membrane separation performance. The addition of the trace oxygen resulted in an increase in selectivity and a moderate decrease in permeability. It is believed that the oxygen in the purge gas can selectively chemisorb onto the edge of ultramicropores in CMS materials during pyrolysis, resulting in a finely tuned molecular sieving window.

When an inert gas purge is used, the inert gas flow rate is also a considerable parameter for CMS membrane formation. An increase in gas flow rate enhances the transfer of decomposition byproducts away from CMS membranes and prevents deposition of further decomposed byproducts on the surface of membranes³¹. Researchers have studied inert flow rate with 50 and 200 cc(STP)/min during pyrolysis and found the effects of flow rate were less significant on the performance of CMS dense films³⁴.

2.3.5 *Post-Treatment of CMS Membranes*

Some post-treatments have been applied to improve separation performance by finely adjusting pore dimensions and distributions in CMS membranes. Post-oxidation is a commonly used method which can increase pore size without broadening the pore size distribution³⁵. In addition, selectivity can be increased with chemical vapor deposition (CVD) by introducing organic species into pore system of CMS membranes³⁶. Coating techniques, on the other hand, can repair defects and minor cracks in CMS membranes

after pyrolysis³⁷. Besides, post-pyrolysis is a treatment that can be used to further decrease membrane pore size³⁸.

While post-treatment methods may be useful in tuning the CMS pore structures, additional complicated techniques and extra process steps are involved in CMS fabrication, resulting in increasing complexity and cost. Hence, post-treatment is not investigated in the current work.

2.4 Gas Transport in Membranes

Two different types of gas separation membrane have been studied in this work: polymer membrane and CMS membrane. The mechanism for gas separations via these two membranes are discussed below.

2.4.1 Permeation

Gas transport through either a non-porous polymer membrane or a CMS membrane is described by the sorption-diffusion model^{39,40}. The permeation is driven by a chemical potential difference across the membrane. Gas molecules first sorb on the membrane on the upstream side, then diffuse through the membrane via a chemical potential gradient, and finally desorb on the downstream side. This membrane separation process mechanism is shown in **Figure 2.4**.

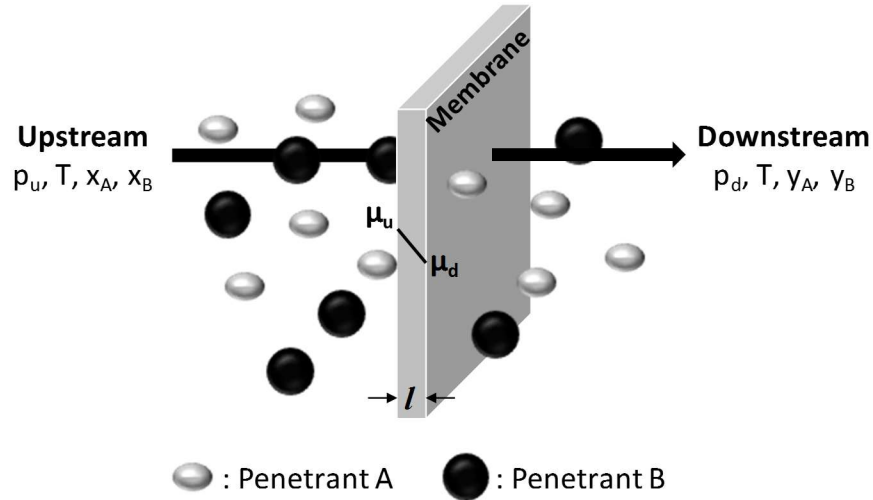


Figure 2.4. Schematic of gas transport through a membrane by solution-diffusion model

Permeability (productivity) and selectivity (separation efficiency) are two intrinsic properties used to evaluate the membrane material performance. Permeability is defined as a partial pressure and thickness normalized flux, given as

$$P_A = \frac{N_A \cdot \ell}{\Delta p_A} \quad (2.1)$$

In **Equation 2.1**, N_A is the flux of penetrant A through the membrane of thickness ℓ , and the partial pressure of A (Δp_A) is the driving force across the membrane. When significant non-ideality in the gas phase exists, the partial pressure is simply replaced by the component fugacities. Typically, Barrer is used as the unit of permeability, where

$$1 \text{ Barrer} = 10^{-10} \frac{\text{cm}^3(\text{STP}) \cdot \text{cm}}{\text{cm}^2 \cdot \text{s} \cdot \text{cmHg}} \quad (2.2)$$

For sorption-diffusion permeation, permeability can also be expressed as a product of an average kinetic diffusion coefficient (\bar{D}_A), and a thermodynamic sorption coefficient (\bar{S}_A), as shown below.

$$P_A = \bar{D}_A \cdot \bar{S}_A \quad (2.3)$$

The ideal permselectivity of a membrane with negligible downstream pressure is equal to the ratio of single-component gas permeabilities, which is also the product of diffusion selectivity ($\frac{\bar{D}_A}{\bar{D}_B}$) and sorption selectivity ($\frac{\bar{S}_A}{\bar{S}_B}$). Separation factor or selectivity (when stage cut is low and the downstream pressure is negligible compared to the upstream pressure) for multicomponent gas mixtures is defined as a ratio of permeate-side (y) and feed-side (x) mole fractions of components A and B . Hence,

$$\alpha_{A/B} = \frac{P_A}{P_B} = \left(\frac{\bar{D}_A}{\bar{D}_B} \right) \cdot \left(\frac{\bar{S}_A}{\bar{S}_B} \right) = \alpha_D \cdot \alpha_S \quad (2.4)$$

$$\alpha_{A/B} = \frac{(y_A/y_B)_{\text{permeate}}}{(x_A/x_B)_{\text{feed}}} \quad (2.5)$$

2.4.2 Sorption

For gas membrane materials with sorption-diffusion model, a penetrant must first sorb on the membrane on the high-pressure side and then diffuse through the membrane. The average sorption coefficient (\bar{S}_A) in **Equation 2.6** is defined as pressure normalized equilibrium concentration of gas penetrant (C_A) sorbed by a material at a given partial pressure (p_A), and depends on the condensability of the gas penetrant as well as the interaction with the sorption material.

$$\bar{S}_A = \frac{C_A}{p_A} \quad (2.6)$$

For glassy polymer materials, dual sorption mode model is often used to describe gas penetrants sorbed on the membranes⁴¹⁻⁴³. This dual sorption mechanism modeled by **Equation 2.7** is defined in terms of Henry's law of solubility (dissolution in dense polymer matrix) and Langmuir sorption (hole filling in microvoids), and the sorption coefficient can be written as in **Equation 2.8**.

$$C_A = C_{DA} + C_{HA} = k_{DA} \cdot p_A + \frac{C'_{HA} \cdot b_A \cdot p_A}{1 + b_A \cdot p_A} \quad (2.7)$$

$$\bar{S}_A = \frac{C_A}{p_A} = k_{DA} + \frac{C'_{HA} \cdot b_A}{1 + b_A \cdot p_A} \quad (2.8)$$

where,

C_{DA} : gas concentration by dissolution (Henry's law)

C_{HA} : gas concentration by hole filling (Langmuir sorption)

k_{DA} : Henry's law of dissolution constant

C'_{HA} : Langmuir saturation constant

b_A : Langmuir affinity constant

For CMS membranes, there is negligible dilation of the rigid CMS structure. Hence, Langmuir sorption is considered to be the only mechanism while the majority of the gas penetrants sorbed into micropores in the CMS membranes. The sorption coefficient is, therefore, given by:

$$\bar{S}_A = \frac{C_A}{p_A} = \frac{C'_{HA} \cdot b_A}{1 + b_A \cdot p_A} \quad (2.9)$$

2.4.3 Diffusion

As the gas penetrant sorb on the membrane on the high-pressure side, it then can diffuse through the membrane by making random jumps from site to site. This diffusion ability is described by a diffusion coefficient as a function of frequency of jumps (f_A) and average jump length (λ_A)⁴⁴:

$$D_A = \frac{f_A \cdot \lambda_A^2}{6} \quad (2.10)$$

Gas diffusion in glassy polymer materials is envisioned to happen in transient gaps that are continuously created and redistributed by thermally stimulated polymer chain segmental motions^{44,45}. When there is a sufficient-sized transient gap occurs adjacent to a

gas penetrant sorbed within the polymer matrix, the penetrant can execute a diffusion jump, as shown in **Figure 2.5**. The gas molecules sitting in the sorption site are in the normal state while those going through the transient gap are considered in the activated state. The size and the frequency of the jumps depend on both the properties of the gas penetrants (size and condensability) and the properties of the polymer (range of motions).

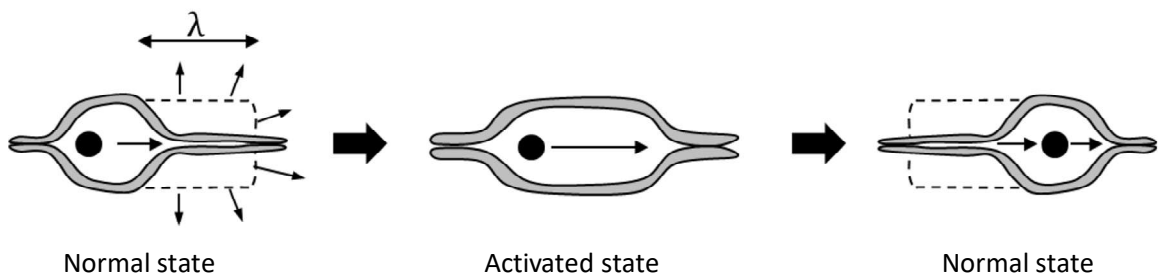


Figure 2.5. Schematic depiction of a diffusion step in polymer membranes⁴⁴⁻⁴⁶

The mechanism for gas transport in CMS membranes is different from that in polymers since the carbonized materials have rigid pore structures. The diffusion process is envisioned to occur when a gas penetrant makes a diffusive jump between adjacent sorption sites in micropores by jumping through a narrow ultramicropore, as shown in **Figure 2.6^{3,47}**. This diffusion requires enough activation energy for the gas penetrant to jump through the ultramicropore. Gas molecules with similar sizes can be separated since the size-dependent activation energy may change greatly with a small difference in molecule size. The ‘slit-like’ structure of CMS materials can restrict the degrees of motional freedom for penetrants, which makes it size-selective sieving. Therefore, the rigid

ultramicropores provide CMS materials with an advantage over polymeric materials with less defined transient gaps. This key difference provides added entropic selectivity, which is absent in polymer membranes⁴⁸. The concept of entropic selectivity in CMS membranes is described in detail in [Section 2.4.5](#)

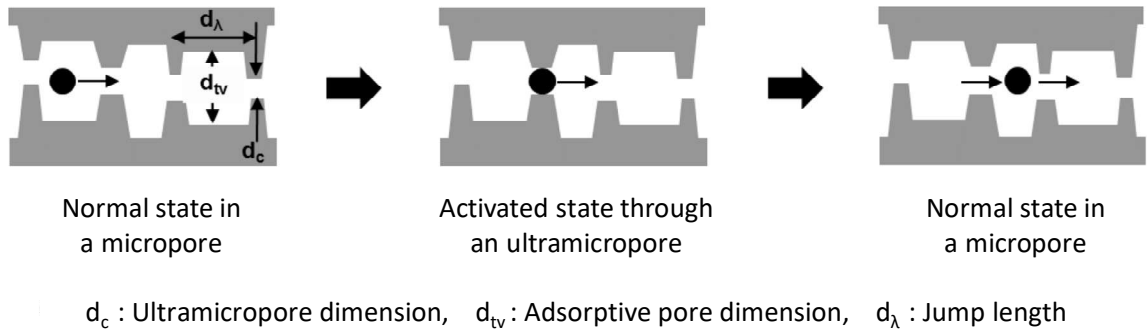


Figure 2.6. Schematic depiction of a diffusion step in CMS membranes⁴⁶

2.4.4 Temperature Dependence of Gas Transport

As described above, size-dependent diffusion of a gas penetrant through either polymer or CMS membranes occurs by an activated process. Hence, an Arrhenius relationship, as shown in **Equation 2.11**, is used to describe the increasing diffusion coefficient with temperature. On the other hand, the thermodynamic sorption coefficient decreases with temperature following a van't-Hoff relationship, as in **Equation 2.12**.

$$D = D_o \cdot \exp\left(\frac{-E_D}{RT}\right) \quad (2.11)$$

$$S = S_o \cdot \exp\left(\frac{-H_S}{RT}\right) \quad (2.12)$$

where,

D_o : pre-exponential factor for diffusion

S_o : pre-exponential factor for sorption

E_D : apparent activation energy for diffusion

H_S : apparent heat of sorption

R : universal gas constant

T : absolute temperature

The temperature dependence of permeation then can be derived by substituting **Equation 2.3** with above correlations, and the resulting **Equation 2.13** follows the Arrhenius relationship. The pre-exponential factor for permeation (P_o) and the apparent activation energy for permeation (E_P) can also be obtained, as shown below.

$$P_A = \bar{D}_A \cdot \bar{S}_A = \left[D_o \exp\left(\frac{-E_D}{RT}\right) \right] \cdot \left[S_o \exp\left(\frac{-H_S}{RT}\right) \right] = P_o \exp\left(\frac{-E_P}{RT}\right) \quad (2.13)$$

$$P_o = D_o \cdot S_o \quad (2.14)$$

$$E_P = E_D + H_S \quad (2.15)$$

As temperature increases, the increase in diffusivity generally outweighs the decrease in sorption coefficient, resulting in an increase in permeability with temperature.

2.4.5 Energetic and Entropic Factors in Diffusion Selectivity

As described in **Equation 2.3**, the overall permeation selectivity is a product of diffusion selectivity and sorption selectivity. The sorption selectivity depends on the condensability of the gas penetrants and the interactions with the sorption material, which reflects the thermodynamic aspects of a separation. On the other hand, the diffusion selectivity depends on the size and shape of the gas penetrants, which reflects the kinetic aspects of a separation. This diffusion selectivity can be further decoupled into an energetic factor and an entropic factor when a transition state theory is applied. The importance of entropic factor in diffusion selectivity for CMS membranes and the derivation of the equations are discussed below.

The pre-exponential factor for diffusion (D_o) can be presented from the Eyring theory of rate processes⁴⁹:

$$D_o = e \cdot \lambda^2 \frac{k \cdot T}{h} \cdot \exp\left(\frac{S_D}{R}\right) \quad (2.16)$$

where k is Boltzmann's constant, h is Planck's constant, and S_D is the activation entropy for diffusion. For a gas pair A and B with similar kinetic diameters (e.g., C_2H_4/C_2H_6), the average diffusive jump lengths (λ) are considered equal for both gas penetrants⁴⁸. The diffusion selectivity then can be derived as:

$$\frac{\bar{D}_A}{\bar{D}_B} = \frac{D_{oA}}{D_{oB}} \cdot \exp\left(\frac{-\Delta E_{D,A-B}}{RT}\right) \quad (2.17)$$

$$= \underbrace{\exp\left(\frac{\Delta S_{D,A-B}}{R}\right)}_{\text{Entropic selectivity}} \cdot \underbrace{\exp\left(\frac{-\Delta E_{D,A-B}}{RT}\right)}_{\text{Energetic selectivity}}$$

where $\Delta S_{D,A-B}$ is the difference in the diffusion activation entropy for penetrants A and B , and $\Delta E_{D,A-B}$ is the difference in the activation energy of diffusion for penetrants A and B .

An equivalent transition state theory description can be presented in terms of the diffusion coefficient as in **Equation 2.18**^{48,49}, and the diffusion selectivity then can be derived as in **Figure 2.19**.

$$D = \lambda^2 \frac{k \cdot T}{h} \cdot \frac{F^\ddagger}{F} \cdot \exp\left(\frac{-E_D}{RT}\right) \quad (2.18)$$

$$\frac{\bar{D}_A}{\bar{D}_B} = \frac{(F^\ddagger/F)_A}{(F^\ddagger/F)_B} \cdot \exp\left(\frac{-\Delta E_{D,A-B}}{RT}\right) \quad (2.19)$$

where F^\ddagger is the partition function of a gas penetrant in the transition state, and F is the partition function of the same penetrant in the normal state. By comparing **Equation 2.17** and **2.19**, the entropic selectivity can be written as:

$$\left(\frac{D_A}{D_B}\right)_{\text{entropic}} = \exp\left(\frac{\Delta S_{D,A-B}}{R}\right) = \frac{(F^\ddagger/F)_A}{(F^\ddagger/F)_B} \quad (2.20)$$

The partition function consists of translational, rotational, and vibrational contributions, as shown below.

$$F = F_{trans} \cdot F_{rot} \cdot F_{vib} \quad (2.21)$$

In the case of CMS membranes, a gas penetrant is in the transition state when it passes through the ultramicropores. The rigid ultramicropores in CMS materials can restrict the translational, rotational, and vibrational degrees of freedom of gas molecules, and this molecular sieving allows for subtle discriminations between similarly sized molecules. Compared to polymer membranes with flexible chains, CMS membranes have added entropic selectivity which is useful for separating penetrants with very little difference in size and shape (e.g., O₂/N₂, C₂H₄/C₂H₆, and C₃H₆/C₃H₈).

2.5 References

1. Pierson, H. O. *Handbook of carbon, graphite, diamond, and fullerenes : properties, processing, and applications*. (Noyes Publications, 1993).
2. Jenkins, G. M. & Kawamura, K. *Polymeric carbons – carbon fiber, glass and char*. (Cambridge University Press, 1976).
3. Steel, K. M. *Carbon membranes for challenging gas separations*. (University of Texas, 2000).
4. David, L. I. B. & Ismail, A. F. Influence of the thermastabilization process and soak time during pyrolysis process on the polyacrylonitrile carbon membranes for O₂/N₂ separation. *J. Memb. Sci.* **213**, 285–291 (2003).
5. Centeno, T. A. & Fuertes, A. B. Supported carbon molecular sieve membranes based on a phenolic resin. *J. Memb. Sci.* **160**, 201–211 (1999).
6. Acharya, M. & Foley, H. C. Spray-coating of nanoporous carbon membranes for air separation. *J. Memb. Sci.* **161**, 1–5 (1999).
7. Song, C., Wang, T., Wang, X., Qiu, J. & Cao, Y. Preparation and gas separation properties of poly(furfuryl alcohol)-based C/CMS composite membranes. *Sep. Purif. Technol.* **58**, 412–418 (2008).
8. Centeno, T. A. & Fuertes, A. B. Carbon molecular sieve gas separation membranes based on poly(vinylidene chloride-co-vinyl chloride). *Carbon N. Y.* **38**, 1067–1073 (2000).
9. Koresh, J. E. & Sofer, A. Molecular Sieve Carbon Permselective Membrane. Part I. Presentation of a New Device for Gas Mixture Separation. *Sep. Sci. Technol.* **18**, 723–734 (1983).
10. Fu, S., Sanders, E. S., Kulkarni, S. S. & Koros, W. J. Carbon molecular sieve membrane structure-property relationships for four novel 6FDA based polyimide precursors. *J. Memb. Sci.* **487**, 60–73 (2015).
11. Park, H. B., Kim, Y. K., Lee, J. M., Lee, S. Y. & Lee, Y. M. Relationship between chemical structure of aromatic polyimides and gas permeation properties of their carbon molecular sieve membranes. *J. Memb. Sci.* **229**, 117–127 (2004).
12. Steel, K. M. & Koros, W. J. Investigation of porosity of carbon materials and related effects on gas separation properties. *Carbon N. Y.* **41**, 253–266 (2003).
13. Jones, C. W. & Koros, W. J. Carbon molecular sieve gas separation membranes-II. Regeneration following organic exposure. *Carbon N. Y.* **32**, 1427–1432 (1994).

14. Hatori, H., Yamada, Y., Shiraishi, M., Nakata, H. & Yoshitomi, S. Carbon molecular sieve films from polyimide. *Carbon N. Y.* **30**, 719–720 (1992).
15. Steel, K. M. & Koros, W. J. An investigation of the effects of pyrolysis parameters on gas separation properties of carbon materials. *Carbon N. Y.* **43**, 1843–1856 (2005).
16. Jones, C. W. & Koros, W. J. Carbon molecular sieve gas separation membranes-I. Preparation and characterization based on polyimide precursors. *Carbon N. Y.* **32**, 1419–1425 (1994).
17. Saufi, S. M. & Ismail, A. F. Fabrication of carbon membranes for gas separation - A review. *Carbon N. Y.* **42**, 241–259 (2004).
18. Williams, P. J. & Koros, W. J. in *Advanced Membrane Technology and Applications* 599–631 (John Wiley & Sons, Inc., 2008). doi:10.1002/9780470276280.ch23
19. Kiyono, M., Williams, P. J. & Koros, W. J. Effect of polymer precursors on carbon molecular sieve structure and separation performance properties. *Carbon N. Y.* **48**, 4432–4441 (2010).
20. Xu, L., Rungta, M. & Koros, W. J. Matrimid?? derived carbon molecular sieve hollow fiber membranes for ethylene/ethane separation. *J. Memb. Sci.* **380**, 138–147 (2011).
21. Xu, L. *et al.* Olefins-selective asymmetric carbon molecular sieve hollow fiber membranes for hybrid membrane-distillation processes for olefin/paraffin separations. *J. Memb. Sci.* **423–424**, 314–323 (2012).
22. Kusuki, Y., Shimazaki, H., Tanihara, N., Nakanishi, S. & Yoshinaga, T. Gas permeation properties and characterization of asymmetric carbon membranes prepared by pyrolyzing asymmetric polyimide hollow fiber membrane. *J. Memb. Sci.* **134**, 245–253 (1997).
23. Bhuwania, N. *et al.* Engineering substructure morphology of asymmetric carbon molecular sieve hollow fiber membranes. *Carbon N. Y.* **76**, 417–434 (2014).
24. Jenkins, G. M. & Kawamura, K. *Polymeric carbons: carbon fibre, glass and char.* (Cambridge University Press, 1976).
25. Singh-Ghosal, A. & Koros, W. J. Air separation properties of flat sheet homogeneous pyrolytic carbon membranes. *J. Memb. Sci.* **174**, 177–188 (2000).
26. Lafyatis, D. S., Tung, J. & Foley, H. C. Poly (furfuryl alcohol)-derived carbon molecular sieves: dependence of adsorptive properties on carbonization temperature, time, and poly (ethylene glycol) additives. *Ind. Eng. Chem. Res.* **30**, 865–873 (1991).

27. Vu, D. Q., Koros, W. J. & Miller, S. J. High pressure CO₂/CH₄ separation using carbon molecular sieve hollow fiber membranes. *Ind. Eng. Chem. Res.* **41**, 367–380 (2002).
28. Rungta, M., Xu, L. & Koros, W. J. Carbon molecular sieve dense film membranes derived from Matrimid® for ethylene/ethane separation. *Carbon N. Y.* **50**, 1488–1502 (2012).
29. Suda, H. & Haraya, K. Gas permeation through micropores of carbon molecular sieve membranes derived from Kapton polyimide. *J. Phys. Chem. B* **101**, 3988–3994 (1997).
30. Kim, Y. K., Park, H. B. & Lee, Y. M. Preparation and characterization of carbon molecular sieve membranes derived from BTDA–ODA polyimide and their gas separation properties. *J. Memb. Sci.* **255**, 265–273 (2005).
31. Geiszler, V. C. & Koros, W. J. Effects of polyimide pyrolysis conditions on carbon molecular sieve membrane properties. *Ind. Eng. Chem. Res.* **35**, 2999–3003 (1996).
32. Kiyono, M., Williams, P. J. & Koros, W. J. Generalization of effect of oxygen exposure on formation and performance of carbon molecular sieve membranes. *Carbon N. Y.* **48**, 4442–4449 (2010).
33. Kiyono, M., Williams, P. J. & Koros, W. J. Effect of pyrolysis atmosphere on separation performance of carbon molecular sieve membranes. *J. Memb. Sci.* **359**, 2–10 (2010).
34. Kiyono, M., Williams, P. J. & Koros, W. J. Generalization of effect of oxygen exposure on formation and performance of carbon molecular sieve membranes. *Carbon N. Y.* **48**, 4442–4449 (2010).
35. Fuertes, A. B. Effect of air oxidation on gas separation properties of adsorption-selective carbon membranes. *Carbon N. Y.* **39**, 697–706 (2001).
36. Soffer, A. *et al.* Method of improving the selectivity of carbon membranes by chemical carbon vapor deposition. (1997).
37. Petersen, J., Matsuda, M. & Haraya, K. Capillary carbon molecular sieve membranes derived from Kapton for high temperature gas separation. *J. Memb. Sci.* **131**, 85–94 (1997).
38. Singh, R. & Koros, W. J. Carbon molecular sieve membrane performance tuning by dual temperature secondary oxygen doping (DTSOD). *J. Memb. Sci.* **427**, 472–478 (2013).
39. Wijmans, J. G. & Baker, R. W. The solution-diffusion model: a review. *J. Memb. Sci.* **107**, 1–21 (1995).

40. Koros, W. J. & Fleming, G. K. Membrane-based gas separation. *J. Memb. Sci.* **83**, 1–80 (1993).
41. BARRER, R. M., BARRIE, J. A. & SLATER, J. SORPTION AND DIFFUSION IN ETHYL CELLULOSE .3. COMPARISON BETWEEN ETHYL CELLULOSE AND RUBBER. *J. Polym. Sci.* **27**, 177–197 (1958).
42. Michaels, A. S., Vieth, W. R. & Barrie, J. A. Solution of gases in polyethylene terephthalate. *J. Appl. Phys.* **34**, 1–12 (1963).
43. Vieth, W. R., Tam, P. M. & Michaels, A. S. Dual sorption mechanisms in glassy polystyrene. *J. Colloid Interface Sci.* **22**, 360–370 (1966).
44. Koros, W. J. in *Barrier Polymers and Structures* **423**, 1 (American Chemical Society, 1990).
45. Koros, W. J. & Madden, W. C. in *Encyclopedia of Polymer Science and Technology* (John Wiley & Sons, Inc., 2002). doi:10.1002/0471440264.pst376
46. Rungta, M. Carbon molecular sieve dense film membranes for ethylene/ethane separations. (Georgia Institute of Technology, 2012).
47. Singh, A. Membrane materials with enhanced selectivity: an entropic interpretation. (The University of Texas at Austin, 1997).
48. Singh, A. & Koros, W. J. Significance of entropic selectivity for advanced gas separation membranes. *Ind. Eng. Chem. Res.* **35**, 1231–1234 (1996).
49. Glasstone, S., Eyring, H. & Laidler, K. J. *The theory of rate processes*. (McGraw-Hill, 1941).

CHAPTER 3. MATERIALS AND EXPERIMENTAL METHODS

3.1 Overview

This chapter describes the materials and experimental procedures used in this work. [Section 3.2](#) introduces the gases for testing and polymers and metal salts for membrane formation. [Section 3.3](#) discusses the formation of both polymeric and carbon molecular sieve (CMS) dense film membranes. [Section 3.4](#) outlines various characterization techniques.

3.2 Materials

3.2.1 Gases

Pure gases including C₂H₄, C₂H₆, C₃H₆, and C₃H₈ (Airgas) were used for gas permeation and sorption measurements. Pure Argon (Airgas) was used as purge gas for pyrolysis. A quaternary mixture containing 54.6 mol% C₂H₄, 17.0 mol% C₂H₆, 15.1 mol% C₃H₆, and 13.3 mol% C₃H₈ (nexAir) was used for mixed gas permeation measurements. This mixed gas is a representative mixture for the feed of a deethanizer column in an ethylene plant.

3.2.2 Polymers

As mentioned before, polyimides are suitable precursors to carbon molecular sieve membranes for gas separations. In this work, the DABA-containing polyimide, 6FDA-DAM:DABA (3:2), was the main precursor, with 6FDA-DAM used as an additional control polymer precursor for characterizing the influence of Fe incorporation without the

DABA group on sorption performance. The rationale for including the DABA moiety will be described in more detail later, but is used to promote uniformity of Fe distribution. The structures of the polymers are shown in **Table 3.1**. Both polyimides were custom synthesized by Akron Polymer Systems, Inc. with a two-step polycondensation reaction, described by several authors^{1,2}. An example of a reaction scheme for 6FDA-DAM:DABA (3:2) synthesis is shown in **Figure 3.1**.

Table 3.1. Chemical structures and names of polymers

Name	Chemical Structure
6FDA-DAM:DABA (3:2)	
	6FDA: 4,4'-(Hexafluoroisopropylidene)diphthalic anhydride DAM: 2,4,6-trimethyl-3,3'-phenylenediamine DABA: 3,5-diaminobenzoic acid
6FDA-DAM	
	6FDA: 4,4'-(Hexafluoroisopropylidene)diphthalic anhydride DAM: 2,4,6-trimethyl-3,3'-phenylenediamine

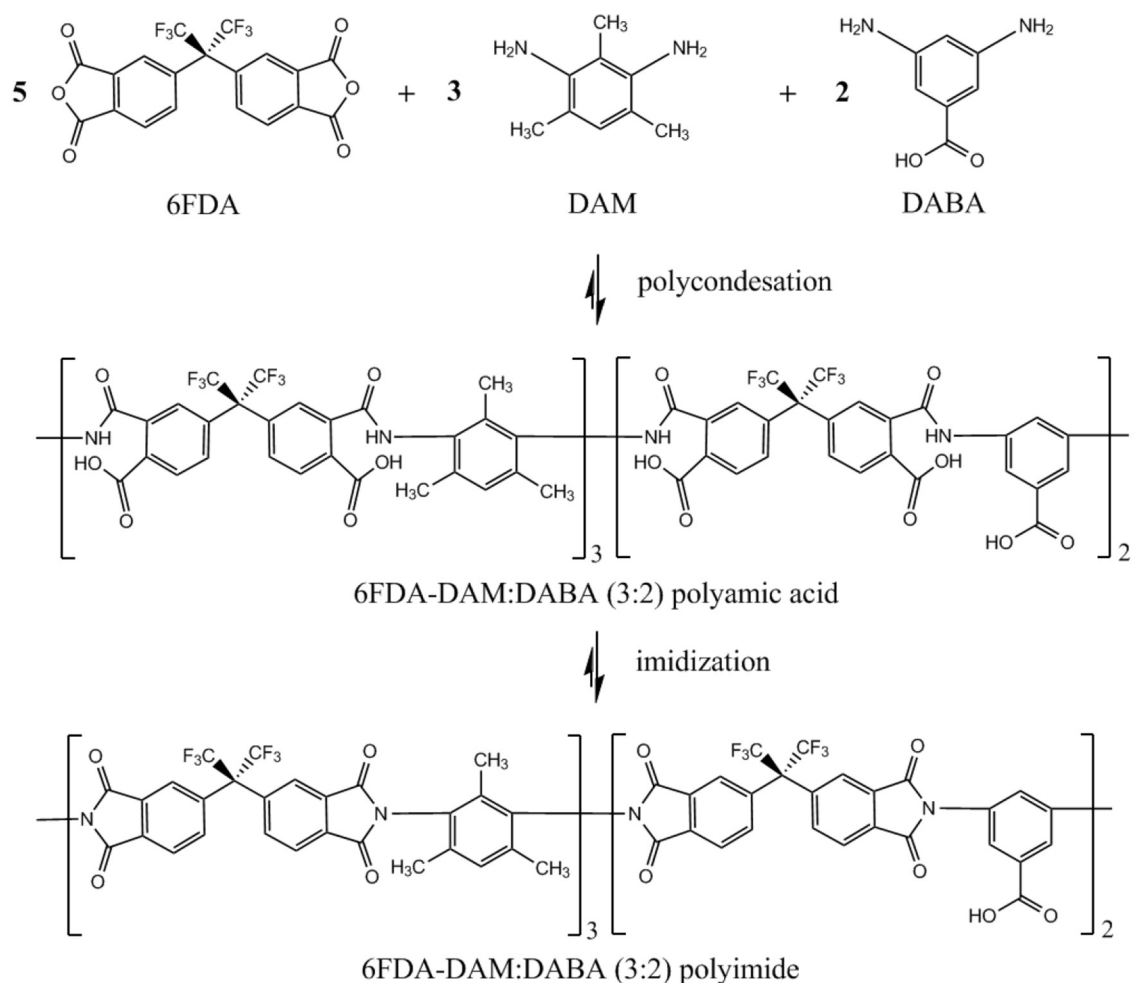


Figure 3.1. Reaction scheme for 6FDA-DAM:DABA (3:2) synthesis

3.2.3 Metal Salts

Metal acetylacetonates $[M(acac)_n]$ were used as the main source of metal for metal-containing polymeric and CMS dense film membranes. The general structure of $M(acac)_n$ is shown in **Table 3.2**. In this work, $Fe(acac)_2$ were the starting materials for Fe-containing polymeric and CMS membranes unless otherwise specified. In Section 5.4, $Fe(acac)_3$, $Al(acac)_3$, $Ni(acac)_2$, $Mn(acac)_2$, and $Mn(acac)_3$ were studied to compare the effects of

various metal species on olefin/paraffin separation performance, and two other Fe(II) compounds, FeCl₂, and Fe(ac)₂, were also studied as the source of metal. All the metal salts were purchased from Sigma-Aldrich.

Table 3.2. Chemical structures of metal salts

Name	Chemical Formula	Chemical Structure
Metal acetylacetonate	M(acac) _n	 $\left[\text{H}_3\text{C}-\text{C}(=\text{O})-\text{CH}=\text{C}(\text{O}^-)-\text{CH}_3 \right]_n \text{M}^{n+}$ $(\text{M}^{n+}=\text{Fe}^{2+}, \text{Fe}^{3+}, \text{Al}^{3+}, \text{Ni}^{2+}, \text{Mn}^{2+}, \text{and Mn}^{3+})$
Iron(II) chloride	FeCl ₂ ·4H ₂ O	
Iron(II) acetate	Fe(ac) ₂	 $\left[\text{H}_3\text{C}-\text{C}(=\text{O})-\text{O} \right]_2 \text{Fe}^{2+}$

3.3 Membrane Formation

3.3.1 Polymer Dense Film Membrane Formation

The polymer powders were dried under vacuum at 110 °C overnight to remove moisture. The dried polymer was dissolved in tetrahydrofuran (THF, >99.9% purity, Sigma-Aldrich) in a 40 ml vial (vial A) to form a 2 to 3 wt% polymer solution, and the solution was then mixed on a rolling mixer overnight for complete polymer dissolution. The specific amount of metal acetylacetonate was separately dissolved in THF in a 20 ml vial (vial B) to form a metal-containing solution. The two solutions were filtered with 0.20 micron PTFE filters (Micropore Corporation) respectively to remove impurity, and the Fe-

containing solution in vial B was added to vial A to form a Fe-containing polymer dope for casting. The compositions of the solutions studied in this work are presented in **Table 3.3**, and with the studied amount of $M(\text{acac})_n$, there was no particle settling in the prepared solutions. The resulting Fe-containing polymer films in this work have a theoretical concentration of Fe between 1.1 and 3.2 wt% based on the loading of $\text{Fe}(\text{acac})_2$ in the precursor. For 6FDA-DAM:DABA (3:2) polymer, as the amount of Fe ion was over a certain range, the mixed casting solution became gel due to a high ionic cross-linking density between Fe and the DABA group, thereby compromising film formation. Although the DABA moiety limits the loading of Fe during polymer film casting, the moiety appears to be necessary for uniformity of Fe distribution, as will be described later. For non-Fe polymer dense films, the casting solution did not contain $\text{Fe}(\text{acac})_2$.

Table 3.3. Casting solution formulation for metal-containing polymer dense films

	Solvent	Solute
Vial A	20 ml THF	0.5 g polymer
Vial B	5 ml THF	0.025–0.075 g $M(\text{acac})_n$

Polymer dense films were prepared by casting the mixed solution into a TeflonTM casting dish inside a glove bag (Cole Parmer) at room temperature as shown in **Figure 3.2**. Two jars containing excess THF were placed inside the glove bag before sealing the glove bag. The glove bag was then purged with nitrogen and allowed to saturate with THF by waiting at least 3 hours before casting. After at least 3 days, the vitrified films were

removed from the bag and dried in a vacuum oven at 130 °C for 24 hours to remove residual solvent. The dried films having a thickness of about 80 microns were then cut into 0.75 inch diameter discs that were then pyrolyzed as described below.

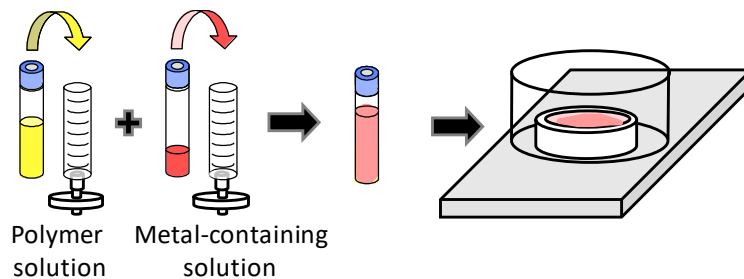


Figure 3.2. Schematic of solution-casting method for polymer dense films

3.3.2 Carbon Molecular Sieve Dense Film Membrane Formation

3.3.2.1 Pyrolysis Setup

Carbon molecular sieve (CMS) dense films were formed by pyrolyzing polymer films with a pyrolysis system which was previously reported^{3,4}, shown in **Figure 3.3**.

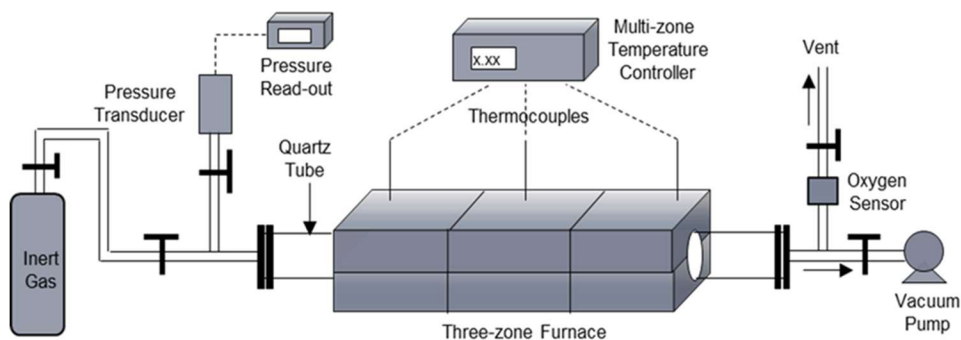


Figure 3.3. Schematic of pyrolysis furnace setup for fabricating CMS materials⁴

The pyrolysis setup includes a three-zone furnace (Thermcraft, Inc., model XST-3-0-24-3C, Winston-Salem, NC) with three thermocouples connected to a multi-channel temperature controller (Omega Engineering, Inc., model CN1504TC, Stamford, CT), allowing for accurate and uniform control of desired temperature profile. A quartz tube (55 mm I.D. x 4 ft length, National Scientific Company, GE Type 214 quartz tubing, Quakertown, PA) was placed inside the furnace and sealed on each side with an assembly of metal flanges and silicon O-rings (MTI Corporation, Richmond, CA). A mass flow controller (MKS Instruments, MA) was used for an accurate flow rate of purge gas during the pyrolysis process. The concentration of oxygen in the pyrolysis atmosphere was monitored by an oxygen analyzer (Rapidox 2100, Cambridge Sensotec, Ltd., Cambridge, England) during the pyrolysis process.

The dried polymer dense films were cut into small discs by using a 0.75” die cutter (McMaster Carr). The discs were placed on a slotted quartz plate (United Silica Products, Franklin, NJ, USA) with spacing between each disc, shown in **Figure 3.4**. The combination

of the discs and the quartz plate were placed into the quartz tube of the pyrolysis system described above.

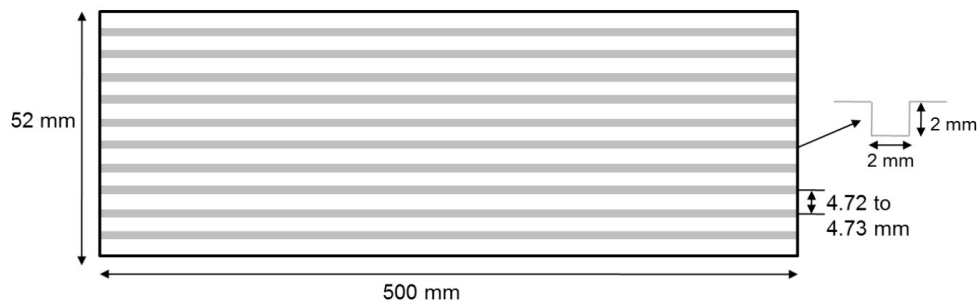


Figure 3.4. Custom made quartz plate for dense film pyrolysis⁴

3.3.2.2 Pyrolysis Protocol

Four different pyrolysis protocols were used in this work for pyrolyzing polymer dense films to CMS dense films, and the programmed heating protocol details are listed below and shown in **Figure 3.5**, where T_{pyro} represents the final pyrolysis temperature (either 550 °C or 675 °C). In this work, the *Fast protocols* were specifically designed for advanced Fe-containing CMS membranes for improving separation performance, as discussed later.

Table 3.4. Programmed pyrolysis heating protocols ($T_{\text{pyro}}=550\text{ }^{\circ}\text{C}$ or $675\text{ }^{\circ}\text{C}$)

Protocol name	Temperature range ($^{\circ}\text{C}$)	Ramp rate ($^{\circ}\text{C}/\text{min}$)
Slow protocol	50 – 250	13.3
	250 – ($T_{\text{pyro}}-15$)	3.85
	($T_{\text{pyro}}-15$) – T_{pyro}	0.25
	120 min soak at T_{pyro}	
Fast protocol	50 – ($T_{\text{pyro}}-50$)	10
	($T_{\text{pyro}}-50$) – T_{pyro}	2

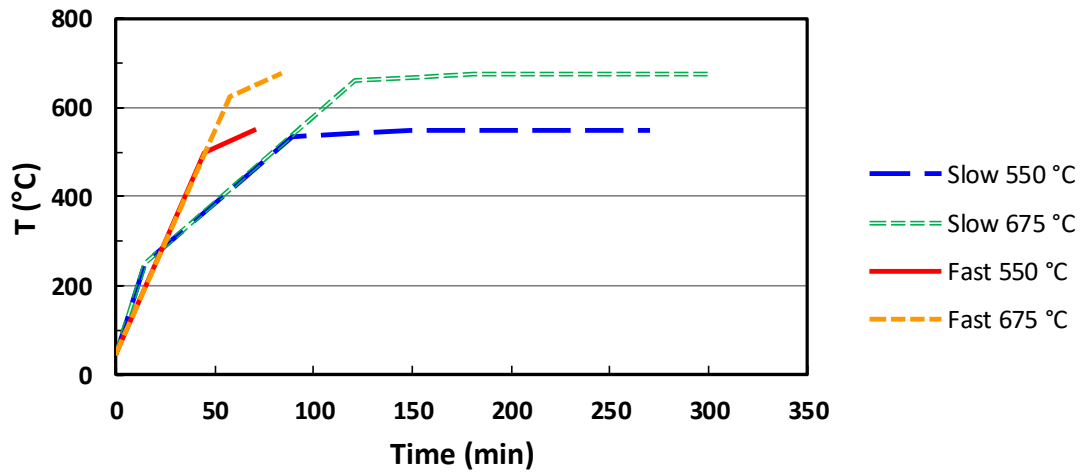


Figure 3.5. Temperature profiles of programmed pyrolysis protocols

For all the protocols, pyrolysis atmosphere was controlled with a continuous UHP Argon flow at a rate of 200 cc(STP)/min during the entire pyrolysis procedures. Prior studies⁵ showed that this flow rate was adequate to avoid external mass transfer resistance complications during pyrolysis. Before heating up, Argon was purged in the quartz tube for at least 10 hours while the oxygen concentration was monitored. After pyrolysis, the

films were allowed to naturally cool to room temperature inside the quartz tube before unloading. Between each pyrolysis cycle, the quartz tube and the quartz plate were rinsed with acetone and baked at 800 °C for 2 hours under an air flow at a rate of 500 cc(STP)/min to remove any residue that may contaminate the subsequent pyrolysis run.

3.4 Characterization Techniques

3.4.1 Dense Film Permeation Measurements

3.4.1.1 Permeation Cell

The permeation properties of both polymeric and CMS dense films were measured with a permeation cell, and a typical assembly of the film and the permeation cell is shown in **Figure 3.6**. The films were first masked by sandwiching between two concentric pieces of impermeable aluminum tape. To provide a cushion, several layers of filter paper were put between the masked film and the base of the cell. On the top of the masked film was a larger aluminum tape with a hole allowing the films to be exposed for permeation. Epoxy was then applied at the interface between the film and the tape for sealing. For CMS dense films, five-minute epoxy (3M, DP-100) was mixed in a weighing boat for 30 seconds and then used for sealing. For polymeric films, Duralco 4525 epoxy has been shown to have better adherence to the polymer materials for preventing seal failure, and this epoxy was used with standard instruction. The permeation cell was finally assembled with O-rings and screws, and then loaded into a permeation system, shown in **Figure 3.7**.

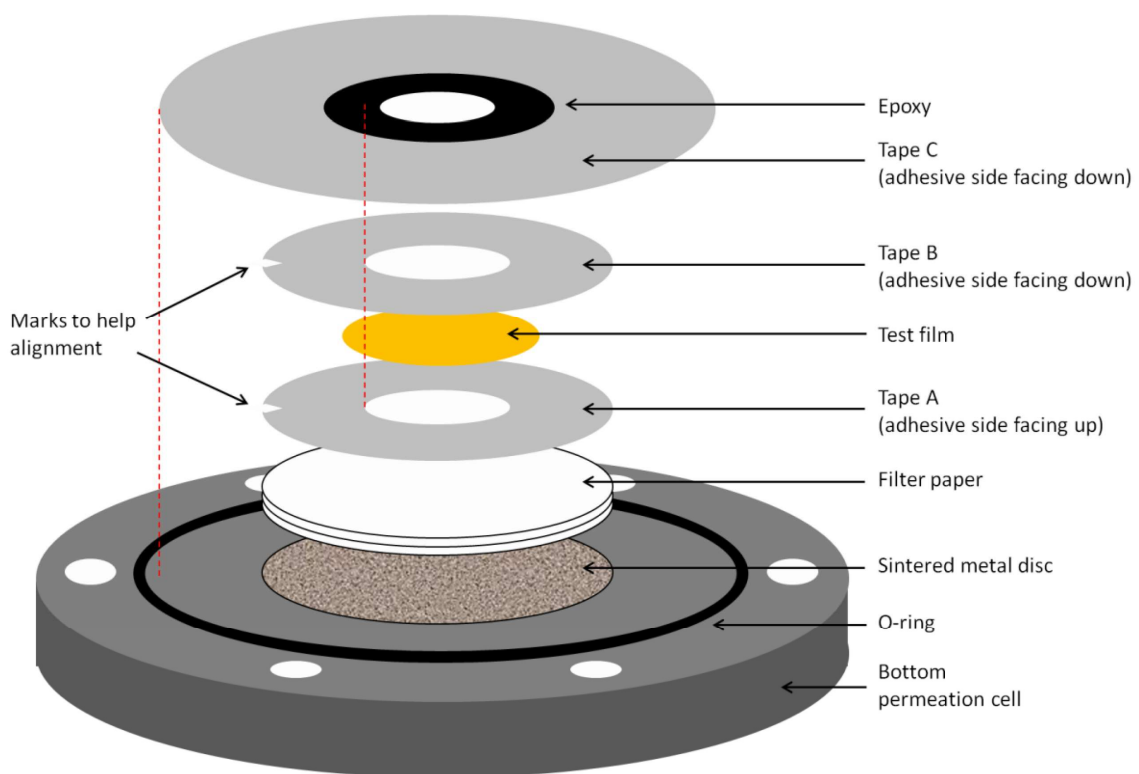


Figure 3.6. Schematic of masking a dense film into a permeation cell⁶

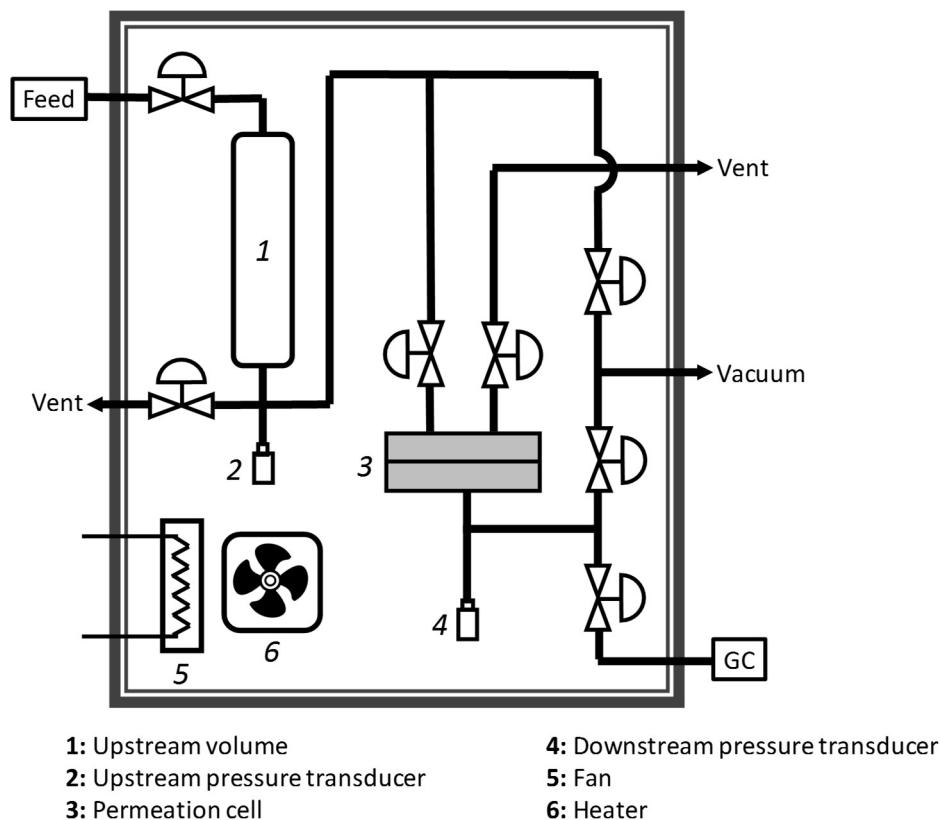


Figure 3.7. Schematic of a constant-volume permeation system

3.4.1.2 Constant-Volume Permeation System

Pure and mixed gas permeation measurements of both polymeric and CMS dense films were performed with a constant-volume permeation system. **Figure 3.7** shows a typical constant-volume permeation system, and the details of which were described previously^{7,8}. The permeation system was stabilized at a desired temperature (i.e., 35 °C, 42.5 °C, and 50 °C) with heating tapes and a fan. Prior to the permeation test, the entire system was evacuated for 18 hours to minimize the outgassing to less than 1% of the permeation of the slowest gas. After evacuation, the upstream was pressurized with feed

gas at about 50 pounds per square inch absolute pressure (psia) while the downstream was kept at vacuum. The pressure rise in a constant, known downstream volume was monitored by a pressure transducer and recorded over time by LabVIEW (National Instruments, Austin, TX) until a steady state was achieved.

Mixed gas permeation measurements were performed with the desired mixture at 50 psia. The flow rate of the retentate over the feed side of the film was controlled by a needle valve. The percentage of the feed permeating through the film, also known as the stage cut, was kept less than 1% to avoid concentration polarization. Permeate compositions were analyzed with a gas chromatograph (Bruker 450) using a thermal conductivity detector (TCD) with He as the carrier gas.

3.4.1.3 Permeability of Dense Films

Permeability of dense film membranes was calculated using **Equation 3.1**,

$$P = \frac{1.764 \cdot 10^6 \cdot V \cdot \ell \cdot (dp/dt)}{(T + 273.15) \cdot A \cdot \Delta p} \quad (3.1)$$

where:

P : permeability (Barrer)

V : downstream volume (cm³)

ℓ : membrane thickness (mil)

$dpdt$: downstream pressure rising rate (torr/s)

A : available area of membrane for permeation (cm²)

Δp : partial pressure difference across the membrane (psia)

The available area of each film for permeation was determined with image scanner and area analysis software (ImageJ). The membrane thickness was determined with a digital micrometer.

3.4.2 *Pressure Decay Sorption*

The equilibrium sorption properties of both polymeric and CMS dense films were measured with a pressure decay sorption system reported earlier⁹, shown in **Figure 3.6**. After casting as described earlier, the polymeric films were cut into small pieces for sorption measurements while the CMS films were gently broken into pieces between two pieces of weighing paper and wrapped with aluminum foil securely. The samples were loaded into the sample cell chamber, and the sorption cell was then placed in an oil bath with a heating circulator to maintain a uniform desired temperature (i.e., 35 °C, 42.5 °C, and 50 °C). The entire system was evacuated for 18 hours before testing. For the measurement at each pressure level, the reservoir cell chamber was filled with feed gas and equilibrated for 20 to 25 minutes. The valve between the reservoir and the sample cell was then opened carefully to introduce gas into the sample cell. The pressure in both the reservoir and sample cell was monitored by a pressure transducer and recorded over time by LabVIEW until the pressure in the sample cell became constant.

The amount of sorbed gas was calculated based on a mole balance⁹. To account for behavior of non-ideal gases, the compressibility factors of the interested gases were calculated using the NIST SUPERTRAP, and the equations are listed in **Appendix A**. Gas uptake by the sample was plotted against equilibrium pressure and the data was fitted using

either a dual mode sorption mode (for polymeric samples) or a Langmuir model (for CMS samples) to obtain sorption isotherms.

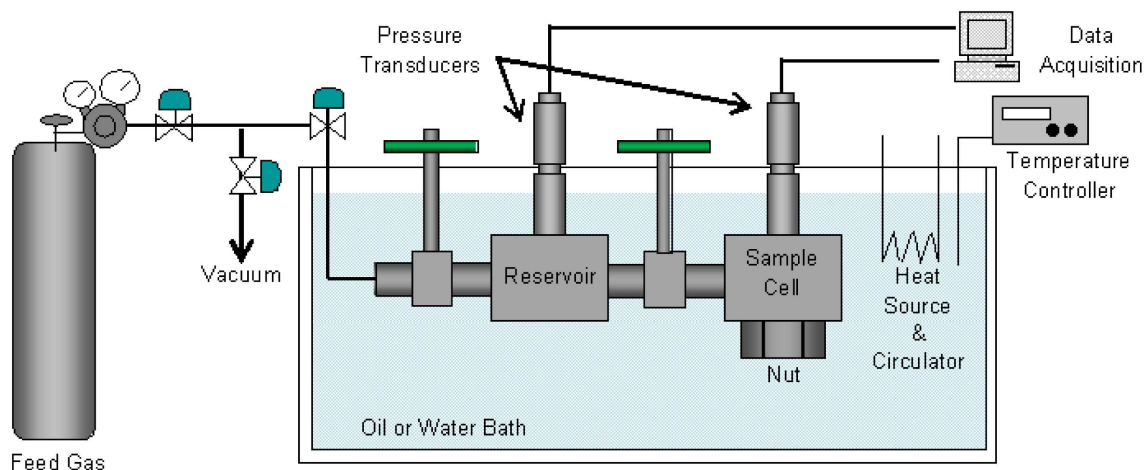


Figure 3.8. Schematic of a pressure decay sorption system¹⁰

3.4.3 X-Ray Absorption Near Edge Structure

X-ray absorption near edge structure (XANES) was performed to determine the valence state of Fe. The Fe K-edge XANES spectra were collected at beamline 5BM-D (DND-CAT) at Argonne National Laboratory, Lemont, IL in transmission mode at room temperature. Data was processed using the Athena software package¹¹.

3.5 References

1. Qiu, W. *et al.* Sub-Tg cross-linking of a polyimide membrane for enhanced CO₂ plasticization resistance for natural gas separation. *Macromolecules* **44**, 6046–6056 (2011).
2. Chen, C.-C. Thermally crosslinked polyimide hollow fiber membranes for natural gas purification. (Georgia Institute of Technology, 2011).
3. Xu, L. Carbon molecular sieve hollow fiber membranes for olefin/paraffin separations. (Georgia Institute of Technology, 2012).
4. Rungta, M. Carbon molecular sieve dense film membranes for ethylene/ethane separations. (Georgia Institute of Technology, 2012).
5. Kiyono, M., Williams, P. J. & Koros, W. J. Generalization of effect of oxygen exposure on formation and performance of carbon molecular sieve membranes. *Carbon N. Y.* **48**, 4442–4449 (2010).
6. Ning, X. Carbon molecular sieve membranes for nitrogen/methane separation. (Georgia Institute of Technology, 2014).
7. Pye, D. G., Hoehn, H. H. & Panar, M. Measurement of gas permeability of polymers. II. Apparatus for determination of permeabilities of mixed gases and vapors. *J. Appl. Polym. Sci.* **20**, 287–301 (1976).
8. Pye, D. G., Hoehn, H. H. & Panar, M. Measurement of gas permeability of polymers. I. Permeabilities in constant volume/variable pressure apparatus. *J. Appl. Polym. Sci.* **20**, 1921–1931 (1976).
9. Koros, W. J. & Paul, D. R. Design considerations for measurement of gas sorption in polymers by pressure decay. *J. Polym. Sci. Polym. Phys. Ed.* **14**, 1903–1907 (1976).
10. Kiyono, M. Carbon molecular sieve membranes for natural gas separations. (Georgia Institute of Technology, 2010).
11. Ravel, B. & Newville, M. ATHENA, ARTEMIS, HEPHAESTUS: data analysis for X-ray absorption spectroscopy using IFEFFIT. *J. Synchrotron Radiat.* **12**, 537–541 (2005).

CHAPTER 4. EVALUATION OF VIABILITY OF IRON IN CARBON MOLECULAR SIEVE MEMBRANES FOR INCREASING OLEFIN/PARAFFIN SORPTION SELECTIVITY

4.1 Overview

Previous work has shown that carbon molecular sieve (CMS) membranes with rigid pore structures are promising for olefin/paraffin separation, based on diffusion selectivity, while sorption selectivity has little influence. In this work, integrating Fe^{2+} into polymer precursors was pursued to improve CMS membrane separation properties for advanced olefin/paraffin separation. Starting materials and processing conditions were investigated in order to explore the impacts on the olefin-selective CMS membranes. The Fe-containing CMS membranes prepared with a carefully designed pyrolysis protocol have improved olefin/paraffin sorption separation performance, which is reported in this chapter.

4.2 Olefin/Paraffin Separation with CMS Membranes

Researchers have studied binary olefin/paraffin separations ($\text{C}_2\text{H}_4/\text{C}_2\text{H}_6$ and $\text{C}_3\text{H}_6/\text{C}_3\text{H}_8$) with carbonized membranes¹⁻⁴, and it is found that CMS membranes are promising with favorable olefin/paraffin separation performance. Rungta⁴ investigated CMS membranes derived from Matrimid[®] and 6FDA:BPDA-DAM (1:1), and she pointed out that the selectivity of C_2H_4 over C_2H_6 is dominated by diffusion selectivity while sorption selectivity has little influence, as shown in **Figure 4.1**. As discussed in [Section 2.4](#), CMS membranes with rigid pore structures can restrict the degrees of motional

freedom for gas penetrants, providing size-selective sieving with moderately high diffusion selectivity.

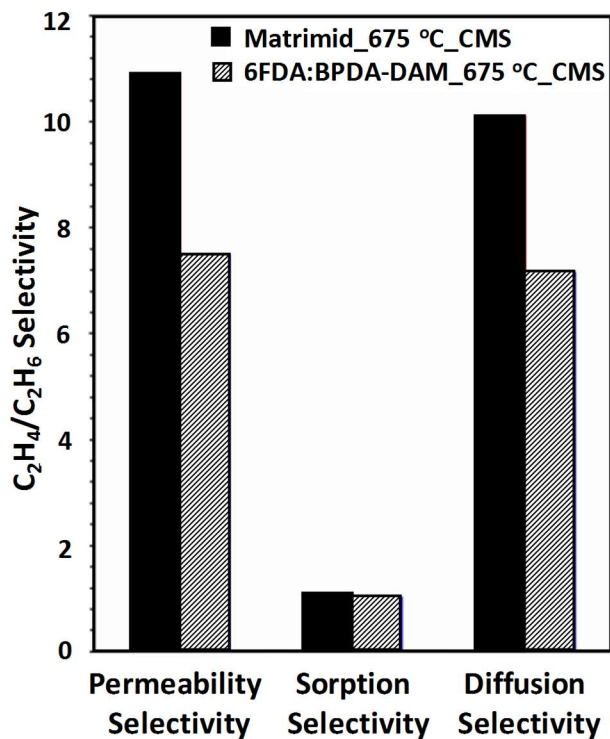


Figure 4.1. C_2H_4/C_2H_6 selectivities based on permeability, sorption, and diffusion for CMS membranes derived from Matrimid[®] and 6FDA:BPDA-DAM (reproduced from reported data⁴)

Since this work focuses on developing olefin-selective CMS membranes for the separation of mixed olefins (C_2H_4 and C_3H_6) from paraffins (C_2H_6 and C_3H_8), improving olefin/paraffin sorption selectivity was felt to be a good strategy to separate the large olefin (C_3H_6) from the small paraffin (C_2H_6) more efficiently. Recalling that sorption selectivity

depends on the condensability of the gas penetrants and the interactions with the sorbent material, modifying the properties of CMS materials to favor olefins may increase olefin/paraffin sorption selectivity, and ultimately permselectivity.

4.3 Selective Olefin/Paraffin Adsorption with Metal-Organic Frameworks

Metal-organic frameworks (MOFs) have emerged as a promising crystalline molecular sieve material for gas separations⁵. MOFs can be formed by coordinating a network with metal ions/clusters and organic ligands, and this fabrication approach provides enormous structural diversity with tailored properties. This type of material has well-defined porous structures, and their performance can overcome the polymer upper bound for gas separations.

Bloch *et al.*⁶ studied olefin/paraffin separation with a MOF material, Fe₂(dobdc) (dobdc⁴⁻: 2,5-dioxido-1,4-benzenedicarboxylate), also referred to as Fe-MOF-74. They found that Fe₂(dobdc) can have C₂H₄/C₂H₆ adsorption selectivity in a range of 13 to 18 and C₃H₆/C₃H₈ adsorption selectivity between 13 and 15. These high olefin/paraffin adsorption selectivities are based on the strong interactions between the carbon-carbon double bonds in the olefins and the open Fe(II) coordination sites in Fe₂(dobdc). Extended work on olefin/paraffin separation with MOFs M₂(dobdc) (M= Mg, Mn, Fe, Co, Ni, Zn) was conducted by Geier *et al.*⁷. They investigated the interaction between olefins and various species of open metal sites in the MOFs, and the results showed that Fe₂(dobdc) and Mn₂(dobdc) exhibit the highest selectivities for the separation of C₂H₄/C₂H₆ and C₃H₆/C₃H₈ mixtures, respectively.

Most studies of olefin/paraffin separation with MOFs are focused on cyclic batch adsorption/desorption processes, but in principle, a steady state membrane process is more attractive⁸. Since MOFs are expensive to produce and difficult to handle, this work did not explore the applications of MOF material for gas separations.

4.4 Strategy for Improving Olefin/Paraffin Separation with Fe in CMS Membranes

With the support of selective interaction between olefins and open metal sites in MOFs, the performance of a CMS membrane with low olefin/paraffin sorption selectivity may be improved by incorporating transition metal ions in the membrane. Several researchers have successfully made metal-containing CMS membranes to improve the separation performance^{9–13}, but none of them have studied the effects of metal on olefin/paraffin separation. To realize a metal-containing CMS membrane, a transition metal can be incorporated during the formation of a polymer precursor to form a metal bearing polymer precursor, and the detailed formation processes are described in [Section 3.3](#).

In this work, iron (Fe) was chosen as the incorporated metal based on a combination of factors including high C₂H₄/C₂H₆ adsorption selectivity⁷, low cost, and stability against contaminants. Iron(II) acetylacetonates [Fe(acac)₂] were used as the source of the metal according to its simple structure, low cost, and moderate solubility in the solvent. It is desirable that Fe is incorporated homogeneously into the polymer on a fine scale, so a DABA-containing polyimide, 6FDA-DAM:DABA (3:2), was used as the polymer precursor, and the Fe ions can be uniformly dispersed by the cross-linking of the DABA carboxylic acid group and Fe ions¹⁴, as illustrated in **Figure 4.2**. The films were then

pyrolyzed with controlled pyrolysis protocols developed in this work to form the Fe-containing CMS membranes for the mixed olefin/paraffin separation. As will be discussed later, in the absence of the DABA group, CMS derived from Fe-containing precursors have poor final separation results.

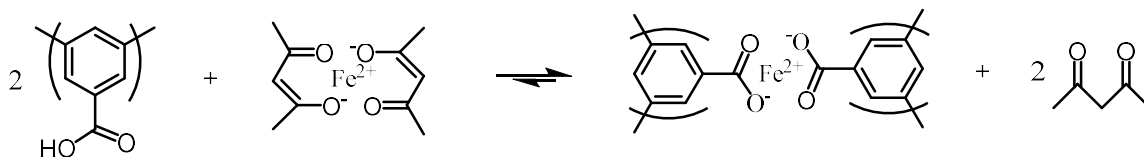


Figure 4.2. Ionic cross-linking of DABA-containing polyimide with Fe(II) acetylacetonate

4.5 Sorption Performance of Fe-Containing CMS Membranes

The interaction between olefins and Fe in the CMS membranes was studied by conducting pressure decay sorption measurements with single-component gas at 35 °C. The loading of Fe in the current studied precursor was 2.2 wt%, which is suitable for forming Fe-containing polymer precursor and for observing the effects of Fe on sorption performance. Since C2 pair olefin/paraffin separation is more challenging than C3 pair and draws much researchers' attention, this work first studied C2 sorption performance of the membranes to evaluate the viability of Fe for increasing olefin/paraffin sorption selectivity. As the suitable formation conditions for Fe were probed, sorption of C3 hydrocarbons was studied as well.

4.5.1 Effects of Pyrolysis Protocols

Pyrolysis protocols allow for adjusting the performance of the resulting CMS membranes. For Fe-containing CMS membranes, pyrolysis protocols may also change the state of Fe in the carbon material and affect the interactions between Fe ions and olefins. In this work, four pyrolysis protocols were studied. In this work, as noted in **Section 3.3.2**, four pyrolysis protocols were studied: *Slow 550 °C* and *Slow 675 °C* protocols have a ramp rate at 3.85 °C/min and a 2-hour thermal soak time while *Fast 550 °C* and *Fast 675 °C* protocols have a faster ramp rate at 10 °C/min and no thermal soak time.

4.5.1.1 Slow Pyrolysis Protocols

The standard *Slow 675 °C* protocol has been studied in depth for C₂H₄/C₂H₆ separation performance of CMS membranes derived from various polyimides, and this pyrolysis protocol was found to be optimum in the past^{3,15}. In the current work, the 2.2 wt% Fe-containing 6FDA-DAM:DABA (3:2) precursor was pyrolyzed with the *Slow 675 °C* protocol, and as shown in **Figure 4.3 (a)**, it is obvious that the resulting CMS membranes have C₂H₄/C₂H₆ sorption selectivity at 50 psia near 1. Another commonly used protocol with lower pyrolysis temperature, the *Slow 550 °C* protocol, was also applied to the 2.2 % Fe-containing precursors, and the resulting CMS membranes have C₂H₄/C₂H₆ sorption selectivity of 1.03, as shown in **Figure 4.3 (b)**. These results indicate the need for additional attention to the pyrolysis conditions for the Fe-containing CMS membranes.

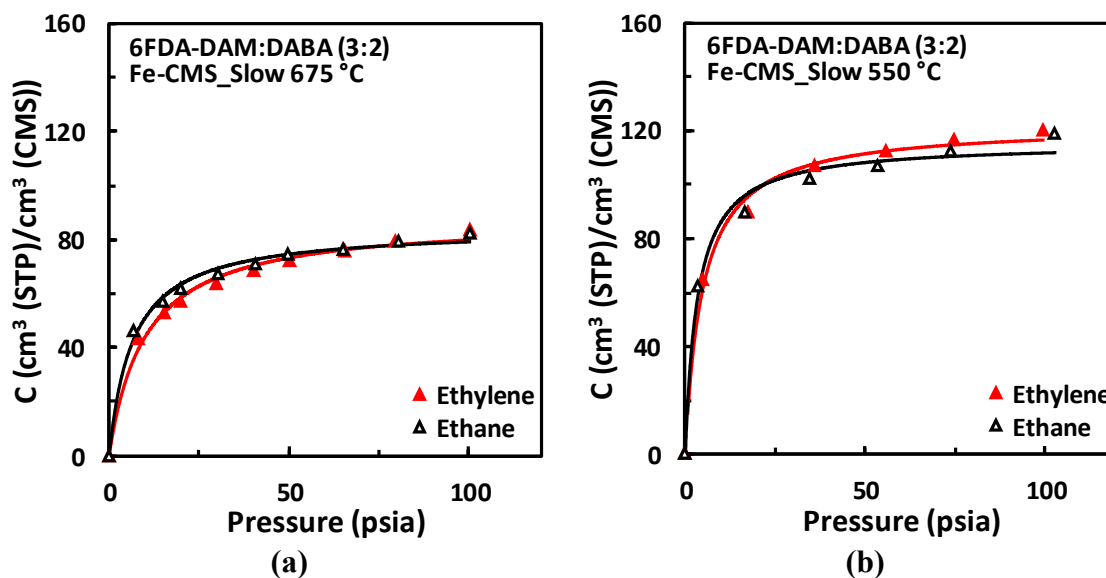


Figure 4.3. Sorption isotherms of single-component ethylene and ethane at 35 °C for Fe-containing 6FDA-DAM:DABA (3:2) derived CMS membranes from (a) Slow 675 °C and (b) Slow 550 °C pyrolysis protocols

The pyrolysis temperature was expected to be influential in determining the molecular scale morphology of the resulting CMS membranes, as well as the state of Fe in the CMS membranes. From the data shown in **Figure 4.3 (a) and (b)**, it is found that the sorption capacity of both C_2H_4 and C_2H_6 increase when the pyrolysis temperature is reduced from 675 °C to 550 °C. Recalling that most of the sorption occurs in micropores in the carbon material, this increasing sorption capacity reflects a more open micropore structure in the Fe-containing CMS membranes derived at the lower pyrolysis temperature, providing more sorption capacity for the gas penetrants (see **Figure 4.4**). Changing the pyrolysis temperature offers an opportunity to tune the performance of CMS membranes. However, the Fe-containing carbon materials derived from the both standard *slow* pyrolysis protocols clearly still lack sorption preference for olefins. While this chapter focuses on

the sorption performance, the effects of pyrolysis temperature on permeation performance of CMS membranes are discussed in [Chapter 5](#).

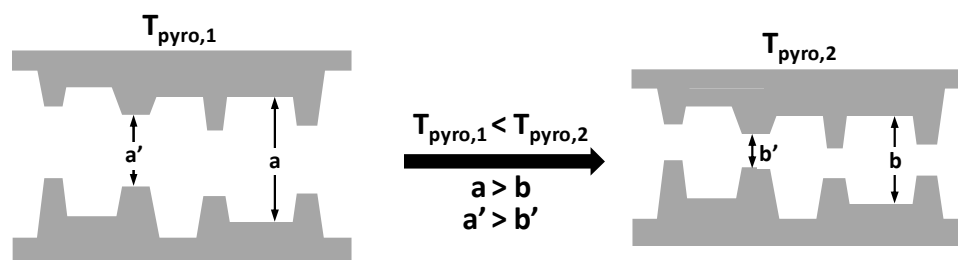


Figure 4.4. Effects of final pyrolysis temperature (T_{pyro}) on idealized pore structures of CMS membranes

Both the pyrolysis protocols with the slower ramp rate and 2-hour thermal soak time lead to indistinct olefin/paraffin sorption selectivity for Fe-containing CMS membranes. Although Fe-containing precursors were prepared successfully, it is important to ensure the Fe ions are effective for the interaction with olefins after pyrolysis. Alternative pyrolysis protocols with modified temperature profiles are discussed in the next section.

4.5.1.2 Fast Pyrolysis Protocols

To maintain active Fe^{2+} cation sites, the pyrolysis protocol must be engineered for the Fe-containing CMS membranes. It is reported that FeO can be formed through reductive decomposition of $\text{Fe}(\text{acac})_3$, and FeO can be converted into Fe_3O_4 after annealing at $500\text{ }^\circ\text{C}$ under an argon atmosphere for 1 hour¹⁶. Therefore, two fast pyrolysis protocols

(*Fast 550 °C* and *Fast 675 °C* protocols) were introduced to control the oxidation state of the iron during pyrolysis. The residence time at high temperature was reduced by increasing the ramp rate from 3.85 °C/min to 10 °C/min and eliminating the thermal soak time.

As shown in **Figure 4.5 (a)**, the Fe-containing membranes derived from the *Fast 675 °C* protocol exhibit C₂H₄/C₂H₆ sorption selectivity at 50 psia of 1.05. For this fast protocol with high pyrolysis temperature, the interaction between the olefin and Fe does not benefit significantly from modifying the temperature profile. However, for the fast protocol with lower pyrolysis temperature (*Fast 550 °C*), the resulting Fe-containing CMS membranes have increased C₂H₄/C₂H₆ sorption selectivity of 1.19 for only 2.2 wt% loading of Fe in the precursor, as seen in **Figure 4.5 (b)**. The results support the hypothesis that olefin/paraffin sorption selectivity for CMS membranes will increase when metals are incorporated carefully with controlled pyrolysis conditions. The trade-off in terms of overall permselectivity and productivity of the various CMS samples (Fe-containing and Fe-free CMS materials derived from different pyrolysis temperatures) will be discussed later, but clearly, an effect of Fe on sorption selectivity is shown here.

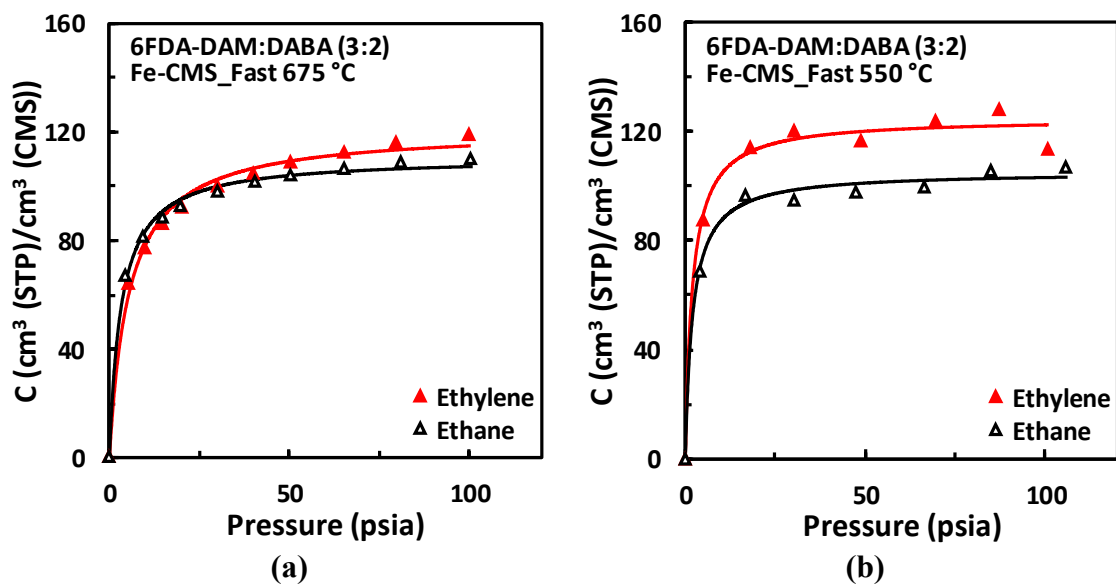


Figure 4.5. Sorption isotherms of single-component ethylene and ethane at 35 °C for Fe-containing 6FDA-DAM:DABA (3:2) derived CMS membranes from (a) Fast 675 °C and (b) Fast 550 °C pyrolysis protocols

A controlled experiment without Fe was conducted to verify the effects of the Fe ions. From **Figure 4.6**, it is shown that CMS membranes derived from the Fe-free polymer with the *Fast 550 °C* protocol have no C₂H₄/C₂H₆ sorption separation ability. This is consistent with the previous results showing that traditional CMS membranes have little sorption effects on olefin/paraffin separation.

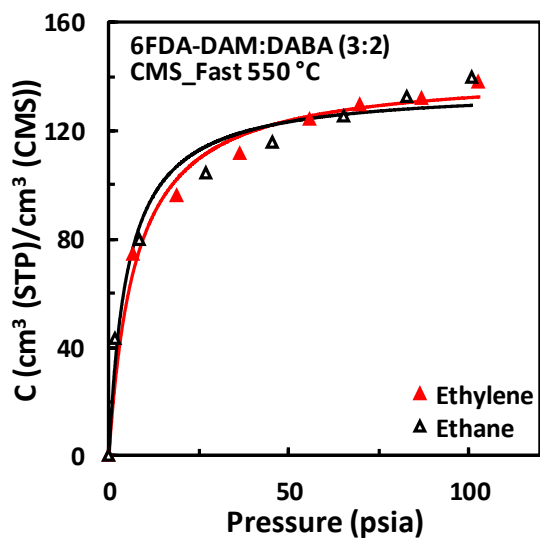


Figure 4.6. Sorption isotherms of single-component ethylene and ethane at 35 °C for Fe-free 6FDA-DAM:DABA (3:2) derived CMS membranes from Fast 550 °C pyrolysis protocol

It is believed that a particular Fe complex having selective interaction with olefins is generated within the carbon material when the Fe-containing precursor was derived from a pyrolysis protocol with a lower temperature and at a faster heating rate (e.g., *Fast 550 °C* protocol). **Figure 4.7** illustrates the conceptual interaction between ethylene and the active Fe complex in micropores of Fe-containing CMS membranes. This *Fast 550 °C* protocol will be the primary focus of successive studies in this work. The oxidation state of Fe in the active Fe complex for the increasing olefin/paraffin sorption selectivity will be discussed later.

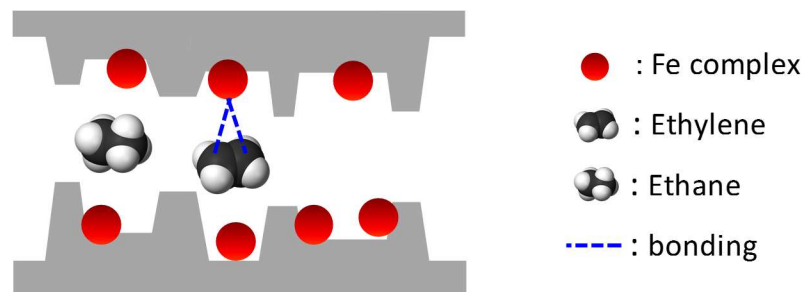


Figure 4.7. Conceptual interaction between ethylene and active Fe complex in idealized pore structures of CMS membranes

4.5.2 Olefin-Selective CMS Membranes with Fe

The results have shown that the *Fast 550 °C* protocol is suitable for improving C_2H_4/C_2H_6 sorption selectivity for Fe-containing CMS membranes. For the C3 olefin (C_3H_6), **Figure 4.8** also shows an enhancement for C_3H_6/C_3H_8 sorption selectivity at 50 psia, which increases 11% by incorporating 2.2 wt% Fe ions in the precursor. The carbon-carbon double bond in C_3H_6 , of course, also has an affinity for the active Fe complex in the Fe-containing CMS membranes derived from the *Fast 550 °C* protocol. This properly prepared CMS membrane with Fe has improved combined C2 and C3 olefin/paraffin sorption selectivity, which is promising for separation of bulk olefins (C_2H_4 and C_3H_6) from paraffins (C_2H_6 and C_3H_8). The overall permselectivity and productivity of the Fe-containing CMS membranes derived from the *Fast 550 °C* protocol will be discussed later, proving the concept of advanced olefin-selective CMS membranes with Fe.

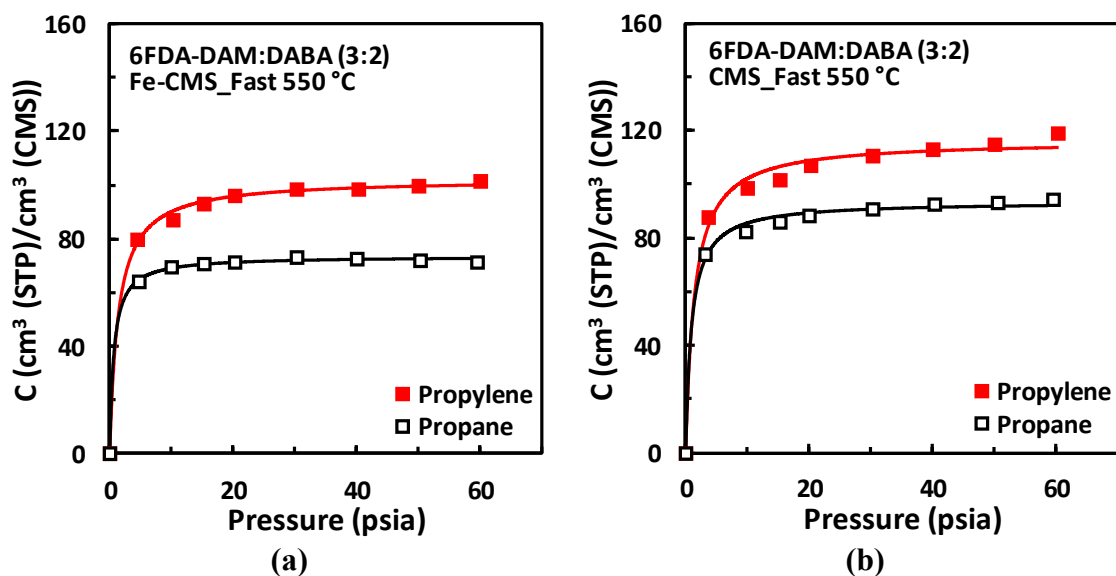


Figure 4.8. Sorption isotherms of single-component propylene and propane at 35 °C for (a) Fe-containing and (b) Fe-free 6FDA-DAM:DABA (3:2) derived CMS membranes from Fast 550 °C pyrolysis protocol

4.5.3 Effects of DABA Group in Polymer Precursor

To determine the necessity of cross-linking between Fe and polymer for uniform dispersion, 6FDA-DAM was investigated as an alternative precursor. The results (see **Figure 4.9**) show that even with the *Fast 550 °C* protocol, CMS membranes derived from the DABA-deficient precursor have similar sorption affinity for C₂H₄ and C₂H₆, probably due to clustering of the iron species, rather than uniform distribution. Therefore, it is believed that coordination with the more or less uniformly distributed DABA carboxylic acid groups within the precursor is critical for the stabilization of the Fe ions.

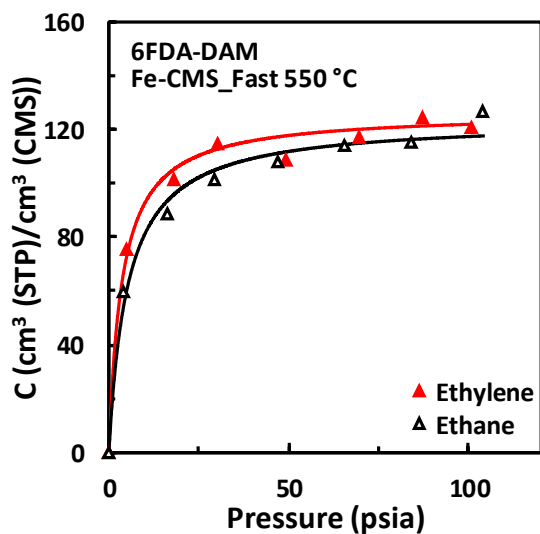


Figure 4.9. Sorption isotherms of single-component ethylene and ethane at 35 °C for Fe-containing 6FDA-DAM derived CMS membranes from Fast 550 °C pyrolysis protocol

4.6 XANES Spectra of Fe-Containing CMS Membranes

As mentioned before, the unsaturated M^{2+} cation sites in MOFs can selectively interact with olefins. It is important to better understand the relationship between the oxidation state of Fe in CMS material and its sorption performance. In this work, X-ray absorption near edge structure (XANES) analysis was performed to determine the valence state and coordination environment of Fe in the CMS membranes derived from 2.2 wt% Fe-containing 6FDA-DAM:DABA (3:2) precursor with the pyrolysis protocols of interest.

The results of XANES spectra are shown in **Figure 4.10**, with the Fe foil representing a zero-valent iron bonding and the iron(III) acetylacetonate representing a Fe^{3+} valence. The Fe-containing CMS membranes derived from the *Slow 550 °C* and *Fast/Slow 675 °C* protocols appear to be a linear combination of the $Fe(acac)_3$ and iron foil

standards as indicated by the presence of isosbestic points at 7127 and 7148 eV. Conversely, the CMS membrane derived from the *Fast 550 °C* protocol appears to have a fundamentally different XANES edge shape indicating a different coordination environment or chemistry.

Each of the XANES scans were fit as a linear combination of iron foil and Fe(acac)₃. These results are shown in **Table 4.1**. Each of the CMS membranes calcined at 675 °C and the Slow 550 °C protocol derived membrane were well-fit by the selected standards (R-factor below 0.0011 in each case). The Fe in the CMS membranes contained between 16 and 44% Fe(acac)₃ with the balance being Fe foil. The Fe-containing CMS membrane pyrolyzed at 550 °C with the fast temperature ramps was not well-fit by the selected standards. The best R-factor achieved was 0.011, which was 10 times greater than the R-factors for the other three CMS samples. This indicates that the *Fast 550 °C* protocol derived CMS membrane has an unique coordination environment of the iron species in the film compared to the others which may provide a reason for the enhancement in olefin/paraffin sorption selectivity. This finding may suggest that iron has transferred into the DABA polymer as was portrayed in **Figure 4.2**.

The X-ray absorption edge energies were determined as the peak in the first derivative plot. Fe foil (7112.0 eV) and Fe(acac)₃ (7126.6 eV) were used as standards for Fe⁰ and Fe³⁺, respectively. Using this calibration for oxidation state, the *Fast 550 °C* protocol derived CMS membrane, with an edge energy of 7122.1 eV has an average oxidation state of Fe^{+2.1}. This further suggests that Fe²⁺ from the Fe(acac)₂ starting material is being cross-linked into the DABA polymer where it is resistant to further oxidation to Fe³⁺ or reduction to Fe⁰. It is possible that if iron is not incorporated into the DABA

polymer in this way, it can convert to some combination of $\text{Fe}(\text{acac})_3$ and iron metal particles, as in the case of the other three membranes.

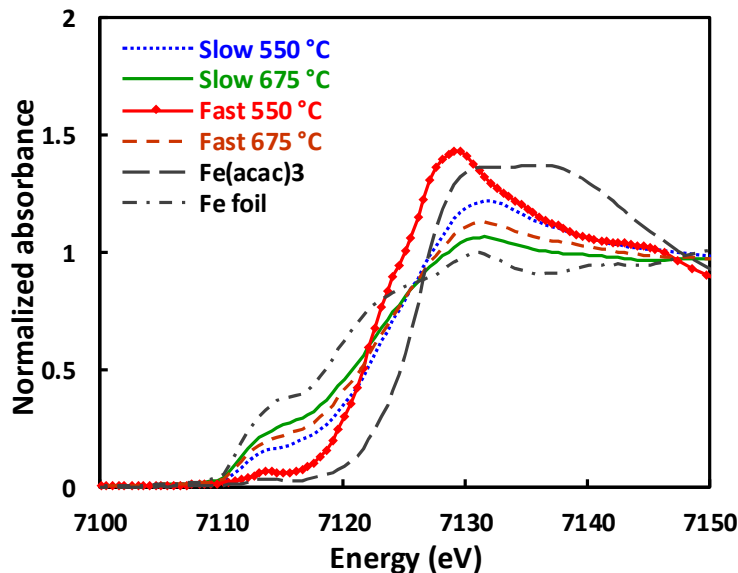


Figure 4.10. XANES spectra of Fe-containing CMS membranes derived from various pyrolysis protocols

Table 4.1. XANES linear combination fitting results

	$\text{Fe}(\text{acac})_3$ %	Fe Foil %	Fit R-Factor
Fe-CMS_Slow 550 °C	44	56	0.0009
Fe-CMS_Slow 675 °C	16	84	0.0011
Fe-CMS_Fast 550 °C		No Fit	
Fe-CMS_Fast 675 °C	28	72	0.0005

4.7 Summary and Conclusions

Fe-containing CMS membranes were successfully prepared by incorporating 2.2 wt% Fe(II) ions into the 6FDA-DAM:DABA (3:2) polymer precursor and then pyrolyzing with controlled pyrolysis protocols. When applying a protocol with a low pyrolysis temperature and a fast ramp rate (e.g., the *Fast 550 °C* protocol), the incorporation Fe into the CMS membranes can improve 19% C₂H₄/C₂H₆ sorption selectivity and 11% C₃H₆/C₃H₈ sorption selectivity relative to the controlled Fe-free CMS membranes derived from the same protocol. X-ray absorption near edge structure (XANES) was performed to determine the valence state and coordination environment of Fe in the CMS membranes. An average Fe oxidation state of between 1.4 and 2.2 is observed in the carbon material derived from the *Fast 550 °C* protocol, and this material appears to have a fundamentally different XANES edge shape relative to the carbon materials derived from other pyrolysis protocols. This finding may provide a reason for the enhancement in olefin/paraffin sorption selectivity for the *Fast 550 °C* protocol derived Fe-containing CMS membranes.

4.8 References

1. Okamoto, K. *et al.* Olefin/paraffin separation through carbonized membranes derived from an asymmetric polyimide hollow fiber membrane. *Ind. Eng. Chem. Res.* **38**, 4424–4432 (1999).
2. Hayashi, J. *et al.* Separation of ethane/ethylene and propane/propylene systems with a carbonized BPDA–pp ‘ODA polyimide membrane. *Ind. Eng. Chem. Res.* **35**, 4176–4181 (1996).
3. Rungta, M., Zhang, C., Koros, W. J. & Xu, L. Membrane-based ethylene/ethane separation: The upper bound and beyond. *AIChE J.* **59**, 3475–3489 (2013).
4. Rungta, M. Carbon molecular sieve dense film membranes for ethylene/ethane separations. (Georgia Institute of Technology, 2012).
5. Zhou, H.-C., Long, J. R. & Yaghi, O. M. Introduction to Metal–Organic Frameworks. *Chem. Rev.* **112**, 673–674 (2012).
6. Bloch, E. D. *et al.* Hydrocarbon separations in a metal-organic framework with open iron (II) coordination sites. *Science (80-.)*. **335**, 1606–1610 (2012).
7. Geier, S. J. *et al.* Selective adsorption of ethylene over ethane and propylene over propane in the metal–organic frameworks M2(dobdc) (M = Mg, Mn, Fe, Co, Ni, Zn). *Chem. Sci.* **4**, 2054–2061 (2013).
8. Ruthven, D. M. Molecular Sieve Separations. *Chemie-Ingenieur-Technik* **83**, 44–52 (2011).
9. Yoshimune, M., Fujiwara, I., Suda, H. & Haraya, K. Gas transport properties of carbon molecular sieve membranes derived from metal containing sulfonated poly (phenylene oxide). *Desalination* **193**, 66–72 (2006).
10. Yoda, S. *et al.* Preparation of a platinum and palladium/polyimide nanocomposite film as a precursor of metal-doped carbon molecular sieve membrane via supercritical impregnation. *Chem. Mater.* **16**, 2363–2368 (2004).
11. Barsema, J. N., van derVegt, N. F. A., Koops, G. H. & Wessling, M. Ag-Functionalized Carbon Molecular-Sieve Membranes Based on Polyelectrolyte/Polyimide Blend Precursors. *Adv. Funct. Mater.* **15**, 69–75 (2005).
12. Kim, Y. K., Park, H. B. & Lee, Y. M. Carbon molecular sieve membranes derived from metal-substituted sulfonated polyimide and their gas separation properties. *J. Memb. Sci.* **226**, 145–158 (2003).
13. Barsema, J. N., Balster, J., Jordan, V., Van derVegt, N. F. A. & Wessling, M. Functionalized carbon molecular sieve membranes containing Ag-nanoclusters. *J.*

Memb. Sci. **219**, 47–57 (2003).

14. Taubert, A., Wind, J. D., Paul, D. R., Koros, W. J. & Winey, K. I. Novel polyimide ionomers: CO₂ plasticization, morphology, and ion distribution. *Polymer (Guildf)*. **44**, 1881–1892 (2003).
15. Rungta, M., Xu, L. & Koros, W. J. Carbon molecular sieve dense film membranes derived from Matrimid® for ethylene/ethane separation. *Carbon N. Y.* **50**, 1488–1502 (2012).
16. Hou, Y., Xu, Z. & Sun, S. Controlled synthesis and chemical conversions of FeO nanoparticles. *Angew. Chemie* **119**, 6445–6448 (2007).

CHAPTER 5. INVESTIGATION OF EFFECTS OF IRON LOADINGS & STUDIES ON ALTERNATIVE METAL SPECIES FOR OLEFIN-SELECTIVE CARBON MOLECULAR SIEVE MEMBRANES

5.1 Overview

The preliminary results in [Chapter 4](#) show that when applying the *Fast 550 °C* protocol, the incorporation of Fe(II) ions in the carbon molecular sieve (CMS) membranes can improve olefin/paraffin separation efficiency in sorption. [Section 5.2](#) pursues advanced olefin-selective CMS membranes by studying the effects of Fe(II) loading between 1.1 and 3.2 wt% on mixed olefin/paraffin separation. The stability of the 2.2 wt% Fe(II)-containing CMS membrane is reported in [Section 5.3](#). Effects of alternative metal species, including Fe(III), Al(III), Ni(II), Mn(II), and Mn(III), are discussed in [Section 5.4](#).

5.2 Effects of Fe Loadings in CMS Membranes

Earlier work presented herein has shown that CMS membranes derived from 2.2 wt% Fe-containing 6FDA-DAM:DABA (3:2) precursor with the *Fast 550 °C* protocol have improved C2 and C3 olefin/paraffin sorption selectivity. It is hypothesized that higher loading of Fe can further improve the separation performance. In the current work, as noted earlier, Fe loadings between 1.1 and 3.2 wt% in the precursor were studied, and the higher Fe loading could not be pursued due to gelation issue during the formation of Fe-containing polymer precursor films, resulting from high ionic cross-linking density between Fe ions and the DABA group. Although the DABA moiety limits the loading of Fe during polymer

film casting, the moiety appears to be necessary for uniformly distributed Fe ions and the enhancement in olefin/paraffin sorption selectivity. This gelation issue could be overcome by incorporating Fe ions during the polyimide synthesis process or infusing Fe ions into the polymer. However, to avoid complexity, the current work did not pursue the above approaches for increasing Fe loading, but instead, focuses on understanding the effects of Fe on olefin/paraffin separation, and the range of Fe loading studied in this work is adequate to that end.

There are several studies on olefin/paraffin separation with C2 or C3 binary mixtures¹, and some studied pure C2 and C3 hydrocarbons². However, only few researchers investigated membrane separation with mixed C2 and C3 hydrocarbons³. In the current work, a quaternary mixture consisting C2 and C3 hydrocarbons was used for permeation measurements. The feed is specifically designed for the use in the hybrid membrane-distillation system reported previously³. The Fe-containing CMS membranes were prepared with the *Fast 550 °C* protocol and then exposed to the 50 psia multi-component mixed gas at 35 °C. Gas permeabilities and selectivities of selected olefin/paraffin pairs are shown in **Figure 5.1 (a)** and **(b)**, where error bars represent standard deviations from multiple film measurements. The large error bars for C₃H₈ related results were caused by the limit of detection in gas chromatography (GC) for the low C₃H₈ concentration (< 0.05 mole%) in the permeate sides for Fe-containing CMS membranes. The compositions of each gas in the feed and the permeate streams are shown in **Table 5.1**.

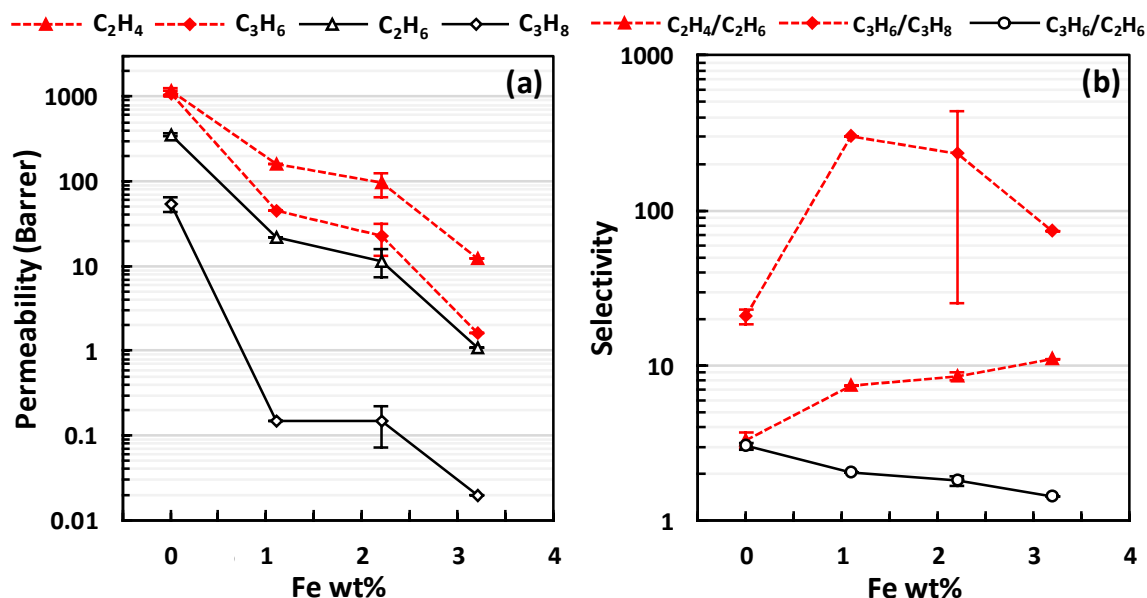
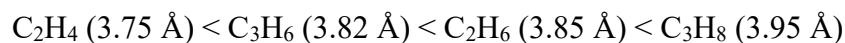


Figure 5.1. Effects of Fe loading on (a) gas permeability and (b) selectivity at 35 °C for 6FDA-DAM:DABA (3:2) derived CMS membranes from Fast 550 °C pyrolysis protocol (50 psia quaternary mixture feed)

Table 5.1. Compositions of feed and permeate streams for CMS membranes derived from 6FDA-DAM:DABA (3:2) precursor with various Fe loadings (50 psia quaternary mixture feed at 35 °C)

		0 wt% Fe	1.1 wt% Fe	2.2 wt% Fe	3.2 wt% Fe
Feed (mol%)		Permeate (mol%)			
C ₂ H ₄	54.6	73.28 ± 3.08	89.45	91.21 ± 0.73	93.93
C ₃ H ₆	15.1	18.92 ± 2.35	6.78	5.41 ± 0.60	3.38
C ₂ H ₆	17.0	6.67 ± 0.53	3.75	3.35 ± 0.16	2.64
C ₃ H ₈	13.3	0.83 ± 0.20	0.02	0.04 ± 0.02	0.04

As shown in **Figure 5.1 (a)**, CMS membranes *without* Fe have olefin-selective potential based on higher combined permeation of C₂H₄ and C₃H₆ than that of C₂H₆ and C₃H₈. This trait of traditional CMS membranes has been observed previously³ and is hypothesized to be due to the rigid size-selective ultramicropores in the carbon materials that can restrict molecules with bulky morphologies. The size of light olefins and paraffins are studied with calibrated slits and space filling CPK models, and it shows the following order in size:



As C₃H₆ is only slightly more compact in molecular sieving size than C₂H₆, CMS membranes still have the ability to perform mixed olefin/paraffin separation. However, the separation efficiency needs to be improved.

Incorporation of Fe into the membranes was proposed for improving mixed olefin/paraffin sorption selectivity and overall permselectivity. A trend was found in **Figure 5.1 (a)** that permeation of each gas decreases with the increasing loading of Fe in the membranes, and C₃H₈ is most impacted. From **Figure 5.1 (b)**, the C₂ pair selectivity increases with higher Fe loadings, and the enhancement is much higher than that has been seen in the previous sorption selectivity study. In addition to improving olefin/paraffin sorption selectivity, the Fe complex also alters the molecular sieve window and has effects on gas diffusions, which will be discussed in [Section 6.3.1](#). On the other hand, the selectivity of larger olefin over smaller paraffin (C₃H₆/C₂H₆) decreases with the increasing Fe loading in the membranes, which does not meet our expectation for developing an advanced olefin-selective membrane. However, integrating Fe ions in CMS membranes is

valuable to promote challenging C2 pair separation with increasing overall selectivity. Hence, the successive work will focus on C₂H₄/C₂H₆ separation for Fe-containing CMS membranes. The trade-off in terms of overall permselectivity and productivity of the various CMS samples (Fe-containing and Fe-free CMS materials derived from different pyrolysis temperatures) will be discussed later.

5.3 Stability of Fe-Containing CMS Membranes

Stability of Fe-containing CMS membranes derived from 2.2 wt% Fe-containing 6FDA-DAM:DABA (3:2) precursor with the *Fast 550 °C* protocol was investigated by continuous testing using the 50 psia multi-component mixed gas at 35 °C over a period around 60 days. **Figure 5.2 (a)** represents permeabilities of mixed olefins and paraffins, showing the transport properties of this Fe-containing CMS membrane are stable after 50 days with the continuous 50 psia feed. The permeability of C₂H₄ decreases moderately over time at the beginning and finally remains higher than 76% of the initial value. This initial decrease in permeability is due to the CMS pore relaxation. The pores in CMS materials have been reported to relax over time to reach some equilibrium state⁴. For the selectivities, C2 pair selectivity and C₃H₆/C₂H₆ selectivity remain high around 9 and 2, respectively. The large deviation of C3 pair selectivity is caused by test limitation of gas chromatography. Since the selectivities do not drop, it is believed that the Fe complex in the CMS membranes derived from the *Fast 550 °C* protocol is stable for olefin/paraffin separation.

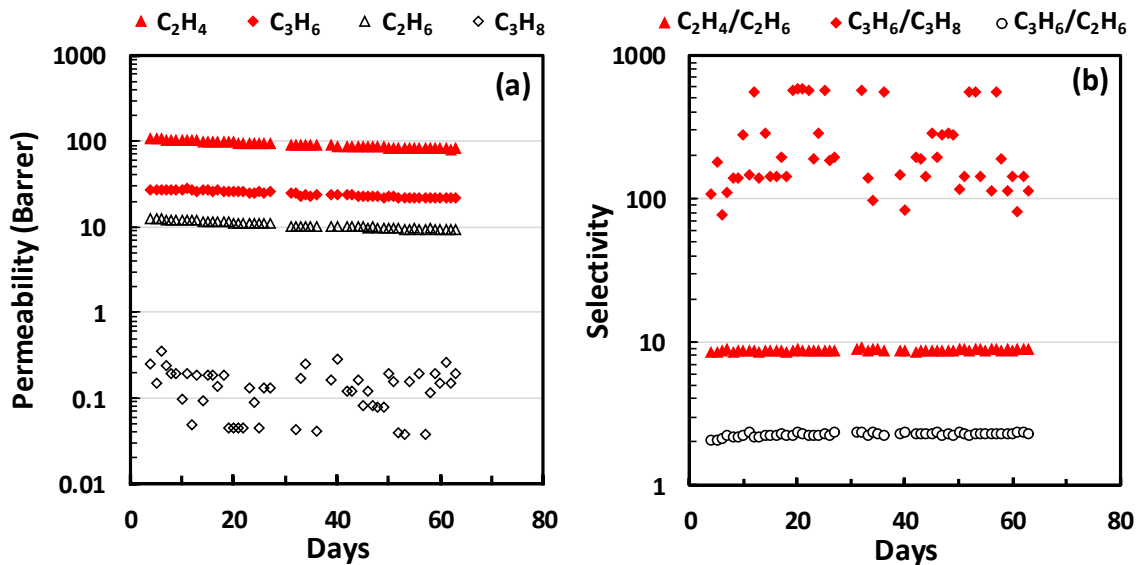


Figure 5.2. (a) Gas permeability and (b) selectivity at 35 °C over ~60 testing days for Fe-containing 6FDA-DAM:DABA (3:2) derived CMS membranes from Fast 550 °C pyrolysis protocol (50 psia quaternary mixture feed)

5.4 Effects of Metal Species for Metal-Containing CMS Membranes

In this work, Fe(II) was chosen as the incorporated metal into CMS membranes based on a combination of factors including high C_2H_4/C_2H_6 adsorption selectivity⁵, low cost, and stability against contaminants. The Fe-containing CMS membranes have shown improved olefin/paraffin separation. Besides Fe(II), there are alternative metal species that may be incorporated into CMS membranes for tuning olefin/paraffin separation. Previous studies have shown that open Fe(II) and Mn(II) coordination sites in the MOF material, $M_2(\text{dobdc})$ ($\text{dobdc}^{4-} = 2,5\text{-dioxido-1,4-benzenedicarboxylate}$; $M = \text{Mg, Mn, Fe, Co, Ni, Zn}$) exhibit the highest adsorption selectivities for the separation of C2 and C3 pairs, respectively⁵. In the current work on metal-containing carbon membranes, besides Fe(acac)₂, other metal acetylacetonates were studied as well, including Fe(acac)₃,

Al(acac)₃, Ni(acac)₂, Mn(acac)₂, and Mn(acac)₃. Two other Fe(II) compounds, FeCl₂, and Fe(ac)₂, were also studied. The chemical structures of the studied metal salts were shown previously in **Table 3.2**.

As described in Section 3.3.1, 0.05 g metal salts were dissolved in 5 ml tetrahydrofuran (THF) as metal-containing solutions for casting polymer films. Among the metal salts studied, only Fe(acac)₂, Fe(acac)₃, and Al(acac)₃ were completely dissolved in THF, and polymer films derived from these metal salts were successfully made. For other metal salts, there were particle settling in the THF solutions even when the solutions were mixed on a Wrist Action Shaker machine overnight. There are alternative paths to overcome this challenge in the formation of metal-containing polymer films by using other metal salts/solvents or pursuing other procedures for the film formation, as will be discussed in Chapter 8. However, to avoid complexity, the current work focuses on comparing effects of Fe(II) and other metal species on the performance of metal-containing CMS membranes, and Fe(III) and Al(III) are adequate for the controlled experiments.

Polymer films were prepared from THF solutions with 0.5 g 6FDA-DAM:DABA (3:2) and 0.05 g metal salts [Fe(acac)₂, Fe(acac)₃, and Al(acac)₃]. The dried polymer films were then derived into CMS membranes by applying the *Fast 550 °C* protocol. The membranes were tested using the 50 psia multi-component mixed gas at 35 °C, and the separation performance is shown in **Figure 5.3 (a)** and **(b)**. Due to GC testing limitation, the C₃H₈ permeabilities were unavailable for Fe(III)- and Al(III)-containing CMS membranes.

The incorporation of Fe(II) or Fe(III) reduces the gas permeability to a similar range; however, the Fe(II)-containing CMS membranes have 47% higher C₂H₄/C₂H₆ permselectivity and 12% higher C₃H₆/C₂H₆ permselectivity than that of the Fe(III)-containing CMS membranes. The permselectivity can be decoupled into a sorption factor and a diffusion factor. Previous results in this work have shown that CMS membranes with Fe(II) have C₂H₄/C₂H₆ *sorption selectivity* of 1.19. On the other hand, the sorption isotherms of single-component ethylene and ethane at 35 °C for the Fe(III)-containing CMS membranes are shown in **Figure 5.4**, and clearly, there is no C₂H₄/C₂H₆ sorption selectivity. Hence, it is hypothesized that both states of Fe alter the CMS pore morphology in a similar manner, affecting gas diffusivity. However, only the incorporation of Fe(II) can improve olefin/paraffin sorption selectivity and achieve the highest C₂H₄/C₂H₆ permselectivity. This finding supports the hypothesis that incorporation of Fe²⁺ into CMS membranes improves olefin/paraffin separation. Hence, the successive work will focus on the studies of Fe(II)-containing CMS membranes, and Fe(acac)₂ were used as the starting material unless otherwise stated.

The CMS film derived from Al(III)-containing precursor is relatively permeable with much lower C₂H₄/C₂H₆ selectivity. Previous studies have shown that aluminum oxide can be formed by pyrolysis of Al(acac)₃ at 420°C under an argon atmosphere⁶. The hypothesis for such permeable CMS film is that Al formed rather large particles (Al₂O₃) that disrupt packing of the turbostratic CMS structures, thereby lowering the selectivity, while increasing permeability.

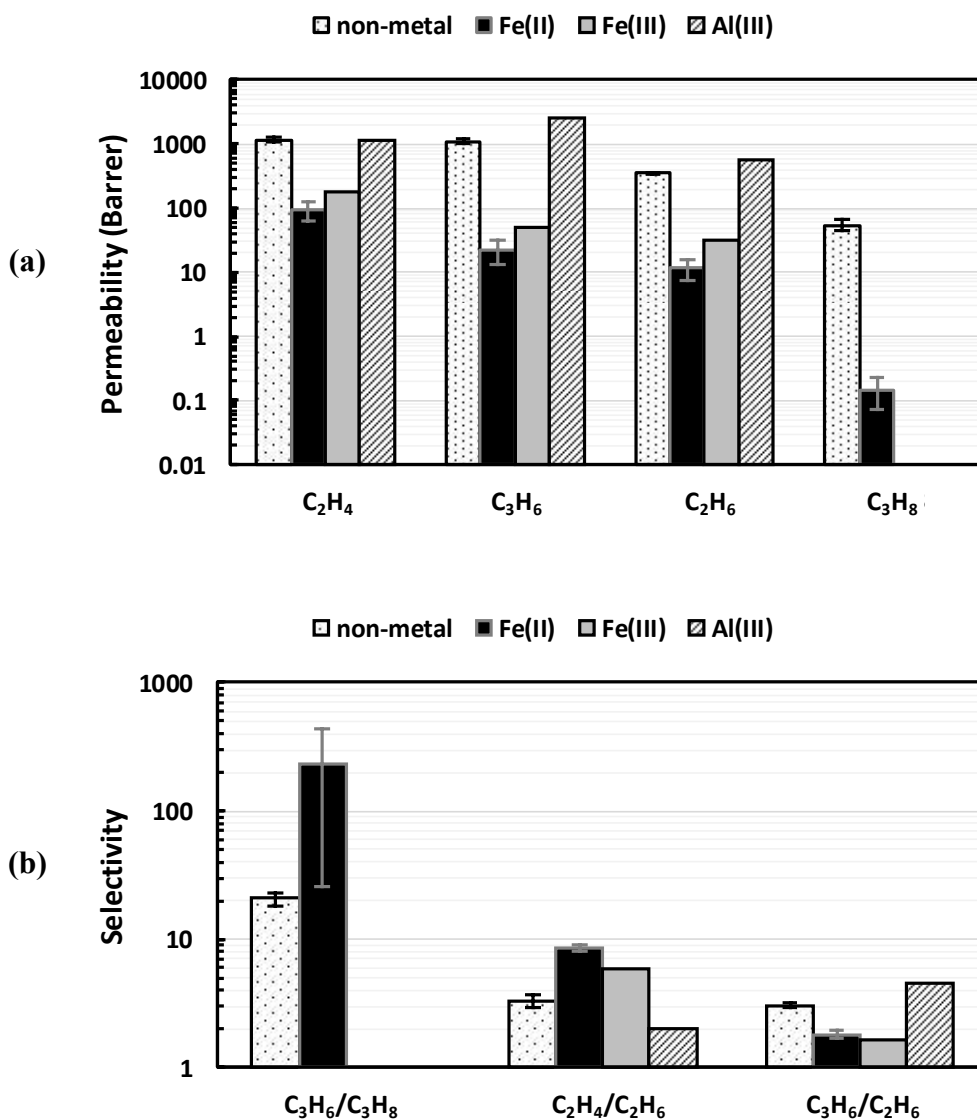


Figure 5.3. Effects of metal species on (a) gas permeability and (b) selectivity at 35 °C for 6FDA-DAM:DABA (3:2) derived CMS membranes from Fast 550 °C pyrolysis protocol (50 psia quaternary mixture feed) (partial C₃H₈ related results were unavailable due to GC testing limitation)

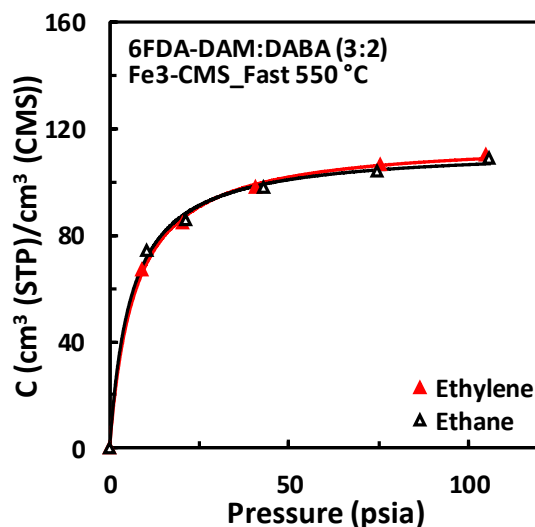


Figure 5.4. Sorption isotherms of single-component ethylene and ethane at 35 °C for Fe(III)-containing 6FDA-DAM:DABA (3:2) derived CMS membranes with Fast 550 °C pyrolysis protocol

5.5 Summary and Conclusions

Fe-containing CMS membranes for mixed olefin/paraffin separation were studied by using 6FDA-DAM:DABA (3:2) and $\text{Fe}(\text{acac})_2$ as the starting materials and applying the *Fast 550 °C* pyrolysis protocol. The loadings of Fe(II) ions in the polymer precursor between 1.1 and 3.2 wt% were investigated, and it was found the incorporation of Fe into the membranes is an applicable approach to tuning olefin/paraffin separation performance. Although Fe does not promote $\text{C}_3\text{H}_6/\text{C}_2\text{H}_6$ selectivity, a significant $\text{C}_2\text{H}_4/\text{C}_2\text{H}_6$ permselectivity near 11 with C_2H_4 permeability above 10 Barrers was observed for the 3.2 wt% Fe loading case. Moreover, the extensively studied 2.2 wt% Fe-containing CMS membranes show stable mixed olefin/paraffin separation performance over 60 testing days. Alternative metal species were explored for the metal-containing CMS membranes, and among the studied metal salts, $\text{Fe}(\text{acac})_2$ leads to the highest olefin/paraffin selectivity.

5.6 References

1. Hayashi, J. *et al.* Separation of ethane/ethylene and propane/propylene systems with a carbonized BPDA–pp ‘ODA polyimide membrane. *Ind. Eng. Chem. Res.* **35**, 4176–4181 (1996).
2. Naghsh, M., Sadeghi, M., Moheb, A., Chenar, M. P. & Mohagheghian, M. Separation of ethylene/ethane and propylene/propane by cellulose acetate–silica nanocomposite membranes. *J. Memb. Sci.* **423**, 97–106 (2012).
3. Xu, L. *et al.* Olefins-selective asymmetric carbon molecular sieve hollow fiber membranes for hybrid membrane-distillation processes for olefin/paraffin separations. *J. Memb. Sci.* **423**, 314–323 (2012).
4. Wenz, G. B. & Koros, W. J. Tuning carbon molecular sieves for natural gas separations: A diamine molecular approach. *AIChE J.* **63**, 751–760 (2017).
5. Geier, S. J. *et al.* Selective adsorption of ethylene over ethane and propylene over propane in the metal–organic frameworks M₂(dobdc) (M = Mg, Mn, Fe, Co, Ni, Zn). *Chem. Sci.* **4**, 2054–2061 (2013).
6. Ajayi, O. B., Akanni, M. S., Lambi, J. N., Jeynes, C. & Watts, J. F. Compositional studies of various metal oxide coatings on glass. *Thin Solid Films* **185**, 123–136 (1990).

CHAPTER 6. ANALYSIS OF EFFECTS OF IRON ON PERFORMANCE OF IRON-CONTAINING CARBON MOLECULAR SIEVE MEMBRANES

6.1 Overview

The preliminary results in [Chapter 4](#) show that when applying a low pyrolysis temperature and a fast ramp rate (e.g., the *Fast 550 °C* protocol), the incorporation of Fe ions in the carbon molecular sieve (CMS) membranes can improve olefin/paraffin separation in sorption. As permeation performance is more attractive for separation applications, this chapter focuses on the effects of Fe on olefin/paraffin separation in permeation. [Section 6.2](#) introduces transport properties for the Fe-containing 6FDA-DAM:DABA (3:2) polymer precursor, as well as the pure polymer precursor. [Section 6.3](#) discusses multi-component mixed gas permeation results for Fe-containing CMS membranes derived from various pyrolysis protocols. The effects of Fe ions on pore size distribution of the resulting CMS membranes are reported in this chapter as well.

6.2 Transport Properties of Polymer Precursors

This section studies the separation performance of the precursors for CMS membranes. The DABA-containing polyimide, 6FDA-DAM:DABA (3:2), was used as the precursor, and the Fe-containing polymer precursor has a theoretical concentration of Fe around 2.2 wt%. The permeation and the sorption performance of the membranes were measured with single-component C_2H_4 and C_2H_6 feeds at 35 °C.

6.2.1 Permeation Performance

The permeation performance of single-component C_2H_4 and C_2H_6 at 35 °C for the pure 6FDA-DAM:DABA (3:2) polymer precursor and the Fe-containing polymer precursor is shown in **Table 6.1**. The pure polymer precursor has C_2H_4 permeation of 3.44 Barrers and a C_2H_4/C_2H_6 permselectivity of 4.10. The incorporation of Fe ions in the membranes have little influence on the permeation performance for the polymer precursor. This little change suggests that the 2.2 wt% of Fe ions have been incorporated homogeneously in the polymer on a fine scale and there is no cluster in the polymer matrix.

Table 6.1. Permeation performance of C_2H_4 and C_2H_6 (50 psia) at 35 °C for Fe-free and Fe-containing 6FDA-DAM:DABA (3:2) polymer precursors

	$P_{C_2H_4}$ (Barrer)	$P_{C_2H_6}$ (Barrer)	$\alpha_{C_2H_4/C_2H_6}$
Fe-free polymer precursor	3.44	0.84	4.10
Fe-containing polymer precursor	4.44	1.1	4.04

The C_2H_4/C_2H_6 separation performance of the chosen polymer precursor in this work was compared with the performance of other reported polyimides¹, as listed in **Figure 6.1**. As seen in the figure, the 6FDA-DAM:DABA (3:2) polymer membranes have competitive olefin/paraffin separation performance based on their position relative to the experimentally observed C_2H_4/C_2H_6 upper bound for polymers². Even with the Fe

incorporation, that the DABA carboxylic acid group provides opportunity to tune the properties of the membranes by incorporating transition metal ions in the polymer precursor. The simpler 6FDA-DAM polymer and the non-DABA containing 6FDA-BPDA-DAM polymer have similar selectivity and much higher permeabilities. All the polymer precursors show the separation performance on or below the polymer upper bound. It is more attractive to study the separation performance of CMS membranes derived from the DABA-containing polymer precursor, which is discussed in [Section 6.3](#).

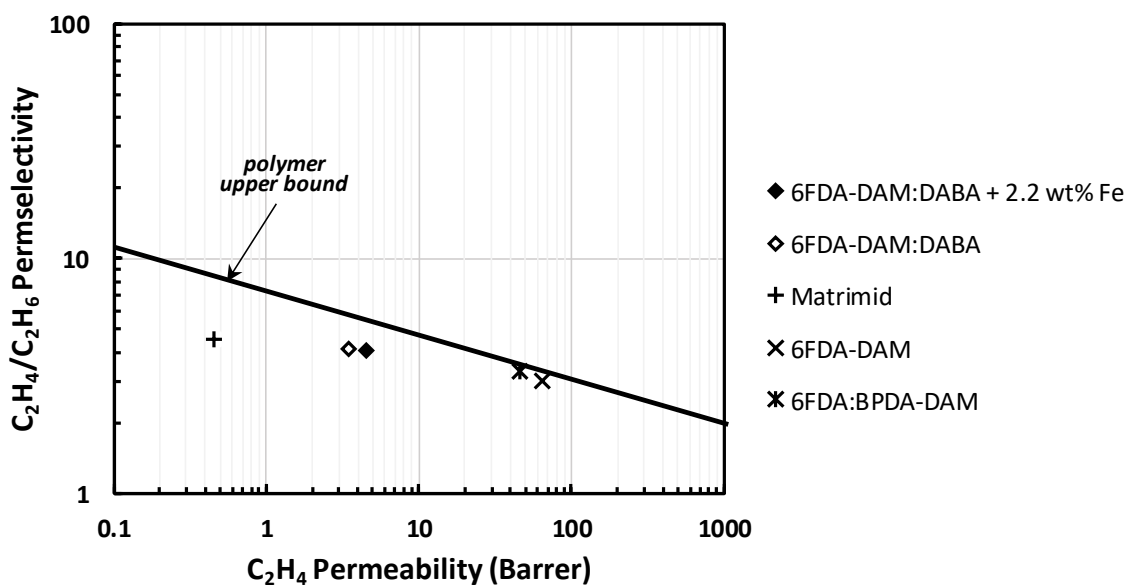


Figure 6.1. Relationship between pure C_2H_4 permeability and C_2H_4/C_2H_6 permselectivity at 35 °C for various polymer precursors (results of non-DABA polyimides are reproduced from reported data¹)

6.2.2 Sorption Performance

The interactions between olefin and the precursors were determined by conducting pressure decay sorption measurements with single-component C₂H₄ and C₂H₆ at 35 °C. The experimental results were fitted with the dual sorption mode model (see **Equation 2.8**) to obtain sorption isotherms, and the plots show sorption concentration in terms of cm³(STP)/cm³ (precursor) as a function of equilibrium pressure for the gas of interest. The olefin/paraffin sorption selectivities were calculated at 50 psia with the fitting parameters.

The sorption isotherms of single-component C₂H₄ and C₂H₆ for the pure 6FDA-DAM:DABA (3:2) polymer precursor and the Fe-containing polymer precursor are shown in **Figure 6.2 (a)** and **(b)**, respectively, and their sorption performance at 50 psia is also presented in **Table 6.2**. The results show that the incorporation of Fe ions in the membranes can increase the sorption affinity to both C₂H₄ and C₂H₆ by around 19% at 50 psia. However, surprisingly, the Fe ions in the polymer do not have sorption preference in olefin, and the C₂H₄/C₂H₆ sorption selectivity remains as low as 1.07 even with Fe ions incorporated in the polymer precursor. Perhaps the complexation of the Fe ions and the DABA groups renders the Fe²⁺ less attractive to the olefins than might be expected, based on the intrinsic attraction between Fe²⁺ and olefins³. As mentioned in Chapter 4, with properly controlled pyrolysis protocols, which removes the DABA groups, the Fe-containing polymer precursor can turn into CMS membranes with improved olefin/paraffin sorption selectivity. Hence, this work focuses on the study of CMS membranes, as discussed in Section 6.3.

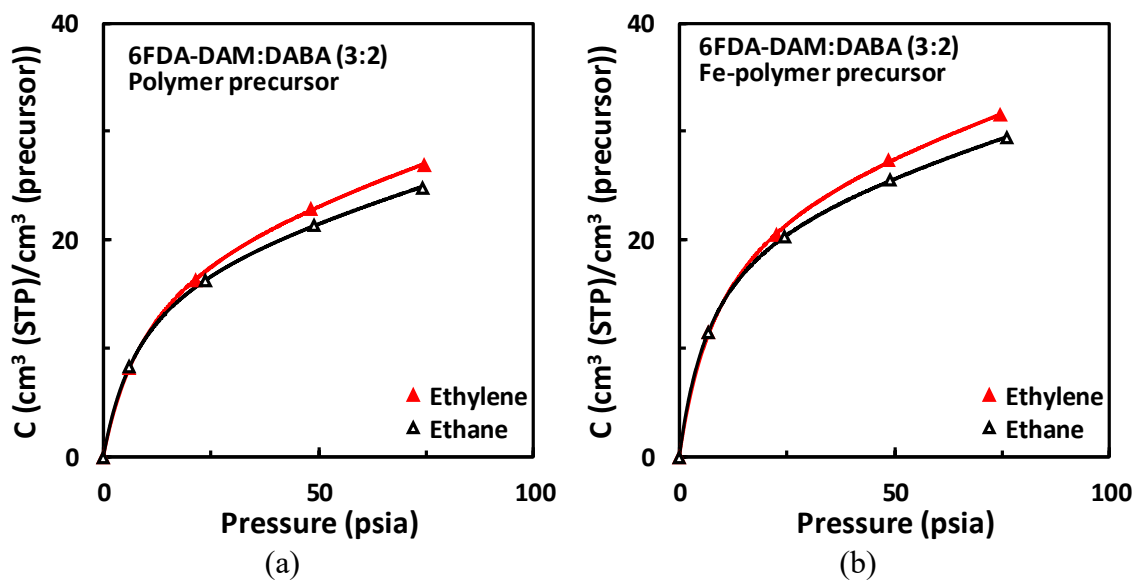


Figure 6.2. Sorption isotherms of single-component ethylene and ethane at 35 °C for (a) Fe-free and (b) Fe-containing 6FDA-DAM:DABA (3:2) polymer precursors

Table 6.2. Sorption performance of C₂H₄ and C₂H₆ (50 psia) at 35 °C for Fe-free and Fe-containing 6FDA-DAM:DABA (3:2) polymer precursors

	$S_{C_2H_4}$	$S_{C_2H_6}$	$\alpha_{C_2H_4/C_2H_6}$
	$\left[\frac{\text{cm}^3(\text{STP})}{\text{cm}^3(\text{precursor}) \cdot \text{cmHg}} \right]$	$\left[\frac{\text{cm}^3(\text{STP})}{\text{cm}^3(\text{precursor}) \cdot \text{cmHg}} \right]$	
Fe-free polymer precursor	0.089	0.083	1.07
Fe-containing polymer precursor	0.106	0.099	1.07

6.2.3 Diffusion Performance

The diffusion coefficients of single-component C₂H₄ and C₂H₆ for the pure 6FDA-DAM:DABA (3:2) polymer precursor and the Fe-containing polymer precursor were back-calculated from permeation and sorption coefficients by using **Equation 2.3**. The diffusion performance is shown in **Table 6.3**. While the precursors have no C₂H₄/C₂H₆ sorption selectivity, the permselectivity is dominated by diffusion selectivity. However, the incorporation of Fe ions in the membranes have little influence on the diffusion performance for the polymer precursor.

Table 6.3. Diffusion performance of C₂H₄ and C₂H₆ (50 psia) at 35 °C for Fe-free and Fe-containing 6FDA-DAM:DABA (3:2) polymer precursors

	$\bar{D}_{C_2H_4}$ (10 ⁻⁹ cm ² /s)	$\bar{D}_{C_2H_6}$ (10 ⁻⁹ cm ² /s)	$\alpha_{C_2H_4/C_2H_6}$
Fe-free polymer precursor	3.86	1.01	3.81
Fe-containing polymer precursor	4.19	1.11	3.77

6.3 Transport Properties of CMS Membranes

This section studies the separation performance of CMS membranes derived from the Fe-containing 6FDA-DAM:DABA (3:2) polyimide. Effects of Fe complex on the size distribution of discriminating ultramicropore in the Fe-containing CMS membranes are analyzed by examining the results from single-component gas permeation and sorption

measurements at 35 °C. Results of mixed olefin/paraffin separation for the CMS membranes derived from various pyrolysis protocols were reported in this section as well.

6.3.1 Sorption and Diffusion Factors in Separation Efficiency

As shown in the previous section, incorporation of Fe ions into CMS membranes can improve C₂H₄/C₂H₆ separation efficiency in sorption and final permeation results. It is therefore important to understand the contribution of Fe on gas sorption and diffusion in the Fe-containing membranes. Both the pure 6FDA-DAM:DABA (3:2) polymer precursor and the 2.2 wt% Fe-containing polymer precursor were pyrolyzed with the *Fast 550* °C protocol, which is suitable for improved olefin/paraffin separation performance. The permeation and sorption performance of single-component C₂H₄ and C₂H₆ at 35 °C for the carbonized membranes were analyzed, since this allows for separating the contributions more clearly.

The relationship between pure C₂H₄ permeability and C₂H₄/C₂H₆ permselectivity for carbonized membranes and their precursors is shown in **Figure 6.3 (a)**. The CMS membrane derived from the pure 6FDA-DAM:DABA (3:2) polymer precursor has higher permeability relative to that of its precursor, due to higher sorption and diffusion coefficients. For the Fe-containing CMS membranes, the incorporation of Fe ions can increase permselectivity by a factor of 3.2 with attractive C₂H₄ permeability around 60 Barrers. This improvement can be further decoupled into a sorption factor and a diffusion factor when the sorption-diffusion model is applied.

Sorption coefficients of single-component C₂H₄ and C₂H₆ at 35 °C for the carbonized membranes and their precursors were analyzed by pressure decay sorption

measurements. As shown in **Figure 6.3 (b)**, after pyrolysis with the *Fast 550 °C* protocol, the carbonized membranes have higher C₂H₄ sorption capacity, and the incorporation of Fe ions increase sorption selectivity by a factor of 1.2. Consistent with the earlier discussion, the active Fe complex presenting in the micropores within the carbon material provides selective sorption affinity to olefins.

The diffusion coefficients of single-component C₂H₄ and C₂H₆ at 35 °C for the carbonized membranes and their precursors were back-calculated from permeation and sorption coefficients and are shown in **Figure 6.3 (c)**. The incorporation of Fe ions clearly boosts diffusion selectivity by a factor of 2.7. It is believed that the active Fe complex is attached to the edge of carbon sheets, partially blocking the larger ultramicropores in the CMS membranes.

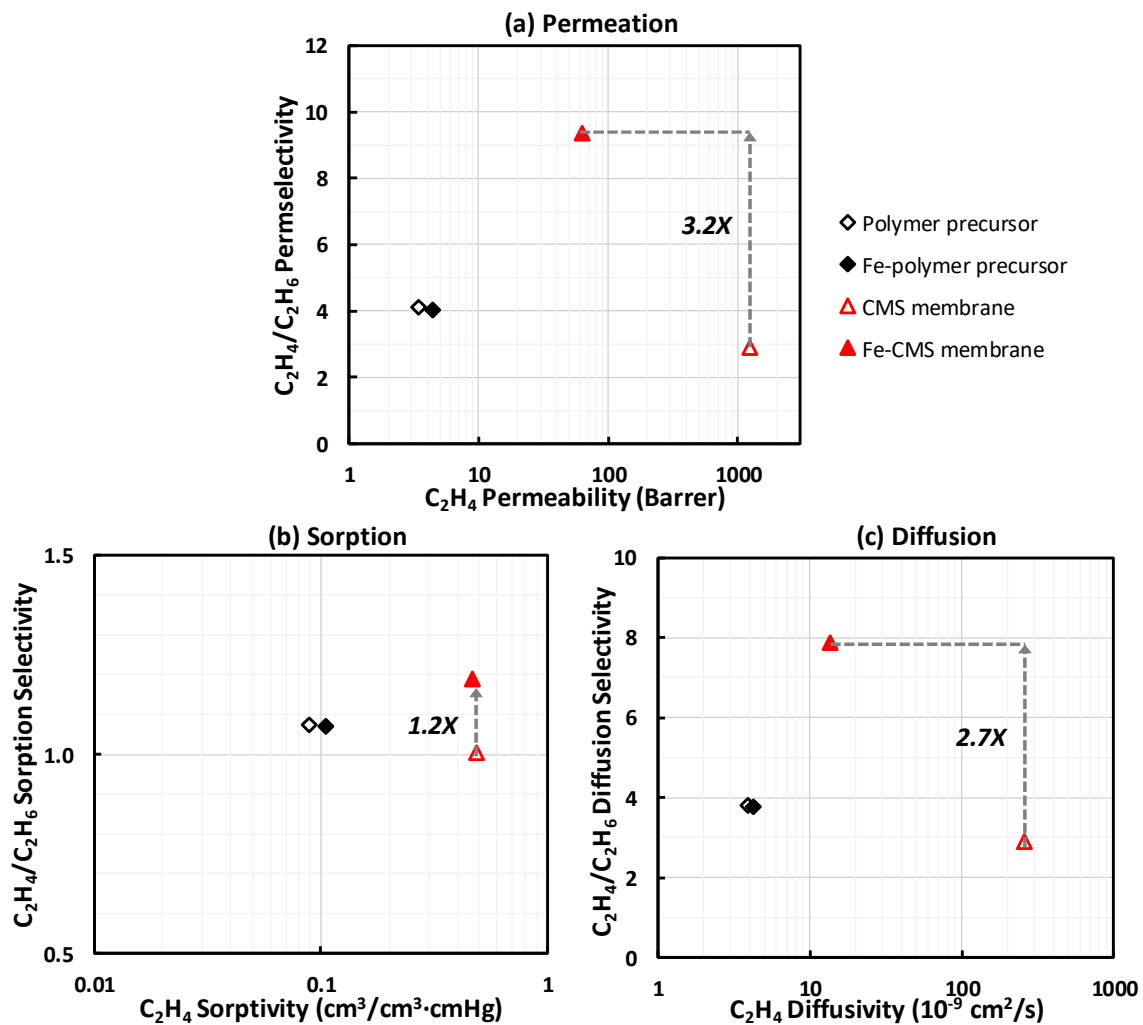


Figure 6.3. C_2H_4/C_2H_6 selectivity in (a) permeation (b) sorption and (c) diffusion at 35 °C for polymer precursors and CMS membranes derived from Fast 550 °C pyrolysis protocol (50 psia single-component gas)

The hypothetical ultramicropore size distribution in Fe-free CMS membranes is illustrated in **Figure 6.4 (a)**. The area below the distribution curve can represent the ability for gas to pass the available pores. Therefore, the C_2H_4/C_2H_6 diffusion selectivity can be represented as the total areas for C_2H_4 and C_2H_6 over the area for C_2H_6 only. For Fe-containing CMS membranes, the Fe complex appears to block the larger ultramicropores, altering the ultramicropores available to diffusion by both penetrants, with a change in the shape of the distribution curve, as illustrated in **Figure 6.4 (b)**. This change of the curve has more impact on the larger molecule, so the diffusion selectivity increases when Fe ions are incorporated into the membranes.

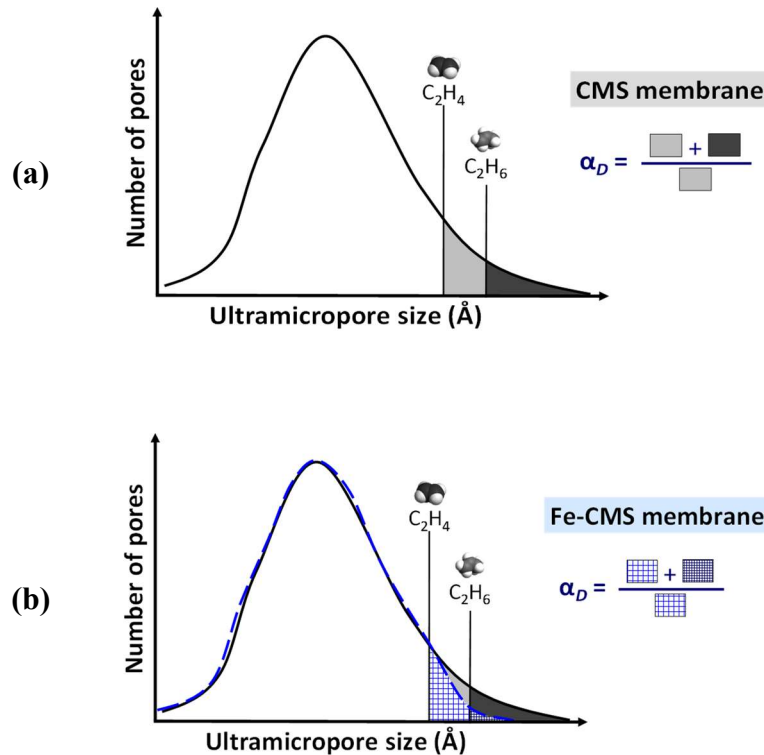


Figure 6.4. Idealized ultramicropore size distribution in (a) Fe-free CMS membranes and (b) Fe-containing CMS membranes

From the improvement of sorption and diffusion performance for the Fe-containing CMS membranes, an idealized pore structure of CMS membranes with Fe complex is proposed, as shown in **Figure 6.5**. The Fe complex, of course, must be in the micropores, providing selective affinity to olefin. However, our results suggest that some Fe complex must also be in the ultramicropores, tightening the molecular sieve window and improving olefin/paraffin diffusion selectivity. Given the XANES results, the state of the Fe in the ultramicropores versus that in the micropores may be different. This outcome reflects a desirable but more complex picture than was originally intended by incorporation of the Fe into the CMS materials.

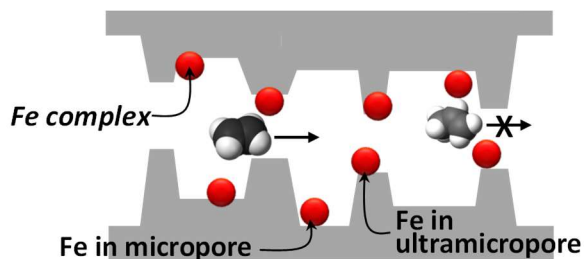


Figure 6.5. Schematic of Fe complex in ultramicropores and micropores of idealized pore structure of Fe-containing CMS membranes based on observed sorption and permeation results

6.3.2 Mixed Gas Permeation Performance

As noted before, Fe chemistry and coordination in the gas separation membranes clearly have effects on final permeation results. The trade-off in terms of overall selectivity and productivity of the various CMS samples (Fe-containing and Fe-free CMS materials

derived from different pyrolysis temperatures) is discussed in this section. The Fe-containing CMS membranes were derived from the 6FDA-DAM:DABA (3:2) polymer precursor with 1.1–3.2 wt% Fe ions, and three different pyrolysis protocols were studied: *Slow 550 °C*, *Fast 550 °C*, and *Fast 675 °C* protocols. The permeation of C2 and C3 hydrocarbons were measured at 35 °C with the 50 psia multi-component mixed gas. As Fe actually lack the ability to promote C₃H₆/C₂H₆ separation, this section only focuses on the C2 pair separation since it is more challenging than the C3 pair.

6.3.2.1 Iron-Free CMS Membranes

Controlled experiments without Fe were conducted to further probe the effects of Fe ions. As shown in **Figure 6.6**, the carbonized materials *without* Fe have C₂H₄/C₂H₆ separation performance well above the polymer upper bound⁴; however, the performance is on or below the CMS upper bound established by Salinas *et al*⁵. The separation performance is further improved by incorporating Fe ions into the membranes. When pyrolyzed at a lower temperature, CMS membranes without Fe derived from the *Slow 550 °C* and the *Fast 550 °C* protocols have similar separation performance for the slow and fast ramp rate and soak. On the other hand, when the pyrolysis temperature increases to 675 °C, the C₂H₄/C₂H₆ permselectivity increases to 4.72 and the C₂H₄ permeability drops to ~300 Barrers. Increasing the pyrolysis temperature for the Fe-free precursors offers an opportunity to tune the performance of CMS membranes, and this situation is not due to changes in sorption selectivity. These results suggest that both micropores and ultramicropores in CMS membranes become more tightened at the higher temperature (as

illustrated in **Figure 6.7**), resulting in a small increase in selectivity and a decrease in permeability.

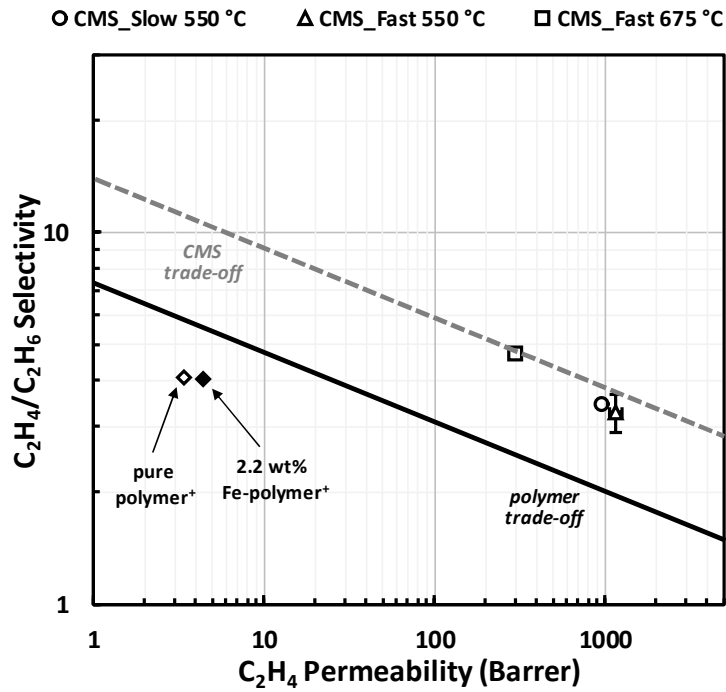


Figure 6.6. C_2H_4/C_2H_6 mixed-gas permeation results at 35 °C for Fe-free 6FDA-DAM:DABA (3:2) derived CMS membranes from various pyrolysis protocols (50 psia quaternary mixture feed)

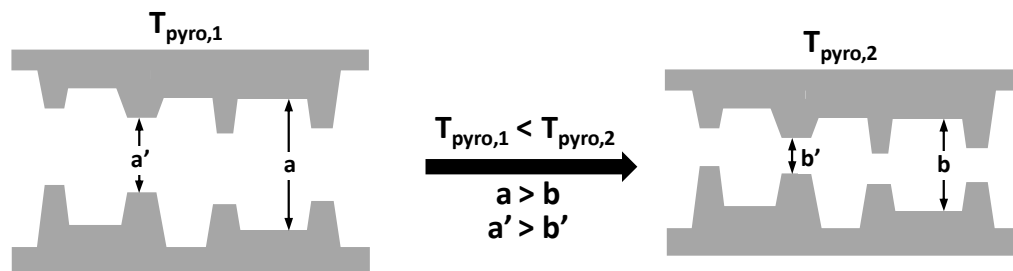


Figure 6.7. Effects of final pyrolysis temperature (T_{pyro}) on idealized pore structures of CMS membranes

6.3.2.2 Iron-Containing CMS Membranes

The Fe-containing CMS membranes were studied in the same manner described previously. As shown in **Figure 6.8**, for the 2.2 wt% Fe-containing CMS membranes, increasing pyrolysis temperature from 550 °C to 675 °C can also tune the olefin/paraffin separation performance. However, the *Fast 550 °C* protocol leads to the highest $\text{C}_2\text{H}_4/\text{C}_2\text{H}_6$ permselectivity of 8.53 ± 0.47 with ~ 100 Barrers C_2H_4 permeability, which is above the CMS upper bound⁵. Clearly, the incorporation of 2.2 wt% Fe ions results in a 1.6 fold increase in the mixed gas permselectivity when the *Fast 550 °C* protocol is applied. This improved performance is based on the Fe complex in CMS membranes improving sorption and diffusion separation efficiency. As discussed previously, higher Fe loading further promotes C_2 pair separation with increasing overall selectivity. Significant results of C_2H_4 permeability above 10 Barrers and $\text{C}_2\text{H}_4/\text{C}_2\text{H}_6$ permselectivity near 11 were achieved with the 3.2 wt% Fe-containing CMS membrane derived from the *Fast 550 °C* protocol. This olefin/paraffin separation performance is competitive with the recent studied PIM-polyimide derived CMS made at 800 °C^{5,6}, as seen in **Figure 6.8**. Clearly, adding more Fe into the 6FDA-DAM:DABA (3:2) or into the PIM-polyimide shown in **Figure 6.8** by

Salinas *et al.* will further increase selectivity for the important gas pair. Most importantly, the approach shown here illustrates a new tool to tailor selectivity and permeability properties for olefin/paraffin pair. Moreover, the increased diffusion selectivity demonstrated here with Fe incorporation may be a broadly applicable approach to tuning diffusion selectivity even for non olefin/paraffin pairs.

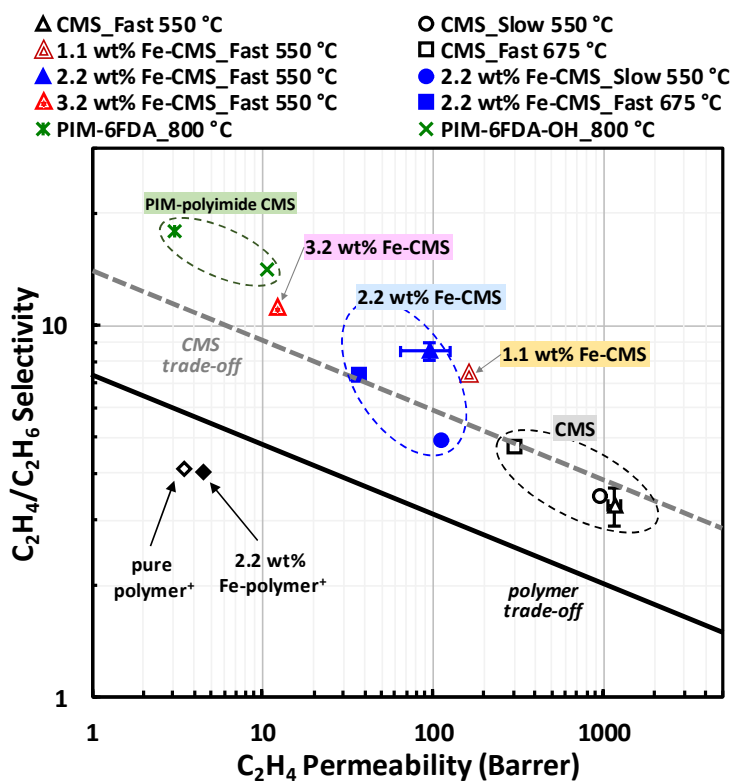


Figure 6.8. C_2H_4/C_2H_6 mixed-gas permeation results at 35 °C for Fe-free and Fe-containing 6FDA-DAM:DABA (3:2) derived CMS membranes with various pyrolysis protocols (results of PIM-polyimide CMS made at 800 °C are reproduced from reported data^{5,6})

6.4 Summary and Conclusions

The incorporation 2.2 wt% Fe ions in the 6FDA-DAM:DABA (3:2) polymer precursor has little influence on C₂H₄/C₂H₆ separation performance for the precursor. However, when pyrolyzed with controlled pyrolysis protocols, Fe-containing CMS membranes exhibit greatly improved separation performance. A pyrolysis protocol with a low pyrolysis temperature and a fast ramp rate (e.g., the *Fast 550 °C* protocol) is most suitable for preparing Fe-containing CMS membranes. With this pyrolysis protocol, active Fe complex can be generated within the carbon material. The C₂H₄/C₂H₆ sorption selectivity increases by 1.2 times since the Fe complex in micropores provides selective affinity to olefin. The C₂H₄/C₂H₆ diffusion selectivity becomes 2.7 times as the Fe complex blocks large less selective ultramicropores. The incorporation of Fe ions can boost the overall olefin/paraffin separation efficiency for CMS membranes as the suitable pyrolysis protocol is used. Clearly, incorporation of higher (> 2.2 wt%) is desirable.

6.5 References

1. Rungta, M. Carbon molecular sieve dense film membranes for ethylene/ethane separations. (Georgia Institute of Technology, 2012).
2. Rungta, M., Xu, L. & Koros, W. J. Carbon molecular sieve dense film membranes derived from Matrimid® for ethylene/ethane separation. *Carbon N. Y.* **50**, 1488–1502 (2012).
3. Bloch, E. D. *et al.* Hydrocarbon separations in a metal-organic framework with open iron (II) coordination sites. *Science (80-.)*. **335**, 1606–1610 (2012).
4. Rungta, M., Zhang, C., Koros, W. J. & Xu, L. Membrane-based ethylene/ethane separation: The upper bound and beyond. *AIChE J.* **59**, 3475–3489 (2013).
5. Salinas, O., Ma, X., Wang, Y., Han, Y. & Pinnau, I. Carbon molecular sieve membrane from a microporous spirobisindane-based polyimide precursor with enhanced ethylene/ethane mixed-gas selectivity. *RSC Adv.* **7**, 3265–3272 (2017).
6. Salinas, O., Ma, X., Litwiller, E. & Pinnau, I. High-performance carbon molecular sieve membranes for ethylene/ethane separation derived from an intrinsically microporous polyimide. *J. Memb. Sci.* **500**, 115–123 (2016).

CHAPTER 7. CHARACTERIZATION OF EFFECTS OF TESTING TEMPERATURE ON OLEFIN/PARAFFIN SEPARATION PERFORMANCE OF IRON-CONTAINING CARBON MOLECULAR SIEVE MEMBRANES

7.1 Overview

Chapter 6 demonstrated that Fe-containing 6FDA-DAM:DABA (3:2) carbon molecular sieve (CMS) membranes derived from the *Fast 550 °C* protocol have great potential with high C₂H₄/C₂H₆ selectivity. Recalling that CMS membranes with the highest Fe loading (3.2 wt%) showed the most impressive performance, however, 2.2 wt% loading was studied here for consistency to the bulk of the studies done in the most of this work. To better understand the properties of the Fe-containing CMS membranes, this chapter investigated the effects of testing temperature on olefin/paraffin separation performance of the CMS membranes, as well as the polymer precursors. The 2.2 wt% Fe-containing and Fe-free 6FDA-DAM:DABA (3:2) precursors were pyrolyzed with the *Fast 550 °C* protocol. The permeation and sorption performance of single-component C₂H₄ and C₂H₆ for the carbonized membranes as well as the polymeric precursors were obtained at 35 °C, 42.5 °C, and 50 °C. Measurements at higher temperature were avoided to prevent possible degradation of epoxy and aluminum tape adhesive used for masking the films. Temperature dependences of permeation, sorption, and diffusion performance for membranes are discussed in this chapter. By analyzing the temperature dependence results, the feature of added diffusion selectivity based on an entropic factor for the CMS membranes is reported in this chapter as well.

7.2 Temperature Dependence of Permeation Performance

The pure gas permeability of C₂H₄ and C₂H₆ for Fe-free and 2.2 wt% Fe-containing 6FDA-DAM:DABA (3:2) polymeric and CMS membranes were obtained at 35 °C, 42.5 °C, and 50 °C. Gas permeability (P) and C₂H₄/C₂H₆ permselectivity (α_p) at 50 psia for the studied films are shown in **Table 7.1**, where the uncertainties of permeability represent standard deviations from multiple film measurements, and the uncertainties of permselectivity were obtained based on the rules for propagation of uncertainty¹.

Clearly, both the carbon materials exhibit significantly higher gas permeability than the polymer precursors, and this observation has been discussed in previous sections. In the range of testing temperature between 35 °C and 50 °C, a trend was found for each type of the films that both C₂H₄ and C₂H₆ permeability increase with the increasing temperature, and this trend is consistent with other studies on polymeric membranes² and CMS membranes³. According to **Equation 2.13**, the temperature dependence of gas permeation is a combination of temperature dependencies of diffusion and sorption. Typically, as temperature increases, diffusion coefficients increase based on positive diffusion activation energies, while sorption coefficients decrease due to typical negative heats of sorption. Several studies have observed that as temperature increases, the increase in diffusion coefficients generally outweighs the decrease in sorption coefficients³⁻⁵. Hence, gas permeations increase with temperature and follow an Arrhenius relationship, which can be rearranged as:

$$\ln(P) = \left(\frac{-E_P}{R}\right) \cdot \frac{1}{T} + \ln(P_o) \quad (7.1)$$

As for the temperature dependence of permselectivity, the C₂H₄/C₂H₆ permselectivity is expected to decrease with increasing temperature in a trade-off for higher permeation. From **Table 7.1**, the studied polymer precursors follow this trend that α_p drops slightly with the increasing temperature. However, the relationship between α_p and temperature is not clear for the CMS films, which is probably due to some uncertainties of the permselectivity including combined uncertainties of the separate permeabilities.

Figure 7.1 shows least-squares fits to the natural logarithm of gas permeability in Barrer versus inverse absolute testing temperature for four types of the films. Based on **Equation 7.1**, the permeation activation energy (E_P) and the permeation pre-exponential factor (P_o) were obtained from the fitting slope and the y-intercept, respectively, and the results including uncertainties are listed in **Table 7.2**. As shown in the table, *positive* permeation activation energies were observed for each type of the films, resulting from the increasing permeations with the increasing temperature. Generally, permeation activation energy depends on size of gas penetrant and membrane material. For the films studied in this work, C₂H₆ generally has higher permeation activation energy than C₂H₄, and this observation is consistent with the previous studies that permeation activation energy increases with penetrant size for gas penetrants of similar condensability³. Surprisingly, this trend was not observed for the CMS materials *without* Fe, and this particular case may be caused by relative low fitting R-squared (~0.9265) for C₂H₆. If the uncertainties of permeation activation energies are considered, this exceptional material (CMS membranes

without Fe) may still follow the typical trend that has been observed for other materials. For the polymer precursors, the incorporation of Fe does not have significant effects on C₂H₄ and C₂H₆ permeation activation energies. Derived from the *Fast 550 °C* protocol, the carbon material *without* Fe has the lowest permeation activation energies, showing less temperature dependence of permeation. For Fe-containing CMS membranes, the permeation activation energies rise to the highest level, presumably due to the formation of Fe complex in both micropores and ultramicropores during pyrolysis. Based on **Equation 2.15**, permeation activation energy is a sum of diffusion activation energy and heat of sorption. The effects of each factor will be analyzed in the following sections.

Table 7.1. Permeation performance of C₂H₄ and C₂H₆ (50 psia) at 35–50 °C for Fe-free and Fe-containing 6FDA-DAM:DABA (3:2) polymeric and CMS membranes

		$P_{C_2H_4}$ (Barrer)	$P_{C_2H_6}$ (Barrer)	α_P
Fe-free polymer precursor	35 °C	3.52 ± 0.99	0.91 ± 0.20	3.89 ± 1.39
	42.5 °C	4.11 ± 0.96	1.16 ± 0.25	3.56 ± 1.14
	50 °C	4.54 ± 1.15	1.31 ± 0.26	3.47 ± 1.12
Fe-containing Polymer precursor	35 °C	2.82	0.62 ± 0.02	4.55 ± 0.15
	42.5 °C	3.26 ± 0.05	0.74 ± 0.03	4.43 ± 0.17
	50 °C	3.53 ± 0.06	0.87 ± 0.02	4.08 ± 0.10
Fe-free CMS Fast 550 °C	35 °C	1244.5	425.2 ± 62.1	2.93 ± 0.43
	42.5 °C	1296.7	434.6 ± 123.4	2.98 ± 0.85
	50 °C	1383.6	461.3 ± 117.0	3.00 ± 0.76
Fe-containing CMS Fast 550 °C	35 °C	63.2	6.8	9.34
	42.5 °C	83.7	10.3	8.13
	50 °C	129.8	15.2	8.54

Table 7.2. Permeation activation energy (E_P) and permeation pre-exponential factor (P_o) of C₂H₄ and C₂H₆ (50 psia) between 35–50 °C for Fe-free and Fe-containing 6FDA-DAM:DABA (3:2) polymeric and CMS membranes

	E_{P,C_2H_4} (kJ/mol)	E_{P,C_2H_6} (kJ/mol)	P_{o,C_2H_4} (Barrer)	P_{o,C_2H_6} (Barrer)
Fe-free polymer precursor	13.99 ± 1.63	20.22 ± 3.60	8.35E+02	2.47E+03
Fe-containing Polymer precursor	12.42 ± 1.82	18.38 ± 0.02	3.63E+02	8.09E+02
Fe-free CMS Fast 550 °C	5.83 ± 0.84	4.48 ± 1.26	1.21E+04	2.42E+03
Fe-containing CMS Fast 550 °C	39.68 ± 5.60	44.73 ± 0.34	3.27E+08	2.59E+08

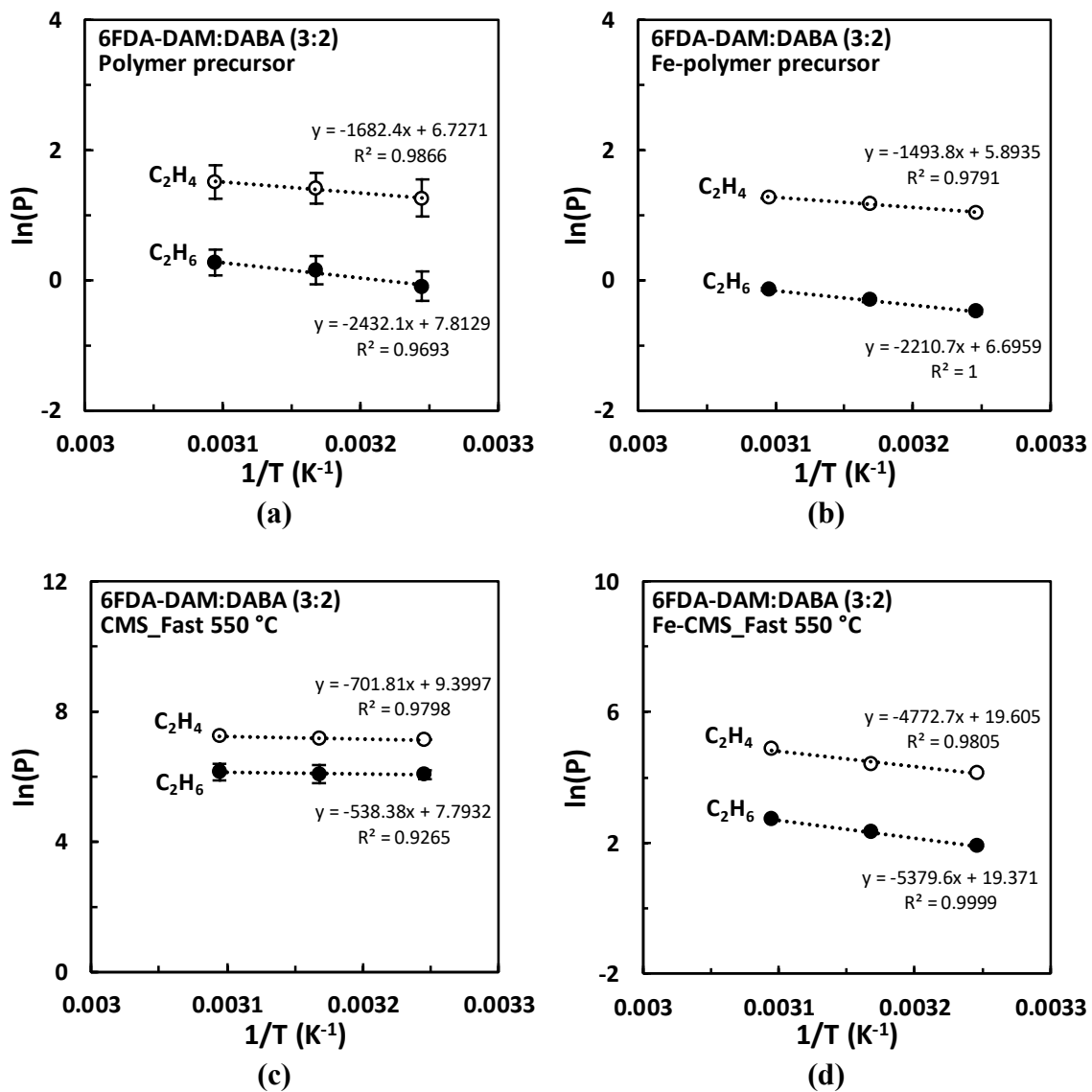


Figure 7.1. Temperature dependence of permeability for C_2H_4 and C_2H_6 (50 psia) for Fe-free and Fe-containing 6FDA-DAM:DABA (3:2) polymeric and CMS membranes (Equations are shown with $\ln(P) = \left(\frac{-E_P}{R}\right) \cdot \frac{1}{T} + \ln(P_o)$)

7.3 Temperature Dependence of Sorption Performance

The C₂H₄ and C₂H₆ equilibrium sorption properties for Fe-free and 2.2 wt% Fe-containing 6FDA-DAM:DABA (3:2) polymeric and CMS membranes were measured at 35 °C, 42.5 °C, and 50 °C. The pressure-dependent sorption coefficients (S) and C₂H₄/C₂H₆ sorption selectivity (α_S) were obtained at 50 psia, as shown in **Table 7.3**, where the uncertainties of sorption coefficients represent standard deviations from multiple sample measurements, and the uncertainties of sorption selectivity were obtained based on the rules for propagation of uncertainty¹.

Clearly, both the carbon materials exhibit significantly higher gas sorptivity than the polymer precursors, and this observation has been discussed in previous sections. In the range of testing temperature between 35 °C and 50 °C, a trend was found for each type of the films that both C₂H₄ and C₂H₆ sorption coefficients decrease with the increasing temperature, and this trend is consistent with other studies on polymeric membranes² and CMS membranes³. According to **Equation 2.12**, the thermodynamic sorption coefficients decrease with temperature due to typical negative heats of sorption, which follows a van't-Hoff relationship. The equation can be rearranged as:

$$\ln(S) = \left(\frac{-H_S}{R}\right) \cdot \frac{1}{T} + \ln(S_o) \quad (7.2)$$

As for the temperature dependence of sorption selectivity, the C₂H₄/C₂H₆ sorption selectivity is expected to increase with increasing temperature. However, in the temperature range from 35 °C to 50 °C, the relationship between temperature and sorption

selectivity is not clear for each type of the films, as shown in **Table 7.3**. Nevertheless, the Fe-containing CMS membranes have notable sorption selectivities at all the testing temperatures.

Figure 7.2 shows least-squares fits to the natural logarithm of gas sorptivity in $\text{cm}^3(\text{STP})/(\text{cm}^3(\text{sample})\cdot\text{cmHg})$ versus inverse absolute testing temperature for four types of the films. Based on **Equation 7.2**, the heats of sorption (H_{S}) and the sorption pre-exponential factor (S_0) were obtained from the fitting slope and the y-intercept, respectively, and the results including uncertainties are listed in **Table 7.4**. As shown in the table, *negative* heats of sorption were observed for each type of the films, resulting from the decreasing sorption coefficients with the increasing temperature. For glassy polymers, heats of sorption of gas penetrants are generally considered as a sum of two contributions⁶, as shown in **Equation 7.3**.

$$H_{\text{S}} = H_{\text{cond}} + H_{\text{mix}} \quad (7.3)$$

H_{mix} represents the enthalpy change when gas penetrants condense into sorption sites, and this change is generally increases with the gas critical temperature. H_{mix} is the enthalpy change resulted from formation of sorption sites and the energy of mixing the condensed gas penetrants within the polymer matrix. Since C_2H_6 has slightly higher critical temperatures (306 K) than C_2H_4 (283 K), the H_{cond} of C_2H_6 is expected to be slightly higher. Surprisingly, for the polymer precursors studied in this work, the effects of gas species on H_{mix} appear to outweigh the effects of gas critical temperature on H_{cond} , resulting in a higher absolute value of H_{S} for C_2H_4 than for C_2H_6 . Besides, with the

incorporation of Fe into the polymer, slightly higher H_S for both the C2 hydrocarbons was observed. For rigid porous CMS materials, H_{mix} is negligible since there is no need to form sorption sites and few, if any polar groups in the micropores. Therefore, H_S is highly dependent on the gas critical temperature for the carbon materials. However, in this work, the relationship between H_S and the gas species is not clear for the CMS materials. This surprising observation may be caused by similar critical temperatures for C₂H₄ & C₂H₆ and also by some uncertainties of the heats of sorption, as shown in **Table 7.4**.

Table 7.3. Sorption performance of C₂H₄ and C₂H₆ (50 psia) at 35–50 °C for Fe-free and Fe-containing 6FDA-DAM:DABA (3:2) polymeric and CMS membranes

		$S_{C_2H_4}$	$S_{C_2H_6}$	α_S
		$\left[\frac{\text{cm}^3(\text{STP})}{\text{cm}^3(\text{sample}) \cdot \text{cmHg}} \right]$	$\left[\frac{\text{cm}^3(\text{STP})}{\text{cm}^3(\text{sample}) \cdot \text{cmHg}} \right]$	
Fe-free polymer precursor	35 °C	0.1001	0.0932	1.07
	42.5 °C	0.0918	0.0858	1.07
	50 °C	0.0793	0.0784	1.01
Fe-containing Polymer precursor	35 °C	0.1005 ± 0.0055	0.0920 ± 0.0070	1.09 ± 0.10
	42.5 °C	0.0875	0.0797	1.10
	50 °C	0.0769	0.0738	1.04
Fe-free CMS Fast 550 °C	35 °C	0.4785	0.4621 ± 0.0146	1.04 ± 0.03
	42.5 °C	0.4528	0.4094 ± 0.0017	1.11
	50 °C	0.4267 ± 0.0067	0.3934 ± 0.0027	1.08 ± 0.02
Fe-containing CMS Fast 550 °C	35 °C	0.4645	0.3909	1.19
	42.5 °C	0.4376	0.3690	1.19
	50 °C	0.3932 ± 0.0016	0.3585 ± 0.0048	1.10 ± 0.02

Table 7.4. Apparent heat of sorption (H_S) and sorption pre-exponential factor (S_0) of C₂H₄ and C₂H₆ (50 psia) between 35–50 °C for Fe-free and Fe-containing 6FDA-DAM:DABA (3:2) polymeric and CMS membranes

	H_{S,C_2H_4} (kJ/mol)	H_{S,C_2H_6} (kJ/mol)	S_{0,C_2H_4} $\left[\frac{\text{cm}^3(\text{STP})}{\text{cm}^3(\text{sample}) \cdot \text{cmHg}} \right]$	S_{0,C_2H_6} $\left[\frac{\text{cm}^3(\text{STP})}{\text{cm}^3(\text{sample}) \cdot \text{cmHg}} \right]$
Fe-free polymer precursor	-12.83 ± 2.10	-9.56 ± 0.39	6.77E-04	2.23E-03
Fe-containing Polymer precursor	-14.74 ± 0.08	-12.19 ± 2.00	3.19E-04	7.81E-04
Fe-free CMS Fast 550 °C	-6.31 ± 0.22	-8.92 ± 2.46	4.08E-02	1.41E-02
Fe-containing CMS Fast 550 °C	-9.17 ± 1.63	-4.79 ± 0.85	1.31E-02	6.01E-02

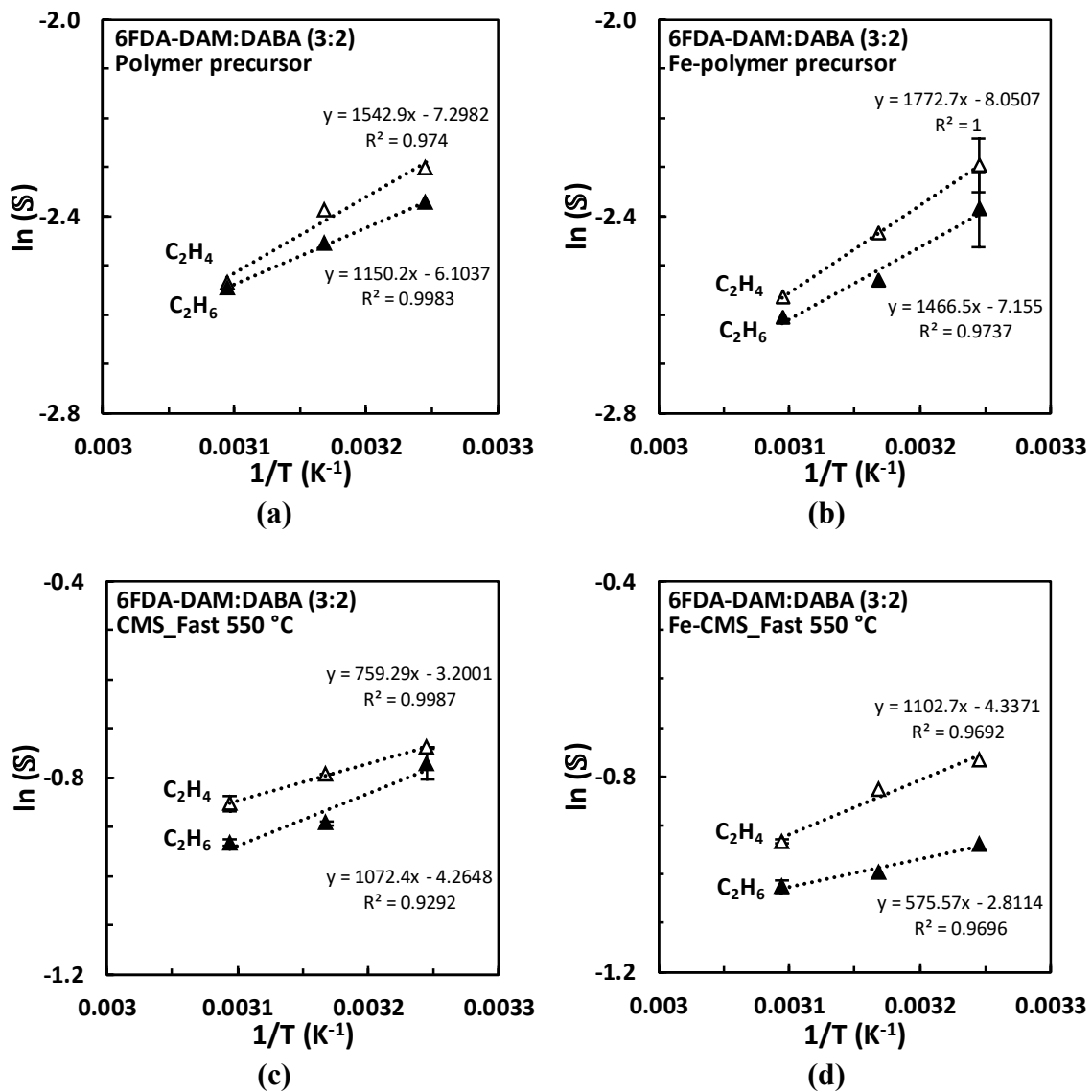


Figure 7.2. Temperature dependence of sorption coefficient for C_2H_4 and C_2H_6 (50 psia) for Fe-free and Fe-containing 6FDA-DAM:DABA (3:2) polymeric and CMS membranes (Equations are shown with $\ln(S) = \left(\frac{-H_S}{R}\right) \cdot \frac{1}{T} + \ln(S_o)$)

7.4 Temperature Dependence of Diffusion Performance

The average diffusion coefficients of C₂H₄ and C₂H₆ for Fe-free and 2.2 wt% Fe-containing 6FDA-DAM:DABA (3:2) polymeric and CMS membranes were calculated based on **Equation 2.3** ($P_A = \bar{D}_A \cdot \bar{S}_A$). The average gas diffusion coefficients (\bar{D}) and C₂H₄/C₂H₆ diffusion selectivity (α_D) at 50 psia for the studied films are shown in **Table 7.5**, where the uncertainties of diffusion coefficients and diffusion selectivity were obtained based on the rules for propagation of uncertainty¹.

Clearly, both the carbon materials exhibit significantly higher gas diffusivity than the polymer precursors, and this observation has been discussed in previous sections. In the range of testing temperature between 35 °C and 50 °C, a trend was found for each type of the films that both C₂H₄ and C₂H₆ diffusion coefficients increase with the increasing temperature, and this trend is consistent with other studies on polymeric membranes² and CMS membranes³. According to **Equation 2.11**, the diffusion coefficients increase with temperature based on an activated process, which follows an Arrhenius relationship. The equation can be rearranged as:

$$\ln(D) = \left(\frac{-E_D}{R}\right) \cdot \frac{1}{T} + \ln(D_o) \quad (7.4)$$

Figure 7.3 shows least-squares fits to the natural logarithm of gas diffusivity in cm²/s versus inverse absolute testing temperature for four types of the films. Based on **Equation 7.4**, the diffusion activation energy (E_D) and the diffusion pre-exponential factor (D_o) were obtained from the fitting slope and the y-intercept, respectively, and the results

including uncertainties are listed in **Table 7.6**. As shown in the table, *positive* diffusion activation energies were observed for each type of the films, resulting from the increasing diffusion coefficients with the increasing temperature. Diffusion activation energy represents the minimum energy for a gas penetrant to jump from one sorbed site to another, and depends on the size of gas penetrant and the intrinsic properties of membrane materials. For each type of the films studied in this work, the larger penetrant, C₂H₆, has higher diffusion activation energy than C₂H₄. The incorporation of Fe does not have significant effects on diffusion activation energies in the polymer precursors. However, the Fe-containing CMS membranes show the highest level of diffusion activation energies among the studied materials. The Fe complex in the CMS films appears to enlarge the temperature dependence of gas diffusion. Moreover, the Fe complex appears to be in ultramicropores of the CMS membrane and have additional size discrimination feature, resulting in greatly improved C₂H₄/C₂H₆ diffusion selectivity. This enhanced diffusion selectivity is contributed from an energetic factor and an entropic factor, as will be discussed in the next section.

Table 7.5. Diffusion performance of C₂H₄ and C₂H₆ (50 psia) at 35–50 °C for Fe-free and Fe-containing 6FDA-DAM:DABA (3:2) polymeric and CMS membranes

		$\bar{D}_{C_2H_4}$ (10 ⁻⁹ cm ² /s)	$\bar{D}_{C_2H_6}$ (10 ⁻⁹ cm ² /s)	α_D
Fe-free polymer precursor	35 °C	3.52 ± 0.99	0.97 ± 0.22	3.62 ± 1.30
	42.5 °C	4.48 ± 1.04	1.35 ± 0.30	3.32 ± 1.06
	50 °C	5.72 ± 1.45	1.67 ± 0.33	3.43 ± 1.11
Fe-containing Polymer precursor	35 °C	2.81 ± 0.15	0.67 ± 0.06	4.16 ± 0.41
	42.5 °C	3.72 ± 0.06	0.92 ± 0.03	4.03 ± 0.15
	50 °C	4.59 ± 0.08	1.17 ± 0.02	3.91 ± 0.10
Fe-free CMS Fast 550 °C	35 °C	260	92.0 ± 13.8	2.83 ± 0.42
	42.5 °C	286	106 ± 30.1	2.70 ± 0.77
	50 °C	324 ± 5.12	117 ± 29.8	2.77 ± 0.77
Fe-containing CMS Fast 550 °C	35 °C	13.6	1.73	7.87
	42.5 °C	19.1	2.79	6.86
	50 °C	3.30 ± 0.14	4.24 ± 0.06	7.79 ± 0.11

Table 7.6. Diffusion activation energy (E_D) and diffusion pre-exponential factor (D_o) of C₂H₄ and C₂H₆ (50 psia) at 35–50 °C for Fe-free and Fe-containing 6FDA-DAM:DABA (3:2) polymeric and CMS membranes

	E_{D,C_2H_4} (kJ/mol)	E_{D,C_2H_6} (kJ/mol)	D_{o,C_2H_4} (cm ² /s)	D_{o,C_2H_6} (cm ² /s)
Fe-free polymer precursor	26.82 ± 0.47	29.78 ± 3.21	1.23E-04	1.11E-04
Fe-containing Polymer precursor	27.16 ± 1.90	30.57 ± 1.98	1.14E-04	1.04E-04
Fe-free CMS Fast 550 °C	12.15 ± 1.06	13.39 ± 1.20	2.96E-05	1.72E-05
Fe-containing CMS Fast 550 °C	48.85 ± 7.24	49.51 ± 1.19	2.50E+00	4.30E-01

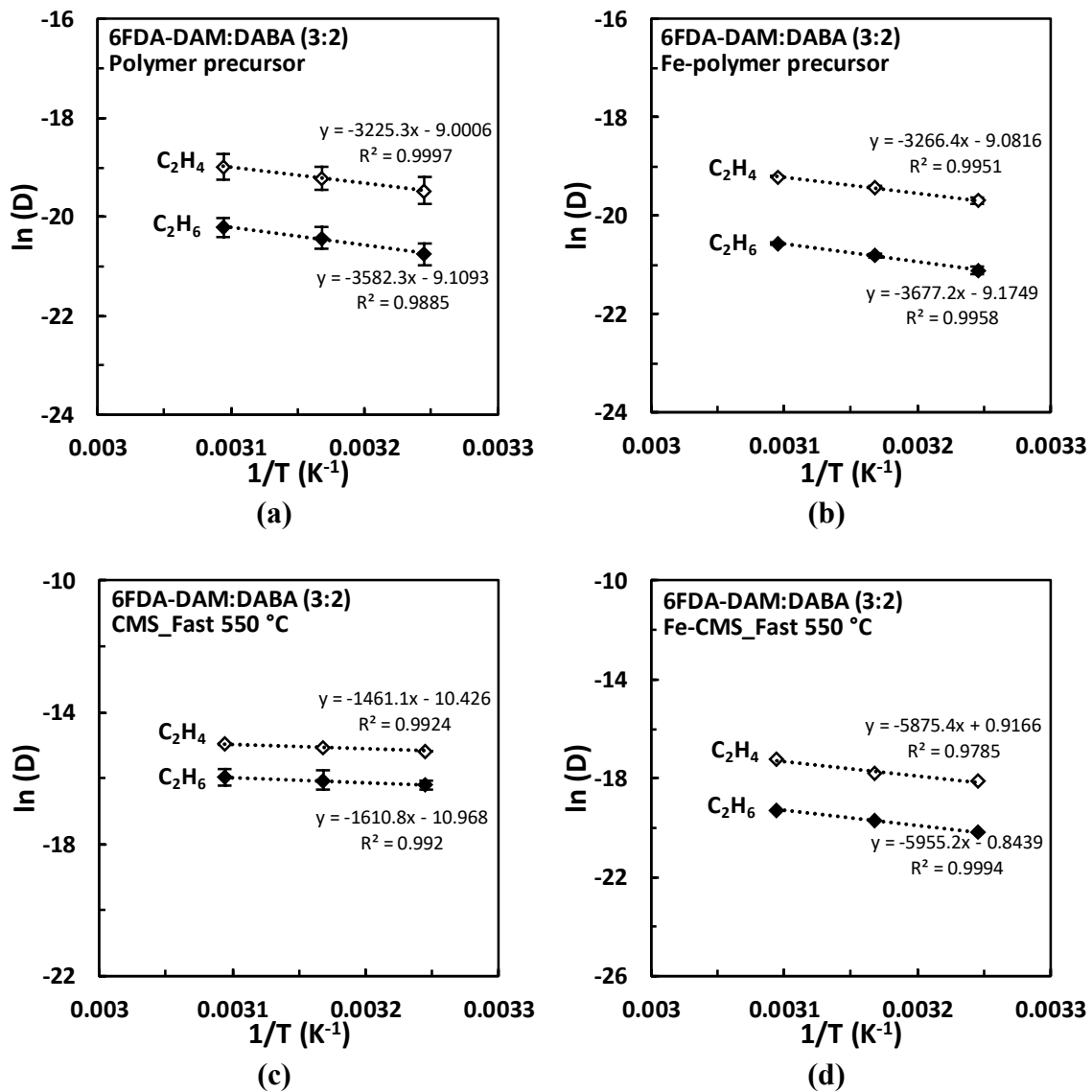


Figure 7.3. Temperature dependence of diffusion coefficient for C_2H_4 and C_2H_6 (50 psia) for Fe-free and Fe-containing 6FDA-DAM:DABA (3:2) polymeric and CMS membranes (Equations are shown with $\ln(D) = \left(\frac{-E_D}{R}\right) \cdot \frac{1}{T} + \ln(D_o)$)

7.5 Energetic and Entropic Factors in Diffusion Selectivity

As mentioned in **Equation 2.4**, a permselectivity ($\alpha_{A/B}$) is a product of diffusion selectivity (α_D) and sorption selectivity (α_S). The average C_2H_4/C_2H_6 permeation, sorption, and diffusion selectivities for each type of the films at the temperature between 35 °C and 50 °C were plotted in **Figure 7.4**, where the error bars represent the standard deviation of the corresponding data in the temperature range. The results shown in **Figure 7.4** are consistent with the previous discussions in Section 6.3.1: the permselectivity is dominated by diffusion selectivity while sorption selectivity has little influence for all the films studied in this work. Although Fe enhances C_2H_4/C_2H_6 sorption selectivity for CMS membranes, Fe increases more notable diffusion selectivity, resulting a ~3X permselectivity relative to the carbon material *without* Fe.

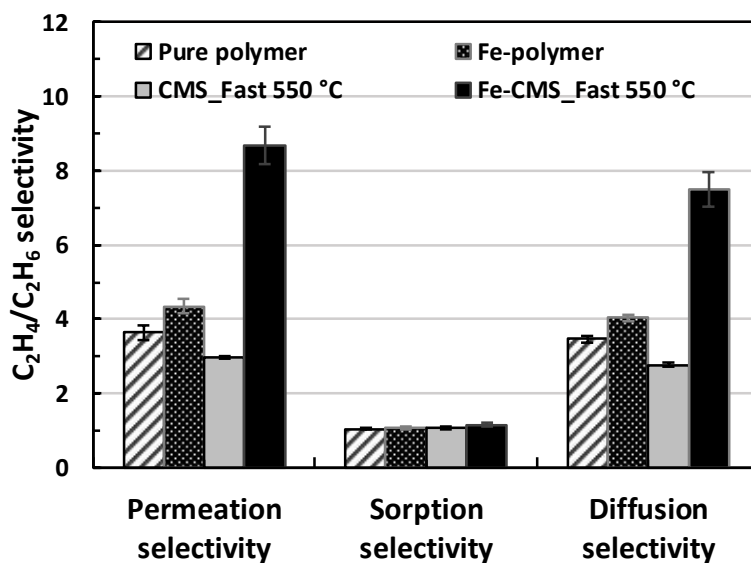


Figure 7.4. Permeation, sorption, and diffusion selectivities of C_2H_4/C_2H_6 (50 psia) between 35–50 °C for Fe-free and Fe-containing 6FDA-DAM:DABA (3:2) polymeric and CMS membranes

According to **Equation 2.17**, the diffusion selectivity can be further decoupled into an energetic factor and an entropic factor. The energetic selectivity is based on the difference in the diffusion activation energies of the two gas penetrants ($\Delta E_{D,A-B}$), while the entropic selectivity reflects the difference in the diffusion activation entropies of the two gas penetrants ($\Delta S_{D,A-B}$). Previous studies^{7,8} have revealed the significance of entropic selectivity for CMS materials for CO₂/CH₄, O₂/N₂, and N₂/CH₄ pairs. The researchers found that the entropic selectivity in polymeric films is close to unity, while entropic selectivity is much higher in CMS films. The results of the studies on C₂H₄/C₂H₆ pair in this work are consistent with this observed trend. As shown in **Figure 7.5**, both types of the CMS films have higher entropic selectivity than the polymer precursors. CMS materials have rigid size-discriminating ultramicropores that can restrict the degrees of motional freedom for gas penetrants, which makes it size-selective sieving. Compared to polymer membranes with flexible chains, CMS membranes have added entropic selectivity which is useful for separating penetrants with very little difference in size and shape. With the incorporation of Fe, the entropic selectivity further increases to the highest level of 5.83, and this entropic factor dominates the increase in diffusion selectivity with Fe.

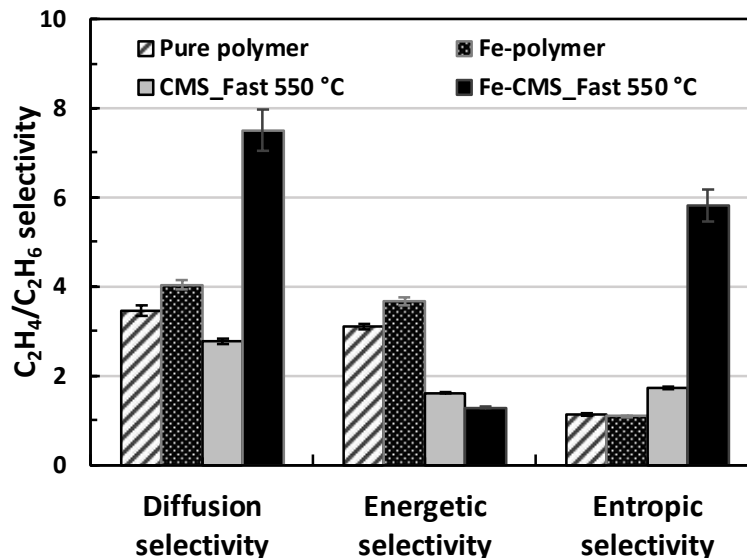


Figure 7.5. Diffusion, energetic, and entropic selectivities of C_2H_4/C_2H_6 (50 psia) between 35–50 °C for Fe-free and Fe-containing 6FDA-DAM:DABA (3:2) polymeric and CMS membranes

Based on the observed improvements in C_2H_4/C_2H_6 diffusion selectivity with Fe in CMS membranes, the Fe complex is hypothesized to be in the ultramicropores, tightening the rigid molecular sieve window and providing added entropic factor for the improved diffusion selectivity. Besides, a slight increase in C_2H_4/C_2H_6 sorption selectivity was shown in this work, apparently resulting from the Fe complex in the micropores providing selective affinity to olefin. Hence, the Fe incorporation clearly changes the pore structure of CMS membranes, and an idealized bimodal pore size distribution in the Fe-containing CMS materials is proposed, as illustrated in **Figure 7.6**. Since Fe clearly affects sorption and diffusion performance, it is envisioned that the Fe complex modifies “large” ultramicropores and “small” micropores. The shaded area is the cross-over region, where is the possible range for Fe complex to present in the CMS membranes. With these

combined contributions derived from the Fe in “large” ultramicropores and “small” micropores, therefore, the Fe-containing CMS membranes derived from the *Fast 550 °C* protocol not only overcome the C₂H₄/C₂H₆ upper bound for polymers⁹ but also surpass the C₂H₄/C₂H₆ upper bound for CMS materials¹⁰, which has been proven in [Section 6.3.2](#).

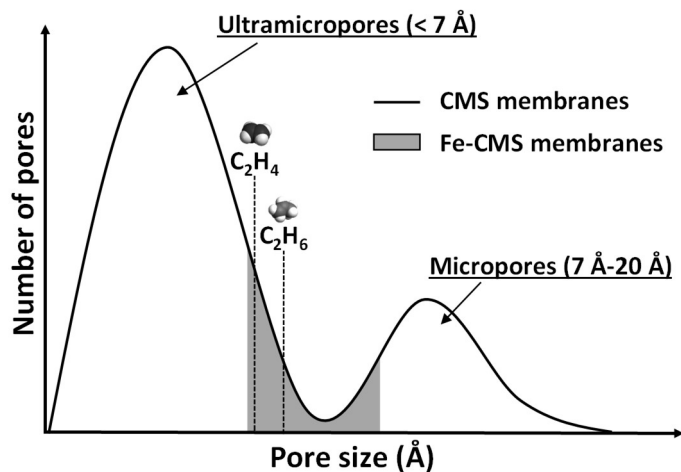


Figure 7.6. Idealized bimodal pore size distribution in Fe-containing CMS materials (shaded area represents cross-over region of “large” ultramicropores and “small” micropores as possible range for Fe complex to present)

7.6 Summary and Conclusions

The temperature dependences of permeation, sorption, and diffusion of C₂H₄/C₂H₆ separation for the Fe-containing CMS membranes are studied in this chapter. The permeation and sorption properties for Fe-free and 2.2 wt% Fe-containing polymer precursor as well as the resulting CMS materials derived from the *Fast 550 °C* protocol were measured at 35 °C, 42.5 °C, and 50 °C. For the films studied in this work, as

temperature increases, the increase in diffusion coefficients outweighs the decrease in sorption coefficients, resulting in an increase in permeation. This work demonstrated that the highly enhanced C_2H_4/C_2H_6 diffusion selectivity was based on the added contribution from entropic selectivity with Fe.

7.7 References

1. Harris, D. C. *Quantitative chemical analysis*. (Macmillan, 2010).
2. Costello, L. M. & Koros, W. J. Temperature dependence of gas sorption and transport properties in polymers: measurement and applications. *Ind. Eng. Chem. Res.* **31**, 2708–2714 (1992).
3. Fu, S., Sanders, E. S., Kulkarni, S. S., Wenz, G. B. & Koros, W. J. Temperature dependence of gas transport and sorption in carbon molecular sieve membranes derived from four 6FDA based polyimides: Entropic selectivity evaluation. *Carbon N. Y.* **95**, 995–1006 (2015).
4. Ning, X. Carbon molecular sieve membranes for nitrogen/methane separation. (Georgia Institute of Technology, 2014).
5. Rungta, M. Carbon molecular sieve dense film membranes for ethylene/ethane separations. (Georgia Institute of Technology, 2012).
6. Ghadimi, A., Norouzbahari, S. & Mohammadi, T. Heat of Sorption of Gases in Glassy Polymers: Prediction via Applying Physical Properties of the Penetrants and Polymers. *J. Chem. Eng. Data* **62**, 1433–1439 (2017).
7. Fu, S. *et al.* The Significance of Entropic Selectivity in Carbon Molecular Sieve Membranes Derived from 6FDA/DETDA: DABA (3: 2) Polyimide. *J. Memb. Sci.* (2017).
8. Singh, A. & Koros, W. J. Significance of entropic selectivity for advanced gas separation membranes. *Ind. Eng. Chem. Res.* **35**, 1231–1234 (1996).
9. Rungta, M., Xu, L. & Koros, W. J. Carbon molecular sieve dense film membranes derived from Matrimid® for ethylene/ethane separation. *Carbon N. Y.* **50**, 1488–1502 (2012).
10. Salinas, O., Ma, X., Wang, Y., Han, Y. & Pinnau, I. Carbon molecular sieve membrane from a microporous spirobisindane-based polyimide precursor with enhanced ethylene/ethane mixed-gas selectivity. *RSC Adv.* **7**, 3265–3272 (2017).

CHAPTER 8. CONCLUSIONS & RECOMMENDATIONS

8.1 Overview

In this work, carbon molecular sieve (CMS) dense film membranes derived from 6FDA-DAM:DABA (3:2) polyimide precursor were studied for separation of mixed olefins (C_2H_4 and C_3H_6) from paraffins (C_2H_6 and C_3H_8). Incorporation of Fe(II) ions into the precursors was pursued to develop olefin-selective CMS membranes with high separation performance. The principal goal of this work is to understand the factors controlling performance of the CMS membranes for the separation, and four specific objectives, as listed in [Chapter 1](#), were pursued. This chapter highlights the key findings and contributions for each objective in this work. Recommendations for the future studies are outlined in the chapter as well.

8.2 Conclusions

There are four specific objectives in this work for the studies on 6FDA-DAM:DABA (3:2) derived CMS membranes for separation of mixed olefins (C_2H_4 and C_3H_6) from paraffins (C_2H_6 and C_3H_8). The key findings and contributions for each objective are described as below.

8.2.1 Evaluation of Viability of Selected Metal in CMS Membranes for Increasing Olefin/Paraffin Sorption Selectivity

To improve olefin/paraffin separation performance, Fe(II) ions were selectively integrated into CMS membranes for improving the sorption selectivity, and ultimately the

permselectivity. The iron salts of $\text{Fe}(\text{acac})_2$ was integrated into the 6FDA-DAM:DABA (3:2) polymer precursor to form a 2.2 wt% Fe-containing polymer precursor. Various pyrolysis conditions (including pyrolysis temperature, ramp rates, and soak time) were studied for tuning the separation performance, and C_2H_4 & C_2H_6 sorption properties of the resulting Fe-containing CMS membranes were measured at 35 °C with selectivity determined at 50 psia. It was found that the *Fast 550 °C* protocol (a protocol with a low pyrolysis temperature at 550 °C, a fast ramp rate at 10 °C/min, and no soak time) was the most suitable pyrolysis protocol for the olefin/paraffin separation for the Fe-containing CMS membranes. The DABA moiety in the polymer was shown to be necessary for the improved separation performance, based on more or less stabilization of the cross-linking with Fe ions in the precursor. After applying the *Fast 550 °C* protocol, the Fe-containing CMS membranes derived from the 2.2 wt% Fe-containing 6FDA-DAM:DABA (3:2) precursor showed a 19% enhancement in $\text{C}_2\text{H}_4/\text{C}_2\text{H}_6$ sorption selectivity and an 11% improvement in $\text{C}_3\text{H}_6/\text{C}_3\text{H}_8$ sorption selectivity relative to the controlled Fe-free CMS membranes derived from the same protocol. From the X-ray absorption near edge structure (XANES) analysis, the *Fast 550 °C* protocol derived Fe-containing carbon material was shown to have a unique coordination environment of the Fe species compared to the materials derived from other pyrolysis protocols, and this particular Fe species was found to have an average oxidation state of $\text{Fe}^{+2.2}$, which may provide a reason for the enhancement in olefin/paraffin sorption selectivity. Deeper studies on Fe-containing CMS membranes for olefin/paraffin separation were pursued in the following objectives.

8.2.2 Investigation of Effects of Iron Loadings & Studies on Alternative Metal Species for Olefin-Selective CMS Membranes

The preliminary results in Chapter 4 have demonstrated that if correctly tailored, CMS membranes derived from the 2.2 wt% Fe-containing 6FDA-DAM:DABA (3:2) precursor exhibit more efficient sorption separation. An advanced olefin-selective CMS membrane was pursued by studying the effects of Fe loadings between 1.1 and 3.2 wt% in the precursor. Higher loadings of Fe could not be pursued due to gelation issue during the formation of polymer precursor films with Fe. The CMS membranes with the studied loadings of Fe were derived from the *Fast 550* °C protocol, and the transport properties of C2 and C3 hydrocarbons in each membrane were measured with a 50 psia quaternary mixture at 35 °C. Surprisingly, a trend was observed that the selectivity of larger olefin over smaller paraffin (C_3H_6/C_2H_6) decrease with the increasing Fe loading in the membranes, which does not meet the expectation for developing an advanced olefin-selective membrane. However, the 3.2 wt% Fe loading CMS membrane achieved the highest C_2H_4/C_2H_6 permselectivity near 11 with C_2H_4 permeability above 10 Barrers, while the 0 wt% Fe loading CMS membrane had a lower selectivity of 3.3. It has been proven that the Fe incorporation provides a valuable tuning opportunity for the challenging C_2H_4/C_2H_6 separation; therefore, most of the studies done in this work focus on the C2 pair separation. Stability of the extensively studied 2.2 wt% Fe-containing CMS membranes were investigated by continuous permeation testing using the 50 psia quaternary mixture at 35 °C over a period around 60 days. The membrane showed some reductions in permeation initially (24% decrease in C_2H_4 permeability) and achieved stable performance after 50 days with the continuous feed. Regardless the initial decrease in permeation caused

by CMS pore relaxation, the 2.2 wt% Fe-containing CMS membrane has been proven to be stable with a competitive C_2H_4/C_2H_6 permselectivity around 9.

In the preliminary studies, Fe(II) was chosen as the incorporated metal into CMS membranes based on a combination of factors including high C_2H_4/C_2H_6 adsorption selectivity¹, low cost, and stability against contaminants. Besides Fe(II), various metal species including Fe(III), Al(III), Ni(II), Mn(II), and Mn(III) were investigated for evaluating their impacts on the mixed olefin/paraffin separation. Each metal species in the form of metal acetylacetonates $[M(acac)_n]$ of 0.05 g was integrated into the 6FDA-DAM:DABA (3:2) precursor of 0.5 g. However, only the films with Fe(II), Fe(III), and Al(III) were applicable while the other metal salts only partially dissolved in the tetrahydrofuran (THF) solvent, preventing film masking. The successfully prepared films were pyrolyzed with the *Fast 550 °C* protocol and exposed to the 50 psia quaternary mixture at 35 °C for measuring the gas transport properties. Among the studied metal species, Fe(II) has been proven to be the suitable specie for the highest C_2H_4/C_2H_6 around 9 while the other metal species provided the selectivity less than 6. Therefore, Fe(II) in the form of $Fe(acac)_2$ was extensively studied as the source of metal in the CMS membranes for improving olefin/paraffin separation.

8.2.3 Analysis of Effects of Iron on Performance of Iron-Containing CMS Membranes

Extensive studies were performed on the 2.2 wt% Fe-containing CMS membranes derived from the *Fast 550 °C* protocol, and the effects of Fe on C_2 pair separation performance were decoupled into a sorption contribution and a diffusion contribution. The permeation and the sorption performance of the Fe-free and Fe-containing CMS

membranes were measured with single-component C₂H₄ and C₂H₆ feeds at 35 °C. It has been discovered that the C₂H₄/C₂H₆ sorption selectivity increases by 1.2 times since the Fe complex in micropores provides selective affinity to the olefin. On the other hand, the C₂H₄/C₂H₆ diffusion selectivity becomes 2.7 times as the Fe complex blocks large less selective ultramicropores. The combined contributions result in a 3.2X permselectivity relative to the Fe-free CMS membrane derived from the same pyrolysis protocol.

This objective also analyzed the trade-off in terms of separation efficiency and productivity of various CMS films (Fe-containing and Fe-free CMS materials derived from different pyrolysis protocols). The results showed when applying the *Fast 550 °C* protocol, the Fe-containing CMS membranes with Fe loadings between 1.1 wt% and 3.2 wt% all have C₂ pair separation performance above the CMS upper bound² reported recently. It has been showed that the 3.2 wt% Fe loading film has the highest selectivity near 11 with C₂H₄ permeability above 10 Barrers, which is competitive with the recent studied PIM-polyimide derived CMS made at 800 °C^{2,3}.

8.2.4 Characterization of Effects of Testing Temperature on Olefin/Paraffin Separation Performance of Iron-Containing CMS Membranes

As the Fe-containing CMS membranes developed in this work have shown impressive olefin/paraffin separation performance, extensive temperature dependence studies were performed on the 2.2 wt% Fe-containing CMS membranes derived from the *Fast 550 °C* protocol. The permeation and the sorption performance of the Fe-free and Fe-containing CMS membranes were measured with single-component C₂H₄ and C₂H₆ feeds at 35 °C, 42.5 °C, and 50°C. The results have proven that for each type of the films, as

temperature increases, the increase in diffusion coefficients outweighs the decrease in sorption coefficients, resulting in an increase in permeation. By analyzing the temperature dependence results, the Fe-containing CMS membranes shown added C₂H₄/C₂H₆ diffusion selectivity contributed from the entropic selectivity with Fe.

8.3 Recommendations

8.3.1 *Exploration of Higher Metal Loadings in CMS Membranes with Alternative Processing Procedures and Precursor Materials*

In this work, CMS membranes with the incorporation of Fe(II) ions have been proven to exhibit improved olefin/paraffin separation performance. Moreover, the CMS membrane derived from the 6FDA-DAM:DABA (3:2) with 3.2 wt% Fe showed the highest C₂H₄/C₂H₆ permselectivity near 11 with a competitive C₂H₄ permeability. This impressive performance may be further pursued by increasing the loading of Fe. However, in the current work, Fe loading could not be pursued due to gelation issue during the formation of Fe-containing polymer precursor films, resulting from high ionic cross-linking density between Fe ions and the DABA group. Alternative approaches are recommended to overcome this gelation issue during the formation of Fe-containing polymer precursors.

Metal ions may be incorporated into polymers during the polyimide synthesis process. Several studies have demonstrated a metal-containing polyimide film can be formed by casting a mixed solution with metal salts and polyamic acid^{4,5}. As the films are thermally cured at a high temperature, the metal ions react with the carboxylic acid groups of the polyamic acid, forming metal-containing polyimide films. Besides, the gelation issue may also be addressed by infusing metal ions into the polymer. This work suggests soaking

a precursor membrane in metal acetylacetonate solutions, allowing for infusion of metal ions into the polymer. This application can be further extended to hollow fiber membranes, which are more appropriate in industry applications. The third proposed approach to increasing metal loading is integrating metal ions with a DABA-free polyimide in the same manner used in this work. Although this work indicated that the DABA moiety appears to be necessary for uniformly distributed metal ions and the improved olefin/paraffin *sorption* selectivity, it is the *diffusion* selectivity dominating the increasing permselectivity. Therefore, alternative polyimide precursors *without* DABA, (e.g., 6FDA-DAM, 6FDA:BPDA-DAM, and 6FDA:BPDA) are suggested as the starting material for the metal-containing CMS membranes with presumably improved diffusion and permeation selectivities.

8.3.2 Investigation of Physical Aging in Fe-Containing CMS Membranes

In the current work, the extensively studied 2.2 wt% Fe-containing CMS membranes derived from the *Fast 550 °C* protocol have shown moderately stable separation performance after 50 days with a continuous feed. Nevertheless, an initial reduction in permeation was observed, presumably caused by CMS pore relaxation. A physical aging phenomenon in CMS materials resulting in time-dependent transport performance was reported previously^{6,7}. The turbostratic carbon sheets in CMS membranes are hypothesized to rearrange to a more stable state with denser packing, which results in a decrease in permeability over time. This phenomenon may explain the initial reduction in permeation for the Fe-containing CMS studied in this work. As the stability of the membrane is critical for real-world applications, conducting thoughtful investigations on the performance stability of the Fe-containing CMS is suggested for the future research.

The storage conditions for the resulting CMS membranes have some effects on the separation performance, and the physical aging phenomena can be amplified when a CMS material is exposed to active vacuum. Hence, storage conditions, including vacuum environment and active inert gas feeds, are recommended for the studies on the stability of CMS membranes. Controlled experiments of CMS membranes *without* Fe are suggested to be performed for analyzing the effect of Fe on physical aging.

8.3.3 *Translation of Fe-Containing CMS Dense Films to Hollow Fiber Membranes*

In the current work, Fe-containing CMS dense film membranes were successfully fabricated and showed an impressive improvement in olefin/paraffin separation performance relative to the starting precursor polymer and even the controlled CMS membranes *without* Fe. Therefore, it is attractive to translate this promising Fe-containing CMS dense film to hollow fiber membranes for scale-up in industrial applications.

Several approaches may be feasible to integrate metal ions into CMS hollow fiber membranes. The first proposed approach, as mentioned before, is to soak an already spun hollow fiber precursor in a metal-containing solution, allowing for infusion of metal ions into the fiber precursor. An alternative suggestion is adding metal ions into the dope solution for fiber spinning. As the dope composition is critical for the solution spinning process, preliminary studies can be started with syringe test to form mimic fibers. This method has been proven as a useful screening tool to identify the influences of dope composition and spinning conditions on resulting fibers⁸.

8.4 References

1. Geier, S. J. *et al.* Selective adsorption of ethylene over ethane and propylene over propane in the metal–organic frameworks M₂(dobdc) (M = Mg, Mn, Fe, Co, Ni, Zn). *Chem. Sci.* **4**, 2054–2061 (2013).
2. Salinas, O., Ma, X., Wang, Y., Han, Y. & Pinnau, I. Carbon molecular sieve membrane from a microporous spirobisindane-based polyimide precursor with enhanced ethylene/ethane mixed-gas selectivity. *RSC Adv.* **7**, 3265–3272 (2017).
3. Salinas, O., Ma, X., Litwiller, E. & Pinnau, I. High-performance carbon molecular sieve membranes for ethylene/ethane separation derived from an intrinsically microporous polyimide. *J. Memb. Sci.* **500**, 115–123 (2016).
4. Sawada, T. & Ando, S. Synthesis, characterization, and optical properties of metal-containing fluorinated polyimide films. *Chem. Mater.* **10**, 3368–3378 (1998).
5. St Clair, A. K. & Taylor, L. T. A comparison of physical and mechanical properties of polyimide films containing different metal ions. *J. Appl. Polym. Sci.* **28**, 2393–2400 (1983).
6. Xu, L. *et al.* Physical aging in carbon molecular sieve membranes. *Carbon N. Y.* **80**, 155–166 (2014).
7. Wenz, G. B. & Koros, W. J. Tuning carbon molecular sieves for natural gas separations: A diamine molecular approach. *AIChE J.* **63**, 751–760 (2017).
8. Carruthers, S. B. Integral-skin formation in hollow fiber membranes for gas separations. (The University of Texas at Austin, 2001).

APPENDIX A.

GAS COMPRESSIBILITY FACTORS

Gas compressibility factors (Z) of the gases were used in this work to account for behavior of non-ideal gases, and is described as follows:

$$Z = \frac{pV}{nRT} \quad (\text{A.1})$$

where:

- p : pressure of the gas
- V : volume of the system occupied by the gas
- n : number of moles of the gas
- R : universal gas constant
- T : absolute temperature of the gas

In this work, the pressure-dependent compressibility factor equations of pure gases were calculated using the Peng-Robinson Equation of State and the National Institute of Standards and Technology (NIST) SUPERTRAPP Software, Version 3.1. These equations of C2 and C3 hydrocarbons at 35–50 °C are listed in **Table A.1**.

Table A.1. Compressibility factor equations of gases, with pressure (p) in psia

Gas	Temperature	Compressibility Equation
C ₂ H ₄	35 °C	$Z = -2.966 \times 10^{-11} p^3 - 8.125 \times 10^{-8} p^2 - 3.519 \times 10^{-4} p + 1$
	42.5 °C	$Z = -1.352 \times 10^{-11} p^3 - 6.807 \times 10^{-8} p^2 - 3.261 \times 10^{-4} p + 1$
	50 °C	$Z = -5.668 \times 10^{-12} p^3 - 5.558 \times 10^{-8} p^2 - 3.027 \times 10^{-4} p + 1$
C ₂ H ₆	35 °C	$Z = -1.681 \times 10^{-10} p^3 - 1.487 \times 10^{-7} p^2 - 4.683 \times 10^{-4} p + 1$
	42.5 °C	$Z = -1.103 \times 10^{-10} p^3 - 1.289 \times 10^{-7} p^2 - 4.355 \times 10^{-4} p + 1$
	50 °C	$Z = -6.943 \times 10^{-11} p^3 - 1.105 \times 10^{-7} p^2 - 4.046 \times 10^{-4} p + 1$
C ₃ H ₆	35 °C	$Z = -2.317 \times 10^{-9} p^3 - 5.100 \times 10^{-7} p^2 - 8.720 \times 10^{-4} p + 1$
	42.5 °C	$Z = -1.254 \times 10^{-9} p^3 - 5.778 \times 10^{-7} p^2 - 7.958 \times 10^{-4} p + 1$
	50 °C	$Z = -1.051 \times 10^{-9} p^3 - 4.341 \times 10^{-7} p^2 - 7.475 \times 10^{-4} p + 1$
C ₃ H ₈	35 °C	$Z = -4.194 \times 10^{-9} p^3 - 4.940 \times 10^{-7} p^2 - 9.922 \times 10^{-4} p + 1$
	42.5 °C	$Z = -2.925 \times 10^{-9} p^3 - 4.760 \times 10^{-7} p^2 - 9.165 \times 10^{-4} p + 1$
	50 °C	$Z = -1.950 \times 10^{-9} p^3 - 4.743 \times 10^{-7} p^2 - 8.464 \times 10^{-4} p + 1$